KOCAELI UNIVERSITY
INSTITUTE OF NATURAL AND APPLIED SCIENCES

DEPARTMENT OF
MECHATRONICS ENGINEERING

THE MASTER'S THESIS

PID AND FUZZY CONTROL OF MAGNETIC LEVITATION SYSTEM

EDISON WVEIMAR AYALA TREJOS

KOCAELI 2019

KOCAELI UNIVERSITY
INSTITUTE OF NATURAL AND APPLIED SCIENCES

DEPARTMENT OF
MECHATRONICS ENGINEERING

THE MASTER'S THESIS

PID AND FUZZY CONTROL OF MAGNETIC LEVITATION SYSTEM

EDISON WVEIMAR AYALA TREJOS

Prof. Dr. Zafer BINGÜL ....
Advisor, Kocaeli University

Asst. Prof. Dr. Selçuk KİZİR ....
Jury Member, Kocaeli University

Asst. Prof. Dr. Metin TOZ ....
Jury Member, Düzce University

Date of Thesis Defense: 12.02.2019

ACKNOWLEDGEMENT

I would like to thank my thesis advisor Prof. Dr. Zafer BINGÜL and Research Assistant Mehmet GÜLEÇ, and my research colleague Mohammad Javad FOTUHI for their support and guidance during the course of my research. I would also like to acknowledge the support of my parents and my friends towards the final product you are now reading; and a special acknowledge to Avril and Bryan for their special understanding.

I would also like to thank The Presidency for Turks Abroad and Related Communities (YTB), without whom this master's degree would not be possible.

January – 2019 Edison Wveimar AYALA TREJOS

TABLE OF CONTENT

ACKNOWLEDGEMENT i
TABLE OF CONTENT ii
LIST OF FIGURES iv
LIST OF TABLES vii
LIST OF SYMBOLS AND ABBREVIATIONS viii
ÖZET x
ABSTRACT xi
INTRODUCTION 1
1. FRAMEWORK 4
1.1. Electromagnetic Principles 4
1.2. Elementary Theory of Electromagnetic 8
1.2.1. Maxwell's equations 8
1.2.2. Flux and circulation 9
1.3. Determination of Losses 9
1.3.1. Magnetic hysteresis losses 10
2. MAGNETIC LEVITATION SYSTEM DESCRIPTION 14
2.1. Core of Somaloy700 14
2.2. Magnetic Levitation System Description 15
2.2.1. Hall effect sensor 17
2.2.2. Electromagnet 17
2.3. Description of the Magnetic Levitation System 18
2.4. Core Permeability 19
2.4.1. Resistivity and temperature coefficients 20
2.4.1.1. Units of electrical conductivity 21
2.4.1.2. Relationship between conductivity and resistivity 21
2.4.1.3. Factors that affect the electrical conductivity 22
2.4.2. Steel ball permeability 23
2.4.2.1. Core design 23
2.4.2.2. Maglev system reluctances 25
2.4.2.3. Determination the number of N-turns at the coil 27
2.4.2.4. Magnetic flux intensity 28
2.4.2.5. Calculating the flux density 28
2.4.3. Electromagnet inductance 29
2.5. Dynamics of Magnetic Levitation 29
2.6. The Electromagnetic Force 31
2.6.1. FMM model simulation 35
2.6.2. Mechanical model 37
2.6.3. Magnetic Levitation 38
2.6.4. Dynamic equations of state space model 39
2.6.5. State equations of a magnetic levitation system 41
3. SYSTEM IDENTIFICATION 42
3.1. Magnetic Levitation System Dynamic Model 42
3.1.1. The temperature effects on maglev system 45

3.2. Magnetic Force ... 46
3.2.1. Complete mathematical model ... 47
3.3. Linear Model ... 49
3.4. Linearization of the Model ... 50
3.5. Plant Transfer Function ... 54
3.5.1. Power gain ... 55
3.6. Dynamic System ... 57
3.7. Model of Laboratory Magnetic Levitation System ... 58
3.7.1. Hall effect sensors on maglev system ... 62
3.7.2. Variation in temperature ... 67
3.8. Behavior of the Magnetic Levitation System ... 69
3.8.1. Determining the best conditions ... 70
3.8.2. Evaluation of obtained data ... 70
3.8.3. Air gap variations ... 72
3.8.4. Power stage ... 73
3.8.5. Frequency variation using a pneumatic system ... 74
3.8.6. Outputs of the alternate pneumatic system ... 75
3.8.7. Frequencies variations using servomotor system ... 76
3.8.8. Outputs of the alternate servomotor system ... 77
3.8.9. HES signal for sinusoidal ball position ... 79
3.8.10. Plant configuration ... 80
4. CONTROLLERS DESIGN ... 81
4.1. PID Controller ... 82
4.1.1. Tuning of the PID ... 83
4.1.2. GOOGOLTECH industrial PC ... 85
4.2. Fuzzy Logic Controller Design ... 86
4.2.1. Fundamental principles of FLC ... 86
4.3. FLC Implementation ... 88
4.3.1. Rule base ... 90
5. RESULTS AND DISCUSSIONS ... 92
5.1. Hall Effect Sensor Bode Diagram ... 92
5.2. System Signal Analysis ... 93
5.3. Performance Error Indices ... 97
6. CONCLUSIONS AND SUGGESTIONS ... 99
REFERENCES ... 102
ANNEX ... 106
PUBLICATIONS AND WORKS ... 108
BIOGRAPHY ... 109

LIST OF FIGURES

Figure 1.1. Magnetizing in a Somaloy700 ferrite bar ... 5
Figure 1.2. Faraday's Induction law... 8
Figure 1.3. A general B-H curve of Hysteresis ... 10
Figure 1.4. B - H hysteresis curve of Somaloy700 material ... 12
Figure 1.5. Somaloy700 3D representation of the magnetization curve in the maglev system... 13
Figure 2.1. Somaloy 700, from powder to 3D Special Shape a) Nano-coated Fe particles, b) Pressing and thermal processing, c) 3D shape ... 14
Figure 2.2. Plant model of magnetic levitation system ... 15
Figure 2.3. Stages that conform the magnetic levitation system... 16
Figure 2.4. Characteristic magnetization B-H curve of Somaloy700 material ... 19
Figure 2.5. Temperature effects in the relation conductivity vs. resistivity from 20 to 100°C of the coil copper ... 23
Figure 2.6. a) Electromagnet cross-section, b) Electromagnet equivalent circuit ... 25
Figure 2.7. Specifications of the electromagnetic coil ... 28
Figure 2.8. Relation between Current (A) and Position (mm) in Magnetic Levitation System ... 32
Figure 2.9. The behavior of the electromagnetic force as function of the position and current ... 33
Figure 2.10. Graphic of the electromagnetic force... 34
Figure 2.11. Electromagnetic force FMM using a 4th order polynomial ... 35
Figure 2.12. Setting the sphere and hall effect sensors before tests of current vs distance... 35
Figure 2.13. FMM-2D Model for magnetic flux density distribution... 36
Figure 2.14. FMM-2D Model for magnetic flux density distribution in absence of the ball ... 37
Figure 2.15. 1-DOF RL circuit for the magnetic levitation system ... 38
Figure 3.1. Illustration of DC magnetic levitation RL circuit ... 42
Figure 3.2. Free body diagram of DC Magnetic Levitation System ... 44
Figure 3.3. Effect of temperature on the magnetic field strength ... 45
Figure 3.4. A 3D Plot concern to the measures which act on the Magnetic Levitation System ... 46
Figure 3.5. Simulink model for comparison of the linear and non-linear response ... 53
Figure 3.6. Non-Linear response... 54
Figure 3.7. Linear response ... 54
Figure 3.8. Poles of the Transfer Function... 55
Figure 3.9. Block diagram for various system signals, (2) The relation between PWM and average current. (1) The relation between controller output and average voltage... 56
Figure 3.10. Block diagram representing the magnetic levitation system ... 57

Figure 3.11. Graph of experimental data from maglev system at room temperature (25°C) 60
Figure 3.12. Graph of experimental data from maglev system at room temperature (100°C) 60
Figure 3.13. Graph of ANSYS Maxwell simulated data at 25°C 61
Figure 3.14. Graph of ANSYS Maxwell simulated data at 100°C 61
Figure 3.15. 3D-FEA model of core magnetization 62
Figure 3.16. Hall effect sensors on Maglev system 63
Figure 3.17. Current Transducer LTS 6-NP 63
Figure 3.18. Diagram of amplifier circuit for hall effect sensor 64
Figure 3.19. PCB amplifier circuit module of hall effect sensor 64
Figure 3.20. Scheme of the OPAM LM358 for thermocouple signal 65
Figure 3.21. PCB circuit of the OPAM LM358 for thermocouple 65
Figure 3.22. Micrometer and movement mechanism 66
Figure 3.23. Data obtained in the response test at 0.02 HZ frequency and 10mm airgap 66
Figure 3.24. Configuration of hall effect and thermocouple sensors on maglev system 67
Figure 3.25. Temperature effects over the magnetic strength of the maglev system 69
Figure 3.26. Magnetic Flux behavior according to temperature, current and tesla parameters 70
Figure 3.27. Variation of magnetic flux vs distance 71
Figure 3.28. a) Magnetic Flux Close up laid with 4A and 4mm airgap, b) The temperature and power consumption effect on maglev system 71
Figure 3.29. a) Magnetic Flux laid close up with 5A and 4mm airgap, b) Temperature increases and power drop on the maglev system 72
Figure 3.30. Hall effect sensor HES_A0 and HES_A1 responses at different frequencies 73
Figure 3.31. Top view of the MOSFET H-Bridge High-Power Driver 30v15 73
Figure 3.32. a) Alternate pneumatic system, work frequency interval at 1-18hz, b) Main pneumatic components 74
Figure 3.33. a) Data acquisition card (DAQ), b) Microcircuit to commute the electropneumatic valve 75
Figure 3.34. Frequency test in 6hz and 8hz data obtained by the alternate pneumatic system 75
Figure 3.35. Servomotor mechanism attached to the maglev system to generate the up/down movement 76
Figure 3.36. Experimental results to different frequencies for the downward-upward sphere movement using HES to capture the magnetic flux variation related to the movement 78
Figure 3.37. a) Experimental data of magnetic flux, b) Hysteresis curve of the magnetic levitation system 79
Figure 3.38. HES signal for sinusoidal ball position 79
Figure 3.39. Setting Maglev system for control test 80
Figure 4.1. Scheme of the magnetic levitation system 81
Figure 4.2. Simulink PID diagram of maglev system 83
Figure 4.3. Region of stability in the space of PID constants 84
Figure 4.4. System response for a 5 mm step input 84

Figure 4.5. Industrial GoogolTech interface 85
Figure 4.6. Control Block Diagram of maglev system 86
Figure 4.7. Basic fuzzy logic controller (FLC) configuration................................ 86
Figure 4.8. Definition of input - output variables for Fuzzy Logic Controller (FLC) 88
Figure 4.9. Airgap between electromagnet and HES 88
Figure 4.10. FLC membership functions of FLC 89
Figure 4.11. FLC Fuzzy Rule Base Analysis surface 91
Figure 5.1. Bode diagram of hall effect sensor 92
Figure 5.2. Magnetic flux vs. distance obtained in the maglev system................... 93
Figure 5.3. HES filtered signal using mid-pass filter 94
Figure 5.4. The equilibrium points and corresponding required current 94
Figure 5.5. Real time response and performance of PID controller for position, Velocity and PWM signal 95
Figure 5.6. Picture of the ball controlled by PID controller.................................... 96
Figure 5.7. Real time response and performance of FLC for position, Velocity and PWM signal 96
Figure 5.8. Levitation of the steel ball using a FLC... 97
Figure A. 1. Parameters for maglev system using Matlab software 107

LIST OF TABLES

Table 1.1. Basic quantities involved in electrical and magnetic phenomena............... 6
Table 2.1. HES Technical Properties 17
Table 2.2. Somaloy700 Magnetic Properties 19
Table 2.3. Data for magnetizing curve (B-H) of Somaloy700.................................. 20
Table 2.4. Resistivity and Conductivity of Copper at 20°C...................................... 21
Table 2.5. Magnetic Properties for Stainless Steel Series 400................................... 23
Table 2.6. FMM simulation airgap outputs for the steel sphere 36
Table 2.7. FMM simulation airgap outputs without steel sphere............................... 37
Table 3.1. Parameters considering for trials on Maglev System................................ 44
Table 3.2. Initial parameters of system identification... 51
Table 3.3. Parameters of magnetic levitation system... 52
Table 3.4. Experimental data at room temperature (25°C) 59
Table 3.5. Experimental data at room temperature (100°C) 59
Table 3.6. ANSYS Maxwell simulated data at 25°C 60
Table 3.7. ANSYS Maxwell simulated data at 100°C 61
Table 3.8. Data obtained through the sensors located in the maglev system............. 67
Table 3.9. Measurement result at 4A and 4mm from the electromagnet center 70
Table 4.1. Linguistic variables set for FLC 90
Table 4.2. FLC rule base... 91
Table 5.1. Definition of basic performance indices 97
Table 5.2. Comparison of performance indices of the PID and FLC controllers 98

LIST OF SYMBOLS AND ABBREVIATIONS

B	: Density of Magnetic field, (V s/m2), (T)
C	: Magnetic Constant
E	: Energy, (J)
F	: Force, (N)
g	: Gravity force, (m/s^2)
H	: Magnetic field strength (A/m)
i	: Current, (Amperes)
L	: Inductance, (H)
Q	: Electric charge (C)
R	: Resistance, (Ohms)
T	: Tesla, it is equivalent to one weber per meter squared ($1Wb \cdot m^{-2}$)
v	: Voltage, (v)
Wb	: A weber equals a volt-second (1 Wb = 1 Vs, 1Tm2)
x	: Object to levitate position, (mm)
Ø	: Magnetic Flux, (wb)
µ	: Relative permeability of the air
μ_r	: Relative permeability
ρ	: Charge density, (C/m3)
σ	: Electrical conductivity
$\dot{x}$	: Derivative of x with respect to time

Abbreviations

AC	: Alternative Current
ADC	: Analog-Digital Converter
DAQ	: Data Acquisition
DOF	: Degrees of Freedom
EC	: Eddy Current
FEM	: Electromagnetic Force
FMM	: Magnetomotive Force
HES	: Hall Effect Sensor
IACS	: International Annealed Copper Standard
IC	: Integrated Circuit
M.K.S.	: Meter Kilogram Second System
MagLev	: Magnetic Levitation
MIMO	: Multiple Input Multiple Output
OPAM	: Operational Amplifier
PCB	: Printed Circuit Board

PWM	: Pulse with Modulation
RL	: Resistive-Inductive circuit
SE	: State Equations
SIP	: Single In Line Package
SISO	: Single Input Single Output
SMC	: Soft Magnetic Composite
Vs	: Voltage in the Surface

MANYETIK LEVITASYON SISTEMININ PID VE FUZZY KONTROLÜ

ÖZET

Bu çalışmada, bir 1 DOF manyetik levitasyon sistemi, hall effect, lazer ve uzaklık sensörleri kullanılarak, manyetik levitasyon sistemini kontrol amacıyla maliyet düşürücü bir sensör geliştirilerek tasarlanmıştır. Buna ek olarak, akış ve sıcaklık arasındaki ilişki de Manyetik Levitasyon Sistemi'nde detaylı biçimde incelenmiştir. Yüksek manyetik akı performansı (B-H) elde etmek için, Somaloy700 denilen Yumuşak Manyeyik Bileşim, elektromanyetik çekirdek için Manyetik Levitasyon Sistemi'nde özel malzeme olarak kullanılmıştır. 1 DOF manyetik levitasyon sisteminin kontrolünü sağlamak için, Oransal İntegral Türev kontrolör (PID) ve Bulanık Mantık Kontrolör (FLC) olmak üzere iki farklı kontrolör uygulanmıştır. Beklendiği gibi, Bulanık Mantık Kontrolör, PID kontrolörden daha iyi sonuçlar verir.

Keywords: Bulanık Mantık Kontrolü FLC, Hall Effect Sensörü, Manyetik Levitasyonu, PID Kontrolü, Somaloy700.

PID AND FUZZY CONTROL OF MAGNETIC LEVITATION SYSTEM

ABSTRACT

In this study, 1 DOF magnetic levitation system is designed and manufactured utilizing hall effect, laser and distance sensors with the aim to develop a cost-effective sensor to control the magnetic levitation system. Moreover, the relationship between flux and temperature is examined in detail in the magnetic levitation system. In order to obtain high flux performance (B-H), Somaloy700 called Soft Magnetic Composites (SMCs) is used as special material in the composition for the electromagnetic core in the magnetic levitation system. Therefore, the laser sensor, distance and hall effect sensors are utilized in the experimental setup. To provide control of the 1 DOF magnetic levitation system it was implemented two different controllers, the Proportional Integral Derivative controller (PID) and Fuzzy Logic Controller (FLC). As expected, the Fuzzy Logic Controller produces better results than the PID controller.

Keywords: Fuzzy Logic Control FLC, Hall Effect Sensor, Magnetic Levitation, PID Control, Somaloy700.

INTRODUCTION

Magnetic levitation is a technology by which an object is suspended in the air with no more support than a magnetic field, for more than 100 years the first magnetic levitation trains appeared and the beginning of the maglev system era was introduced, but the scope of magnetic levitation not only stayed in maglev trains but also extended to more uses, from the point of view of engineering science they can be described as transportation, environmental, aerospace, military, nuclear, biomedical and chemical engineering.

The use of magnetic fields is a method of actuation which has been considered for over four decades. The initial applications of magnetic actuation were in solenoid actuators, magnetic cranes and electrical switches. About three decades ago, the first magnetic levitation train was proposed and initiated as a high-speed mass transportation vehicle. Various experimental and a large number of theoretical studies have been done in Japan, Germany and the United States and have resulted in interesting outcomes. After several years, changing market requirements have forced manufacturers to develop new technologies of actuation. In the high-tech industry (which increasingly relies on micro-assembly) product requirements drive manufacturers to change their production strategies [1].

Keeping objects suspended without mechanical contact by means of a magnetic field is known as magnetic levitation. At present; the widespread use of this phenomenon is observed in magnetic levitation trains; designs of roller coasters with magnetic levitation or the propulsion of spaceships by means of this same phenomenon; where the design of systems and controllers for this type of systems require high precision; such uses are observed in [2-5]. To maintain levitation in a system the use of a closed-loop is propitious. One of the concepts used in control engineering is the concept of feedback. Feedback is a principle by means of which the information coming from a sensor (output from the plant) is contrasted with respect to a reference value with the aim of giving order to an actuator to execute a corrective action [6].

The magnetic levitation system can be considered as a system of multiple outputs; because it is necessary to know variables such as position, speed of the object to be levitate and electrical current to the moment of generate a magnetic field through an electromagnet; and with an input signal that can be the electrical potential applied to the electromagnet. Magnetic levitation system is a non-linear system, due to the continuous changes of parameters, it implies that to utilize linear control methods it is necessary to linearize the system around of point of work (set point), whereas non-linear control methods can work directly with non-linear systems [7-8].

To make a good controller it is necessary to have a good knowledge of the system, when making a mathematical model, mainly in a non-linear system, a high degree of uncertainly is obtained because it is complex to model all the disturbances that affect the system [9-10]. From the matrix formulation, it is feasible to apply the complete state feedback and state estimation methods as a method of solving the stability problem and follow it in a linear way as Acedo mentioned it in [11].

We present a nonlinear control by linearization and the comparison with a traditional PID and a Fuzzy Logic Controller (FLC), throwing as conclusion that the FLC is more efficient, in the present work a comparison of two often used controllers PID and FLC is developed. Linear control was chosen because it is the fundamental basis for robust control in addition to its widespread industrial use due to its low computational cost and good performance. Many of these products need to be manufactured under highly controlled environments. As of recently, magnetic actuation has been shown to be a possible solution for high performance actuators, delivering ultra-fine positional control. The studies carried out in this thesis are examined under 6 main headings.

In Chapter 1, general information about electromagnetic principals and basic electromagnetic theories are given.

In Chapter 2, information concerning the description of the plant and description of the several models required in the modelling for the dynamic of the Force in a Magnetic Levitation System are provided.

In Chapter 3, the identification of the System, the mathematical modelling for the System, the linearization and the equilibrium points, the start-up of the maglev plant, and the execution of tests and preliminary samplings to levitate ferromagnetic objects are presented.

In Chapter 4, accuracy testing the designed controllers using an algorithm of a Proportional-Integral-Derivative (PID) and Fuzzy Logic Control (FLC) which is conducted to find an optimal response is performed.

In Chapter 5, all results obtained within the scope of this thesis are summarized and the comparison indices as result are obtained.

In Chapter 6, the final conclusions about of the use of Somaloy700, hall effect sensor are speech in detail.

1. FRAMEWORK

In this section, some basic characteristics about of electromagnetism are presented, which will be important at magnetic levitation system project. Comprehension the equations that involves the force between the magnet and the metal, magnetic induction, intensity magnetic and the correct selection of parameters and proper management task, those are some questions that to do necessary this section.

1.1. Electromagnetic Principles

Magnetic flux: The magnetic flux is the product of the magnetic induction or magnetic flux density given by polar surface of the magnet. Therefore, the unit of magnetic flux is equal to the product of the unit of magnetic induction and the unit of area. The magnetic flux of a magnet expresses the total value of its magnetic effect. The Weber is the Magnetic Flux unit Wb, where 1wb = VS and [Ø] = VS

$$\emptyset = B.A \tag{1.1}$$

Magnetic Permeability: Magnetic permeability is the ability of a substance or medium to pass through a magnetic field. This is given by the relationship between the magnetic induction present and the magnetic field strength within the material. Thus, it can be considered as the degree of magnetization of a material in response to a magnetic field, thus defining the absolute permeability.

$$\mu = \frac{B}{H} \tag{1.2}$$

Where B is the induction of the magnetic field and H is the intensity of the magnetic field.

Electromagnetic: If a ferromagnetic material is placed in a solenoid and a current is circulated through it, its magnetic field increases considerably because the ferromagnetic material is transformed to a magnet. The resulting magnetic field is a result of the coil turns and the material type; it can be hundreds of thousands of times bigger than the original field due only to the current. This type of solenoid with a ferromagnetic nucleus is known as electromagnet.

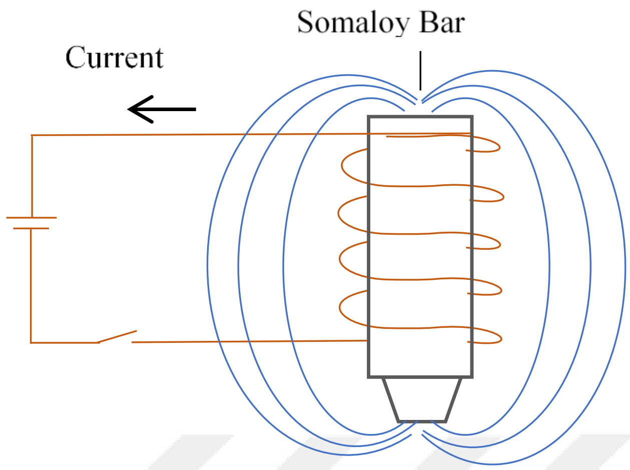

Figure 1.1. Magnetizing in a Somaloy700 ferrite bar

The force of the electromagnet depends on 4 factors:

- The material of the core
- The dimensions and shape of the core
- The number of turns in the coil
- The value of the current on the coil

In general, the magnet will become stronger if:

- The material of the nucleus has a higher permeability
- The material of nucleus has the biggest section slide area and more short longitude to the flux lines. this will permit a lower reluctance.
- The number of turns and the current are high. This will result in a larger magnetomotive force value.

Maxwell’s equations give a comprehensive understanding on which the fundamentals of electromagnetic phenomena are based. The description of electromagnetic phenomena is relatively simple when compared with various other fields of physical sciences and technology [12], since all of the field’s relevant equations can be written as a single group of equations. The basic quantities involved in the phenomena are the following five vector quantities and one scalar quantity [13] (see Table 1.1).

In electrical engineering theory, the other laws, which were initially discovered empirically and then later introduced in writing, can be derived from the following fundamental laws presented in complete form by Maxwell. To be independent of the shape or position of the area under observation, these laws are presented as differential equations.

Table 1.1. Basic quantities involved in electrical and magnetic phenomena

Quantity	Symbol	Unit
Electric field strength	E	[V/m]
Magnetic field strength	H	[A/m]
Electric flux density	D	[C/m2]
Magnetic flux density	B	[V s/m2] [T]
Current density	J	[A/m2]
Electric charge density, dQ/dV	ρ	[C/m3]

A current flowing from an observation point reduces the charge of the point. This law of conservation of charge can be given as a divergence equation.

$$\nabla . J = -\frac{\partial \rho}{\partial t} \tag{1.3}$$

Which is known as the continuity equation of the electric current. Maxwell's actual equations are written in differential form like so:

$$\nabla \times E = -\frac{\partial B}{\partial t} \tag{1.4}$$

$$\nabla \times H = J + \frac{\partial D}{\partial t} \tag{1.5}$$

$$\nabla . D = \rho \tag{1.6}$$

$$\nabla . B = 0 \tag{1.7}$$

The Relation (1.4) of an electric field is Faraday's induction law that describes how changing magnetic flux creates an electric field around it. The Relation (1.5) for magnetic field strength describes the situation where a changing electric flux and current produce magnetic field strength around them. This is Ampere's law. Ampere's law also yields a law for conservation of charge Equation (1.3) by a continuity

Equation (1.5), since the divergence of the curl is identically zero. In some textbooks, the curl operation may also be expressed as ∇×E = curl, E = rot.

A current flowing from an observation point reduces the charge of the point. This law of conservation of charge can be given as a continuity Equation (1.6) of an electric flux. This law is also known as Gauss's law for electric fields. Magnetic flux, however, is always a circulating flux with no starting or end point. This characteristic is described by the continuity of the magnetic flux density in Equation (1.7). This is Gauss's law for magnetic fields. The divergence operation may also be expressed as ∇.D = div D. Maxwell's equations often prove useful in their integral form; Faraday's induction law.

$$\oint_l E\,.dl = \frac{d}{dt}\int_s B.d\mathbf{S} = -\frac{d\Phi}{dt} \quad (1.8)$$

States that the change of a magnetic flux Φ penetrating an open surface S is equal to a negative line integral of the electric field strength along the line l around the surface. Mathematically, an element of the surface S is expressed by a differential operator dS perpendicular to the surface. The contour line l of the surface is expressed by a differential vector dl parallel to the line.

According to Faraday's law, the changing magnetic flux affects the ferromagnetic ball and, induces an electrical field (and hence current flow) in the object which allows it to levitate [14].

Faraday's law together with Ampere's law are extremely important in electrical machine design. At its simplest, the equation can be employed to determine the voltages induced in the windings of an electrical machine. The equation is also necessary for instance in the determination of losses caused by eddy currents in a magnetic circuit, and when determining the skin effect in copper. Figure 1.2 illustrates Faraday's law. There is a flux Φ penetrating through a surface S, which is surrounded by the line l. In other words, Ampere's Law means that the magnetic flux density integrated around a closed contour equals the net current through the surface bounded by the contour, Faraday's Law show the mechanisms by which a lift force acts in an electrodynamic levitation system.

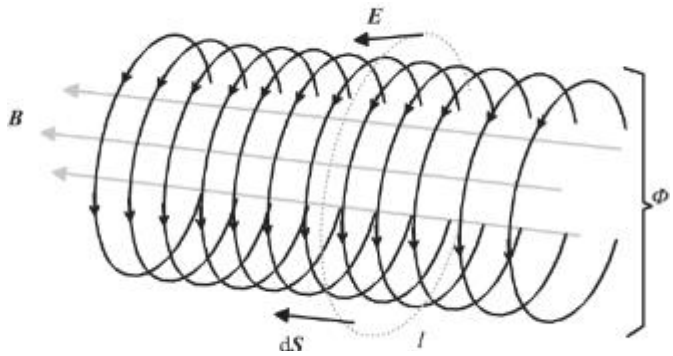

Figure 1.2. Faraday's Induction law

A typical surface S, defined by a closed line l, is penetrated by a magnetic flux Φ with a density B. A change in flux density creates an electric current strength E. The circles illustrate the behavior of E. dS is a vector perpendicular to the surface S.

1.2. Elementary Theory of Electromagnetic

In traditional electrical engineering science, at the macroscopic level all electrical phenomena can be interpreted as being evolved from the forces acting between stationary or moving 'point' charges (electrons and protons).

1.2.1. Maxwell's equations

In fact, this phenomenon can be interpreted from four concise equations, commonly referred to as Maxwell's equations. These equations show that magnetic energy storage is dominant (as compared to energy stored in the electrical field) and wave phenomena are small enough to be ignored [14]. Those equations are sufficient to describe all known macroscopic field interactions in electrical science and are described in a minimalist mathematical form:

Flux D = charge enclosed
Flux B = 0
Circ H = I + rate of change of electric flux (1.9)
Circ E = rate of change of magnetic flux

At first sight these equations may seem perplexing and perhaps incomprehensible, but once the symbols and the terminology are established, and the historical development is explained, the obscurity should disappear. To this end, the following symbol identifications and further definitions are appropriate.

- Electric charge (Q), which may be either positive or negative, is conserved in all electrical operations.
- The electric current through any surface is the rate at which charge passes through the surface: that is I = ρvA, where ρ is the charge density in C/m3, v is the velocity of moving charge in m/s, while A is the area in m2 through which charge is passing. The unite of I are C/s, which is an Ampere in the metre.kilogram.second (m.k.s.) system.
- The electric current through any closed surface is the product of -1 and the rate of change of the charge enclosed within the surface I = -dQ/dt. This is a general statement of Kirchoff's law, which for circuit engineers generally appears in the more familiar form ΣI = 0 at a network junction.

In Equation (1.9) the vector quantities E and B (denoted by bold type) are the fundamental electric and magnetic field quantities in electromagnetism, while D and H are auxiliary fields. Materials embedded within electrical systems are defined electrically by three parameters, namely conductivity (σ, mhos/m), permittivity (ε, F/m) and permeability (μ, H/m).

1.2.2. Flux and circulation

The flux and circulation integrals embedded in Equation (1.9) can be further defined in a relatively non-mathematical form, if averaging (in essence integration) can be considered to be a process that is not excessively remote from common sense [15]. Consequently, we have for an arbitrary vector A:

$$\text{Flux } A = A_n \times dS \tag{1.10}$$

The introduction of vector algebra in (1.10) permits a 'short hand' representation of the process. For an infinitesimally small area (dS), which can be considered to be directionally aligned with a unit vector n normal to its surface, then a simple dot product gives:

$$\text{Flux } A = A \cdot dS \tag{1.11}$$

1.3. Determination of Losses

It is inevitable that in the mechanisms and apparatuses of daily consumption do not present an efficiency of 100% [16], reason given to its operating principles and materials of construction [17], in this sense we can find own characteristics such as driver losses [18], skin and eddy losses [19]. The losses that can occur in a material are:

Iron losses: Iron loss is caused by the alternating flux in the core and consists of hysteresis and eddy current losses.

Hysteresis Loss: Hysteresis loss is associated with the phenomena of hysteresis and is an expression of the fact that when a ferromagnetic material is involved, not all the energy of the magnetic field is returned to the circuit when mmf is removed the remaining energy is known as hysteresis loss. The core of an electromagnet is subject to an alternating magnetizing force and for each cycle of fmm a hysteresis loop is traced out. A great deal of information can be learned about the magnetic properties of a material by studying its hysteresis loop [20]. A hysteresis loop shows the relationship between the induced magnetic flux density B and the magnetizing force H. It is often referred to as the B - H curve. Below, Figure 1.3 shows an example of a hysteresis loop [6].

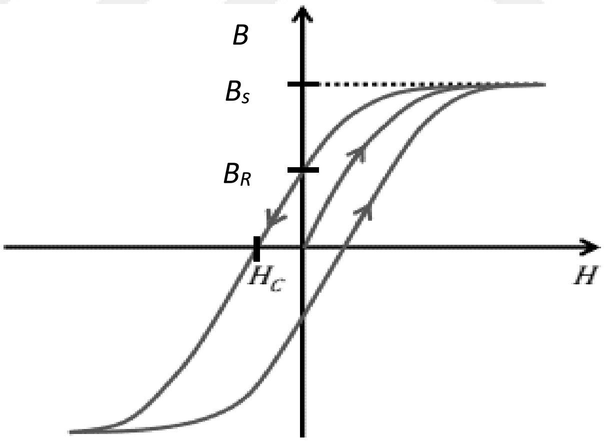

Figure 1.3. A general B-H curve of Hysteresis

1.3.1. Magnetic hysteresis losses

The lagging effects on a ferromagnetic material due to the reversal of magnetization core are explained as such; When ferromagnetic materials are placed within a coil of wire carrying an electric current, the magnetizing field, or magnetic field strength H caused by the current forces some or all of the atomic magnets in the material to align with the field. The net effect of this alignment is an increase in the total magnetic field, or magnetic flux density B. The aligning process does not occur simultaneously or in step with the magnetizing field but lags behind it.

If the intensity of the magnetizing field is gradually increased, the magnetic flux density B rises to a maximum, or saturation value at which all of the atomic magnets are aligned in the same direction. When the magnetizing field is diminished, the magnetic flux density decreases, again lagging behind the change in field strength H In fact, when H has decreased to zero, B still has a positive value called the remanence, residual induction, or retentivity, which has a high value for permanent magnets. B itself does not become zero until H has reached a negative value. The value of H for which B is zero is called the coercive force. A further increase in H (in the negative direction) causes the flux density to reverse and finally to reach saturation again, when all the atomic magnets are completely aligned in the opposite direction. The cycle may be continued so that the graph of the flux density lagging behind the field strength appears as a complete loop, known as a hysteresis loop. The energy lost as heat (which is known as the hysteresis loss) in reversing the magnetization of the material is proportional to the area of the hysteresis loop. Therefore, cores of transformers are made of materials with narrow hysteresis loops so that little energy will be wasted in the form of heat [21].

The soft magnetic compounds (SMCs) with their unique magnetic properties, opens a completely new applications field [22], as the case of Somaloy700 used for the magnetic levitation system, this being composed of pure iron particles coated with an insulating layer provides a reduction of eddy current losses, this represents one of the advantages compared to traditional steel plates, in addition, these materials can adopt any kind of geometry or shape that steel plates cannot because they are limited to 2D-shape. In Somaloy700 the losses due to hysteresis are lower than those with steel plates, because they present a small amount of ferromagnetic iron in their composition. Figure 1.4, shows how narrow is the hysteresis curve in somaloy700, this is very appropriate when the electromagnet is magnetized and demagnetized by the current flow.

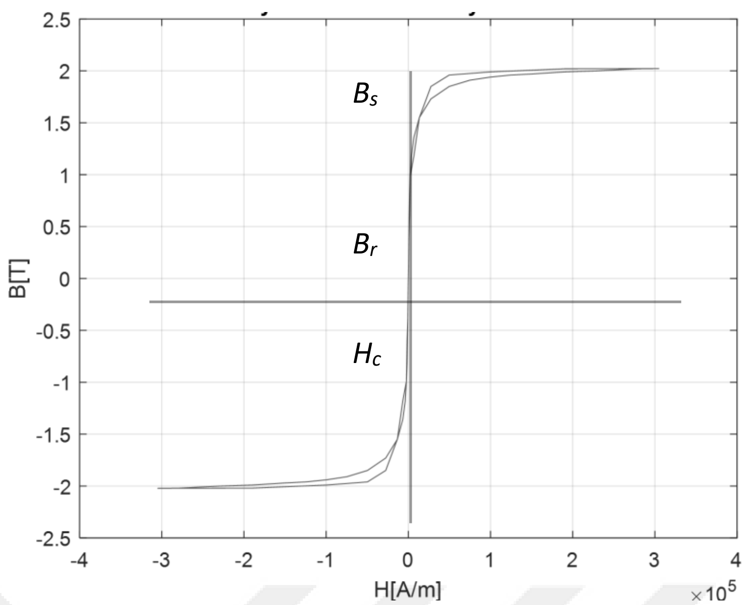

Figure 1.4. B - H hysteresis curve of Somaloy700 material

When we analyze the magnetic and electrical parameters, we can see the moment of hysteresis as a function of the current that flows through the plant and the magnetization of it, we find that the core with N = 1090 turns, with the value of the reluctance and a maximum current of 4 A as maximum current which gradually is increases in steps of 0.1A.

According to formula (1.12) taking the value of reluctance, the current and the number of turns of the magnetic model, we can find the value of the magnetic intensity H.

$$\varphi_T = \frac{Ni}{R_{eq}} \tag{1.12}$$

In Figure 1.5 the coil current has been set to 4 A, because above this value, the electromagnet enters in a state of saturation, this state produces overheats in the core of the magnetic levitation system, the force in the magnetic flux decreases and damages to the magnetic permeability properties in the electromagnetic, under the tests carried out, it was determined that around 4 A is the ideal current where the magnetic flux and the temperature of the system can be maintained constants.

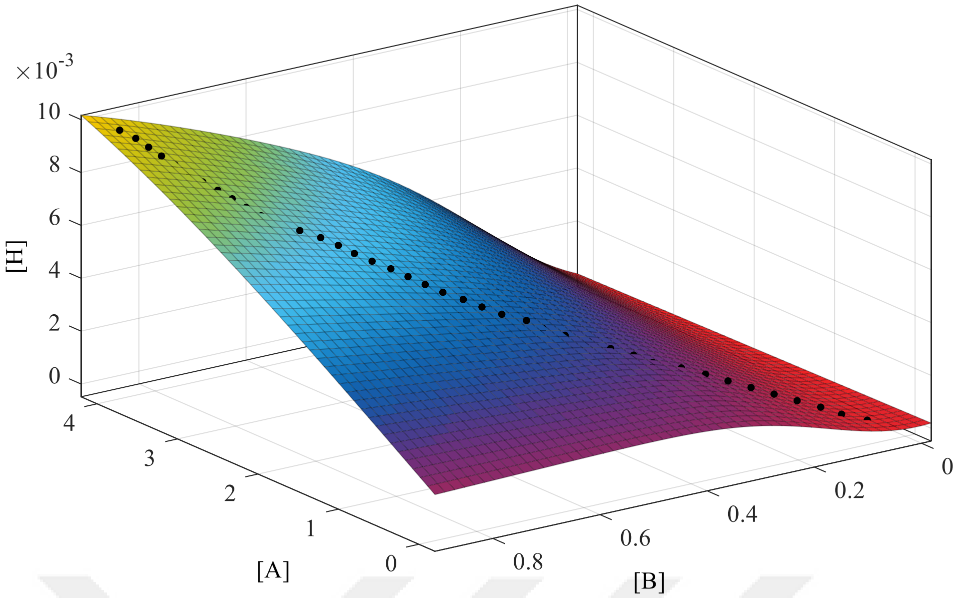

Figure 1.5. Somaloy700 3D representation of the magnetization curve in the maglev system

2. MAGNETIC LEVITATION SYSTEM DESCRIPTION

In this chapter it is discussed in detail how the magnetic levitation system is constituted, it is important to emphasize that Somaloy700 is the main component for the constitution of the electromagnetic core.

2.1. Core of Somaloy700

The actual project of magnetic levitation utilizes soft magnetic composite (SMC) in the magnetic core of the levitation system, this material is called Somaloy700 and is produced by Hgans AB Company. The metal powder is produced utilizing atomization techniques, a stream of molten metal is atomized by an inert gas or high-pressure water which leads to the formation of small droplets of molten metal which subsequently solidify resulting in fine powder particles [23]. It is the most innovative aspect and the most differentiating feature compared to other magnetic levitation systems. Somlaoy700 is highly permeable composed of surface-insulated iron powder particles, which in one single step can be compacted to form components with complex shapes, tight tolerances [24], high permeability and capacity to handle losses due to very low hysteresis, in comparison to other systems where, common iron bars or steel plates are used in its cores.

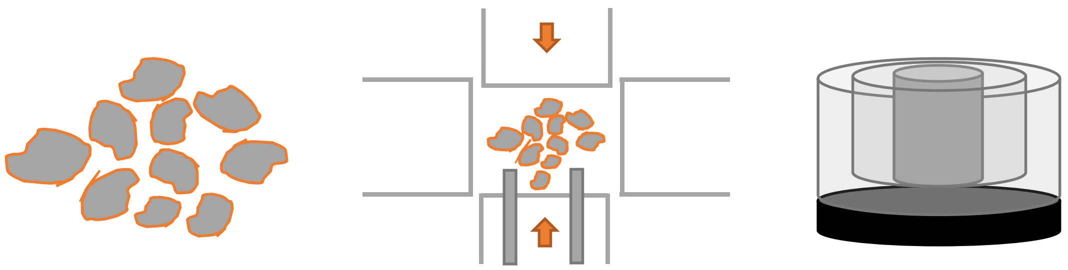

(a) (b) (c)

Figure 2.1. Somaloy 700 from powder to 3D Special Shape a) Nano-coated Fe particles, b) Pressing and thermal processing, c) 3D shape

The core as shown in Figure 2.1 means that soft iron dust particles are composed, which improves the strength of the magnetic field produced by the electromagnet and will allow to reduce problems caused by width hysteresis. Its responsibility is to generate a focal magnetic pole within the work area of the system. Longitudinally the core is an E-shaped component designed to increase the concentration of magnetic flux within the airgap.

2.2. Magnetic Levitation System Description

In the maglev levitation system, a ball of ferromagnetic material and mass m is drawn upward by a magnetic force generated through the electromagnet, since the ball has a weight, there is also a gravitational force that pulls it down. In this way, when a balance occurs between both the magnetic force and the gravitational force are equal in magnitude the ferromagnetic ball is held in suspension state in the air. Since the position of the sphere is never the same, as the system is easily destabilized, the magnetic force has to be controlled. This is achieved by using a sensor which is continuously observing the position of the ball and a driver which sends a control signal to the power stage according to the error signal, this signal is the difference between the desired levitation position and the sensed position.

The control signal reaches the power stage and an amplified control signal is produced which regulates the amount of current flowing through the electromagnet; With this the magnetic force necessary for the ball reach the desired position is applied.

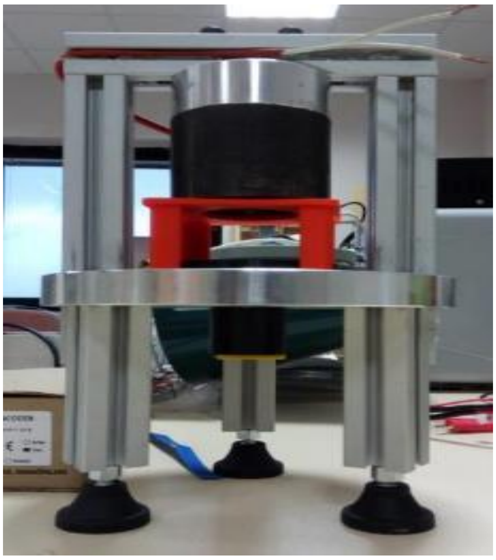

Figure 2.2. Plant model of magnetic levitation system

The maglev device consists of the following elements principally, a set of sensors, the electromagnet, and the driver, in Figure 2.2 a schematic representation of the plant model of the maglev system is shown.

Mainly the maglev system consists of three stages, each of them is vital for the linearization process of the magnetic levitation system and for the stabilization of the ball. In the stages which make up the magnetic levitation system are described, moreover, these stages can be classified as follow:

- Sensing stage: It is the stage where the continuous observing of the position of the ball is carried out by the set of hall effect sensors and the laser sensor, the output voltage signal generated by this stage is transmitted to the controllers' stage.

- Controller’s stage: This stage defines the controllers that are used for the magnetic levitation system; an integral and derivative proportional controller PID and a fuzzy logic controller FLC. The voltage signal coming from the sensing stage is used as the output error value of the magnetic levitation system, a closed loop in the system uses the output signal as feedback and to verify with the setpoint set. The controllers take the difference of the signal setpoint and the output signal to adjust the parameters of Kp, Ki and Kd in the case of the PID controller, and the linguistic variables and base rules in the case of FLC.

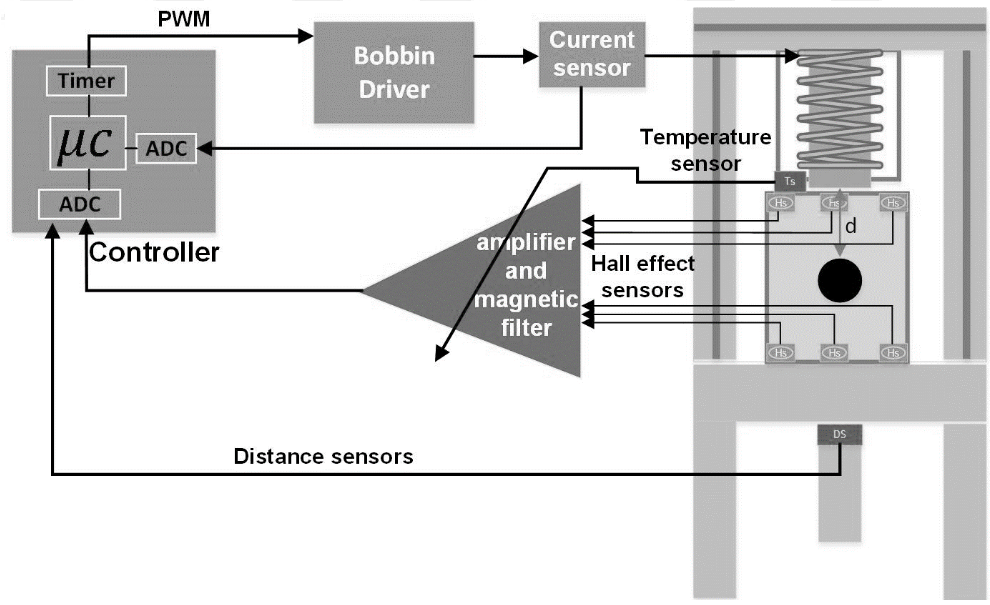

Figure 2.3. Stages that conform the magnetic levitation system.

Power stage: The power stage consists of a physical driver which acts as a separating bridge between the control voltage signal coming from the controllers’ stage and the current flow that feeds the electromagnet, this driver interacts directly with the electromagnet by varying the current flow according to the PWM signal coming from the controllers' stage. The pulse width modulation PWM allows to the magnetic levitation system to have adequate performance in the duty cycle for the average voltage of the coil.

2.2.1. Hall effect sensor

The CYSJ362A linear hall effect sensors reference is used in the magnetic levitation system, where the maximum sensitivity is given between 3.1-4.1 (mV/mT), for a measuring range of 3 T.

The series of this hall-effect is an ion-implanted magnetic field sensor made of monocrystal gallium arsenide (GaAs) semiconductor material group III-V using ion-implanted technology. It can convert a magnetic flux density signal linearly into voltage output. According to the data sheet, below are key sensor parameters.

Characteristics:
- High Linearity
- Superior Temperature Stability
- Miniature Package

Table 2.1. HES Technical Properties

Characteristic	Measure
Input/output Resistance	1000 ~ 1500 kΩ/1800 ~ 3000kΩ
Max. Supply	12 V
Linearity	2%
Max. Sensitivity	3.1 ~ 4.1 mV/mT
Measuring range	3 T
Package/Size	SIP/2.7x2.35x0.95 mm
Temperature range	-40°C ~ +125 °C

2.2.2. Electromagnet

In the magnetic levitation system, the electromagnet core is formed by a soft magnetic component (SMC) material called somaloy700, this offers several advantages over cores formed with steel sheets, for example, isotropic magnetic properties, very low losses due to eddy current, high magnetic permeability. Moreover, the electromagnet is responsible for generating the electromagnetic force that allows the levitation of the ball by adjusting the current that passes through the electromagnet.

2.3. Description of the Magnetic Levitation System

The stability of the vertical suspension of the steel sphere in the magnetic levitation system can be tied to the functional dependence of the terminal inductance and using energy methods to calculate the levitation force. An electrical model to evaluate the driving of the impedance point at the coil R_{coil} is the coil resistance in the free space due to the finite electrical conductivity in the wire, L(x) is the inductance, R(x) is the resistance due to the eddy losses current in the lifted ball.

When the ball is being attracted near the coil, R(x) increases and the terminal inductance at the coil decreases due to the induced currents. It is important to note that R_{coil} has a functional dependent of the operation frequency, due to the entrance of magnetic field into sphere. A magnetic field that affects on the ball, induces eddy currents over the same object too. These perturbations increase exponentially, this depends in the same way in the distance of the levitated object in front the coil. The variation in the inductance between those two terminals depends on variations of position, composition and dimensions of the ball too [25].

$$L(x) = L_0 + L_r e^{-\frac{x}{a}} \tag{2.1}$$

The term L_0 is the terminal inductance in the coil when this is away from the sphere $x = \infty$. the term L_r is the final inductance which decreases when the coil is close to the sphere $x = 0$, due to the eddy currents induced and a is positive constant [26]. The inductance is a function of the position x of the bobbin above the sphere.

The magnetic co-energy of the system is a function of the coil current i and the separation x:

$$W(i,x) = \frac{1}{2} L(x) i^2 \tag{2.2}$$

The magnetomotive force that acts on the sphere is given by:

$$F_{em} = \frac{\partial W}{\partial x} = \frac{L_r}{2a} i^2 e^{-\frac{x}{a}} \tag{2.3}$$

2.4. Core Permeability

Before continuing, we need to define some concepts about permeability and relative permeability for the elements used in the magnetic system, as such elements are the core of the magnetic system and the steel sphere.

Somaloy® 700 is the material by which the core of the magnetic system is formed, according to [24]. In following Table 2.2 the magnetic characteristics of Somaloy 700 are shown.

Table 2.2. Somaloy700 Magnetic Properties

Magnetic properties	Unit	Measure	Standards
@4000A/m	[T]	1.18	IEC 60404-4
B@10000A/m	[T]	1.45	IEC 60404-4
H_c	[A/m]	227	IEC 60404-4
μ_r -max	-	540	IEC 60404-4

The magnetic flux increases notably by magnetic induction in the iron core. The relationship between the flow deficit (B) and the field strength (H) is shown in Table 2.3, where we can see the permeability (μ) that Somaloy700 presents, which indicates that it possesses a high facility of magnetization.

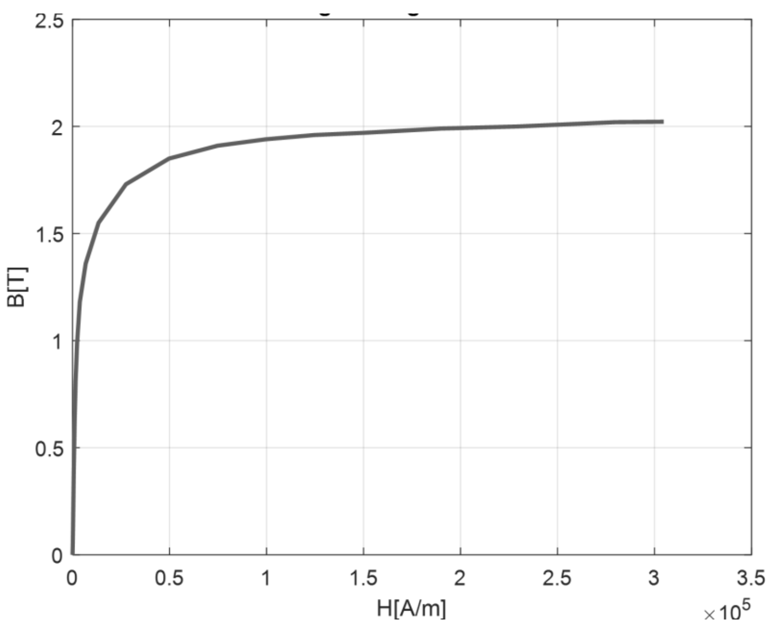

Figure 2.4. Characteristic magnetization B-H curve of Somaloy700 material

The magnetization curve can also be expressed in terms of permeability of the material used, it is not constant. The state reached when any subsequent increase in an external magnetization field H occurs does not cause an increase in the magnetization of the material. Table 2.3 below shows the values of the magnetization curve for Somaloy700.

Table 2.3. Data for magnetizing curve (B-H) of Somaloy700

H[A/m]	μ0M[T]	B[T]
0	0.00	0.00
84	0.03	0.03
146	0.06	0.06
257	0.13	0.13
358	0.20	0.20
632	0.39	0.39
1063	0.61	0.61
1582	0.81	0.81
2351	0.99	1.00
3738	1.18	1.18
6779	1.36	1.37
13409	1.55	1.56
27511	1.73	1.76
49741	1.85	1.92
74741	1.91	2.00
99741	1.94	2.06
124741	1.96	2.11
149741	1.97	2.16
189741	1.99	2.23
229741	2.00	2.29
279741	2.02	2.37
304741	2.022	2.40

2.4.1. Resistivity and temperature coefficients

Electrical conductivity is the measure of the amount of electrical current that a material can carry, or its ability to carry a current. Electrical conductivity is also known as specific conductance. Conductivity is an intrinsic property of a material.

In the project arises the case where the temperature in the copper nucleus produced by the passage of the current must be considered. This can be deduced from the previous results obtained during the tests carried out, where the temperature increment increases the resistivity and it causes the conductive potential of copper to fall.

The International Annealed Copper Standard (IACS) establishes a standard for the conductivity of commercially pure annealed copper [27]. Table 2.4 gives us the values required to calculate the effects when the temperature experiences an increase over the maglev system more specifically on its core.

Table 2.4. Resistivity and Conductivity of Copper at 20°C

Material	ρ (Ω•m) at 20 °C	σ (S/m) at 20 °C	α (T/°C) at 20 °C
Copper	1.68×10^{-8}	5.8001×10^{7}	0.00386

Where ρ is Resistivity, σ is Conductivity and α is the Temp coefficient

2.4.1.1. Units of electrical conductivity

Electrical conductivity is denoted by the symbol σ and has SI units of siemens per meter (S/m). In electrical engineering, the Greek letter κ is used.

The Temperature Coefficient of Copper (near room temperature) is +0.386 percent per degree C. This means if the temperature increases 1 °C, the resistance will increase 0.393 %. According to followed norms in scientific work, 20 °C is used as the standard temperature instead of 0 °C.

2.4.1.2. Relationship between conductivity and resistivity

Conductivity and Resistivity are inverses of each other [28]. Electrical conductivity (σ) is the reciprocal of the electrical resistivity (ρ):

$$\sigma = \frac{1}{\rho} \tag{2.4}$$

where resistivity for a material with a uniform cross section is:

$$\rho = \frac{RA}{l} \tag{2.5}$$

Where R is the electrical resistance, A is the cross-sectional area, and l is the length of the material.

Electrical conductivity gradually increases in a metallic conductor as the temperature is lowered. Below a critical temperature, resistance in superconductors drops to zero, such that an electrical current could flow through a loop of superconducting wire with no applied power.

2.4.1.3. Factors that affect the electrical conductivity

There are three main factors that affect the conductivity or resistivity of a material:

Cross Sectional Area: If the cross section of a material is large, it can allow more current to pass through it. Similarly, a thin cross section restricts current flow.

Length of the Conductor: A short conductor allows current to flow at a higher rate than a long conductor. A real-life analogy would be trying to move a number of people through a hallway.

Temperature: Increasing temperature makes particles vibrate or move more. Increasing this movement (increasing temperature) decreases conductivity because the molecules are more likely to get in the way of current flow, so it is expected that they interfere more with the flow of electrons. If the temperature change is not too great, the resistivity of metals usually increases nearly linearly with temperature [29]. The generic formula for temperature effects on resistance is as follows:

$$R = R_{ref}[1+\alpha(T-T_{ref})] \tag{2.6}$$

Where,

R = Conductor resistance at temperature "T".
R_{ref} = Conductor resistance at reference temperature T_{ref}, usually 20°C.
α = Temperature coefficient of resistance for the conductor material.
T = Conductor temperature in degrees Celsius.
T_{ref} = Reference Temperature that α is specified at for the conductor material.

According to the values for each parameter we have individual values as follow below:

R = 14 ohm
R_{ref} = 20 °C
α = 0.00386
T = 100 °C

Using the Equation (2.6) we have the total value for the resistance: R = 14 [1+0.0386 (100-20)], R = 18.32 Ohms

Taking into account copper's coefficient of resistance, we can use Equation (2.6) to observe the relationship between copper conductivity versus temperature. Figure 2.5, shows how the resistance increases with the presence of temperature, as expected, this relative variation of the resistance leads us to expect a proportional change, which depends on the temperature.

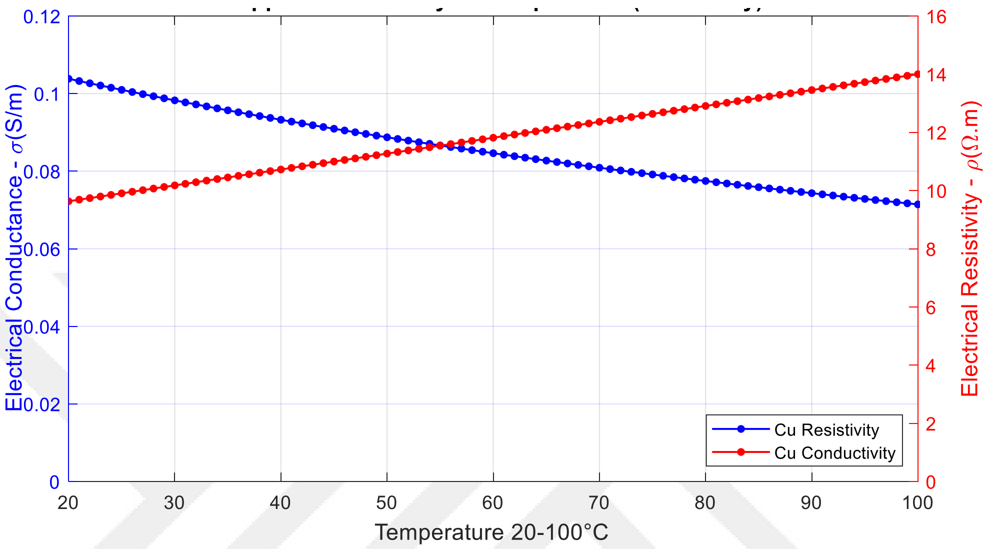

Figure 2.5. Temperature effects in the relation conductivity vs. resistivity from 20 to 100 °C of the coil copper

2.4.2. Steel ball permeability

In the project steel balls are used when the levitation process is carried out, so we need to know the relative permeability for the steel ball too. In this case Italian steel is the material by which the ball is formed. In order to make the test with the magnetic levitation system the steel ball used correspond to ball of stainless-steel series 400 [30]. Thus, knowing this, the characteristics magnetics and electrics in the steel spheres are shown below.

Table 2.5. Magnetic Properties for Stainless Steel Series 400

Property	Symbol	U.o.M.	Type	Notes	Value
Relative magnetic permeability	µ	-	Magnetic Ferromagnetic	Ferromagnetic	200

2.4.2.1. Core design

The core is made of soft magnetic iron powder Somaloy700 and is used to generate a closed loop magnetic flux. This increases the intensity of the magnetic field and the working gradient. In addition, the core is responsible for aligning the magnetic field lines generated in the north pole and curving them until they enter the south pole. Since the weight of the levitated object results in a force in the direction of gravity, the alignment of the lines of the magnetic field in the vertical direction will result in a higher magnetic force opposed to the weight of the object.

As mentioned before, the electromagnet is represented through a longitudinal section to show its dimensions and thereafter the calculation of the reluctance, the force, the magnetic flux and finally the magnetic intensity. Hence, we must consider the followings steps:

- Getting the equivalent circuit.
- Reluctance calculates in each parts of equivalent circuit.
- Reluctance total.

The core presents the following measurement specifications:

l_1 = 0.01m, core upper base height

l_2 = 0.08m, it is the total core width

l_3 = 0.02m, correspond to the width of the central limb

l_4 = 0.05m, length outer limb

w = 0.01m, width outer limb

x = 0.005m, this is value for Airgap

Figure 2.6 shows the model for the equivalent circuit of the core reluctance. In the figure, R_g represents the reluctance of the airgap between the end of the core and the object to be levitated. R_{sp} represents the reluctance between the steel sphere and the outer part of the core. N is the total number of wire-turns, I is the current in the coil and φ is the magnetic flux with the SI unit of Weber (Wb).

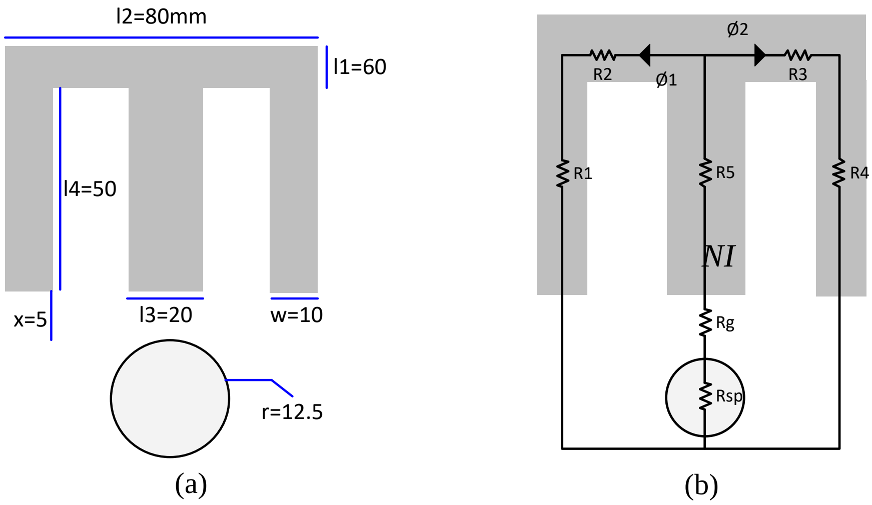

Figure 2.6. a) Electromagnet cross-section, b) Electromagnet equivalent circuit

According to the analysis rules of the model, the equivalent circuit for the magnetic levitation system is obtained using the general equation of reluctance:

$$R_s = \left(\frac{l_s}{\mu_0 \mu_s A_s}\right) \tag{2.7}$$

Where A_s represent the flux penetration surface [31], μ_0 is the Somaloy700 permeability and μ_s is the air permeability, which are used to obtain the specific reluctance in each surface of the plant.

2.4.2.2. Maglev system reluctances

In order to find the reluctances values we have the following constants:

μ_{sp}=200H/m; Relative Permeability of steel spheres

μ_c=540H/m; Relative Permeability of core (Somaloy700)

μ_{air}=1H/m; Relative Permeability of air

$\mu_0=4\pi x10^{-7}$; Relative Permeability of free space

Here the reluctances for each independent surface of the electromagnet core is solved, the main equation for this is related to Equation (2.7).

$$R_3 = R_2 = \left(\frac{\frac{l_2}{2}}{\mu_0\mu_s A_s}\right); \left(\frac{\frac{0.08m}{2}}{(4\pi x10^{-7})(540)(0.004m^2)}\right) = 147366H/m$$

$$R_4 = R_1 = \left(\frac{l_4}{\mu_0\mu_s A_s}\right); \left(\frac{0.05m}{(4\pi x10^{-7})(540)(0.005m^2)}\right) = 147366H/m$$

$$R_5 = \left(\frac{l_4}{\mu_0\mu_c l_3}\right); \left(\frac{0.05m}{(4\pi x10^{-7})(540)(0.01m)}\right) = 73682.8H/m$$

Due to the use of a steel sphere, then, it is necessary to get the reluctance of the steel sphere, according to this, we calculate the area of the surface of the sphere that is affected by the magnetic flux, which is given by the following equation.

$$A = 4\pi r^2 \tag{2.8}$$

Where a steel sphere with radius r = 12.5 mm is used, when we operate, we obtain the area of the surface to calculate the reluctance in the steel sphere, $A = 1.963x10^{-3}m^2$. Since now we are able to find the steel sphere reluctance (R_{sp}).

$$R_{sp}=\left(\frac{d}{\mu_0\mu_{sp}A_{sp}}\right); \left(\frac{0.05m}{(4\pi x10^{-7})(220)(1.963x10^{-3}m^2)}\right); R_{sp}= 46066.7H/m$$

The reluctance in the airgap is also obtained:

$$R_g = \left(\frac{x}{\mu_0\mu_{air}l_3}\right); \left(\frac{0.005m}{(4\pi xE^{-7})(1)(0.02m)}\right); R_g= 198944\ H/m$$

The reluctance on left and right side is equal, so the total reluctance and equivalent reluctance below is found as:

$$R_{eq} = \left(\frac{R_3+R_4}{2}\right)+R_5 \tag{2.9}$$

$$R_{eq} = \left(\frac{147366+147366}{2}\right)+73682.8$$

$$R_{tot} = 221049\ H/m$$

2.4.2.3. Determination the number of N-turns at the coil

The number of N-turns used in the model is determined by the following technical specifications for the coil and core, thus we have the following:

The resistance (Ohm), the length and the width (mm), the number of wire layers of the coil are the parameters which constitute the coil, we got those parameters by measured directly from the physical plant model and were used to find the approximate number of wire N-turns at the coil.

Coil length = 50 mm

No of Layers = 15 mm

Inner length = 10 mm

Coil resistance = 14.6 ohm

Copper wire diameter = 0.6711 mm

Using these parameters, we can calculate the total number of turns for the electromagnetic system coil. The inner length is divided by the wire diameter in order to obtain the number of layers around of the nucleus for a cross-section.

$$C_{Layers} = \frac{10mm}{0.6771mm} = 14.7689 \tag{2.10}$$

As above the same process is carried out to find the core length factor, in this case the value of the coil length divided over the diameter of the wire.

$$F_{Length} = \frac{50mm}{0.6771mm} = 66.7689 \tag{2.11}$$

Finally, these two obtained results are multiplied themselves allowing us to find with a good accurate value the number of N-turns with which the electromagnet’s coil was constructed (see Figure 2.7), here N ≅ 1090 turns.

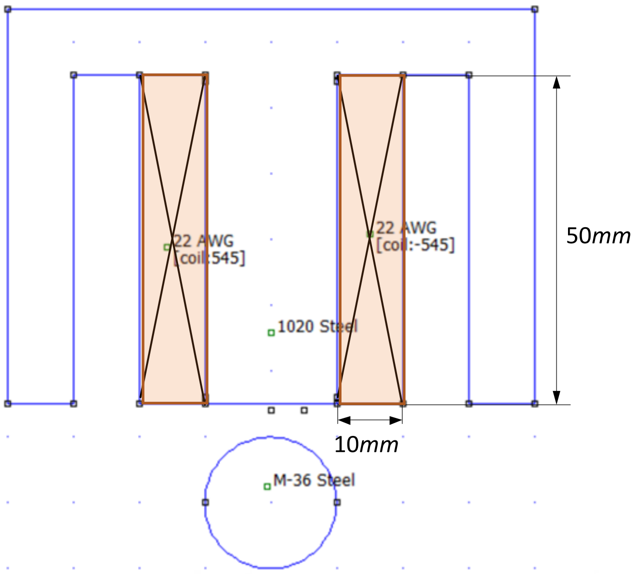

Figure 2.7. Specifications of the electromagnetic coil.

2.4.2.4. Magnetic flux intensity

Since we have the equivalent reluctance (R_{tot}), using Equation (2.12) we can find the magnetic flux intensity that runs through the system.

$$\phi_T = \frac{Ni}{R_{eq}} \tag{2.12}$$

Replacing the corresponding values in Equation (2.12) we have:

N = 1090 turns

V = 30 vdc

i = 1 to 4 A

$$\phi_T = \frac{1090(4A)}{221049\ H/m} = 1.9724x10^{-2}Wb$$

2.4.2.5. Calculating the flux density

Using the Equation (2.13) which is defined by (B_T) the flux density was found.

$$B_T = \frac{\phi_T}{A} \tag{2.13}$$

But here A represents the area which is affected and is represented as $A = l_3$ hence Equation (2.14) is changed, where w_d is the diameter width of the central core which yields:

$$B_T = \frac{\phi_T}{w_d} \tag{2.14}$$

$$B_T = \frac{1.9724x10^{-2}Wb}{0.020m} = 0.986\ T$$

The value the magnetic flux (B_T) was measured using Tesla units, when the 25 mm diameter steel ball is located at a distance of 0.5 mm from the electromagnetic core.

2.4.3. Electromagnet inductance

For the value of the inductance, it is taken into consideration that a value in the order of microHenries (μH) will not be efficient in current storage and its magnetic field will be minimal, and the order of the Henrys H are outliers that need a lot of material, therefore a coil in the order of the milli-henries mH will serve for the purpose of inducing manageable current and not saturating the electromagnet.

L = 150 mH

l = 50 mm

B = Tesla (Magnetic flux density)

Coefficient of self-induction

$$L = \frac{\mu_m N^2 A}{l} \tag{2.15}$$

2.5. Dynamics of Magnetic Levitation

The considered magnetic levitation system is a non-linear system, unstable and above all affected by uncertainties due to the lack of control about any of its parameters such as magnetization, hysteresis, temperature, etc. [32].

The levitation of the ferromagnetic ball is achieved when the electromagnetic force cancels the gravitational force [33] . At that moment the acceleration of the ball is zero and the movement of the system is described by the equation:

$$mg = C\left[\frac{I_0}{X_0}\right] \tag{2.16}$$

The expression (2.16) indicates that the parameter C varies according to the point of levitation (equilibrium point) which is characterized by the pair $x_{1eq} = X_0$, $x_{3eq} = I_0$. This means that the parameter is not constant, even if it is considered constant, a good approximation of the model is obtained for a balance point [34]. However, this model where the constant parameter C is considered will not be a general model in a situation where the levitation of the ferromagnetic ball is desired at several distances such as in the case of tracking a sinusoidal signal.

To determine the equilibrium position X_0 and the equilibrium current I_0, as well as the value of parameter C, an experimental approach [35] is used where the circuit current and the position of the ball are measured [36].

The ferromagnetic ball is located on a non-magnetic shelf directly below the electromagnet. The exact position is recorded by the position sensor, then a soft voltage ramp is applied to the magnetic circuit and the resulting position and the current consumed by the electromagnet is measured [37].

In the first moment of movement of the ball when the magnetic force is equal to the force of gravity the position of the ball $x(t) = X_0$ and the value of the current $i(t) = I_0$ is saved. These values represent different equilibrium points for the magnetic levitation system. Therefore, the force constant X is determined using the experimental values for X_0, I_0 and the expression (2.17), after the substitution in the measured values for the position and current.

$$C = \frac{mg}{\left(\frac{I_0}{X_0}\right)^2} \tag{2.17}$$

The physics established in the plant model is such as the created in [38] with the exception that in the current project the gravity acts to widen the air gap. In that sense taken from (2.17) we get the main equation produced through the electromagnet.

$$F = C\left(\frac{I_0}{X_0}\right)^2 \tag{2.18}$$

2.6. The Electromagnetic Force

Different mathematical models are considered to analyze the electro-magnetomotive force and its behavior. To give a major sense to the total mathematical model of the system even for its simulation the transformation into state equations is performed. The magnetic force is expressed as follows:

$$f(x,i) = -K\frac{i^2}{(x+C)^2} \tag{2.19}$$

Where K and C depend on the electromagnetic characteristics, the geometry, material and the mass of the body that is to be levitated.

The differential equation that describes the interaction of the levitating ball with the electromagnet is given by the second Newton law as follows:

$$\ddot{x} = -\frac{k}{m}\frac{i^2}{(x+C)^2}+g \tag{2.20}$$

When the object is levitating, the equilibrium between the gravitational force and magnetic force is established, this means that the net acceleration of the object that levitate is zero, this situation is described in:

$$0 = g-\frac{K}{m}\frac{i^2}{(x+C)^2} \tag{2.21}$$

The objective is to establish a relation among the current flowing across the electromagnet and the object position. Solving for the current i in the Equation (2.21) we obtain:

$$i = \sqrt{\frac{mg}{K}}x + \sqrt{\frac{mg}{K}}C \tag{2.22}$$

Observing carefully, we can determine that the relation between current and position is a linear relation and is in equilibrium, this corresponds to a straight-line equation of form $y = px + b$ (being p the slope, and b the intercept with the axis y). Therefore, given a position x, it is possible to establish a functional relationship between the current at which the magnetic and gravitational forces are equalized, and then the parameter K and C can be obtained according to the following:

$$K = \frac{mg}{p^2} \tag{2.23}$$

$$C = \frac{b}{\sqrt{\frac{mg}{K}}} \tag{2.24}$$

And observing to what current (approximately) the electromagnet has the capacity to attract the ball towards the nucleus. Thus, a set of readings is obtained whose tendency is very linear, as expected with the model. A linear regression was carried out, obtaining a coefficient very close to unit (1), this is shown in Figure 2.8, as well as the equation of the line obtained by the least square's method. The linear equation obtained is shown in Equation (2.25) and the correlation coefficient found is $R^2 = 0.9873$.

$$y = 0.0668x + 0.1645 \tag{2.25}$$

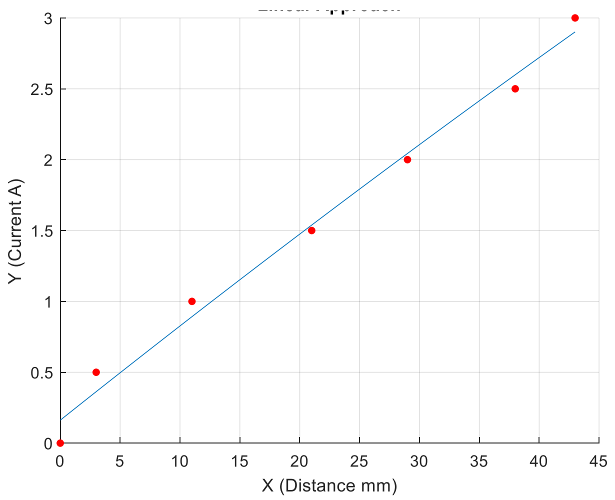

Figure 2.8. Relation between Current (A) and Position (mm) in Magnetic Levitation System

In this way using (2.23) and (2.24), m = 0.0110 kg, g = 9.8 $\frac{m}{s^2}$, and the value for p and b obtained of linear regression, thus K and C are obtained as shown K = 24.1583 and C = 2.4538.

The units of K are given in N$\frac{m^2}{A^2}$ and c are given in m, with these values the electromagnetic force which attracts the body with mass m to obtains the levitation is given according to Equation (2.19), replacing the constant values obtained we have the electromagnetic Equation (2.26) force which it represents a decreasing linear function with negative values for the gain K. Thus, an approximation of the behavior of the magnetic levitation system due to the movement of the sphere is made (see Figure 2.10).

$$f(x,i) = -24.1583 \frac{i^2}{(x+2.4538)^2} \tag{2.26}$$

The graphic associate to the magnitude of this function |f(x,i)| is shown in Figure 2.9.

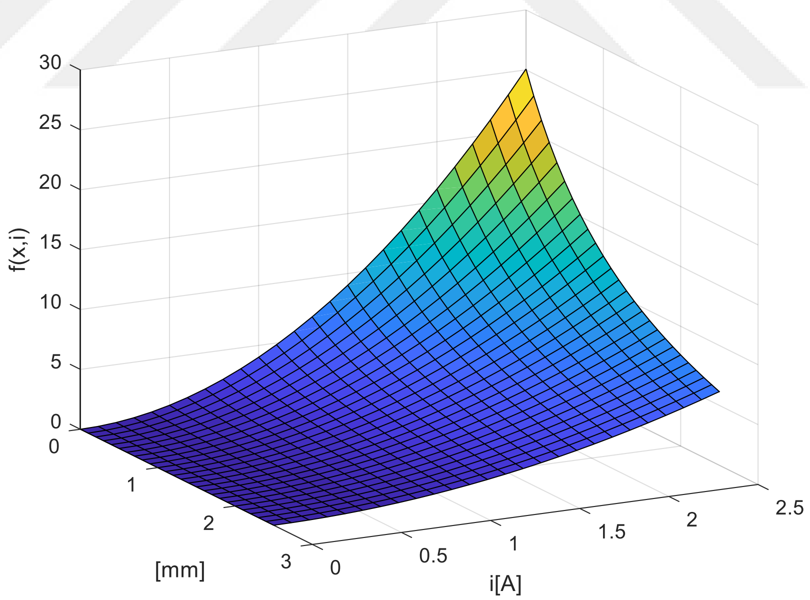

Figure 2.9. The behavior of the electromagnetic force as function of the position and current

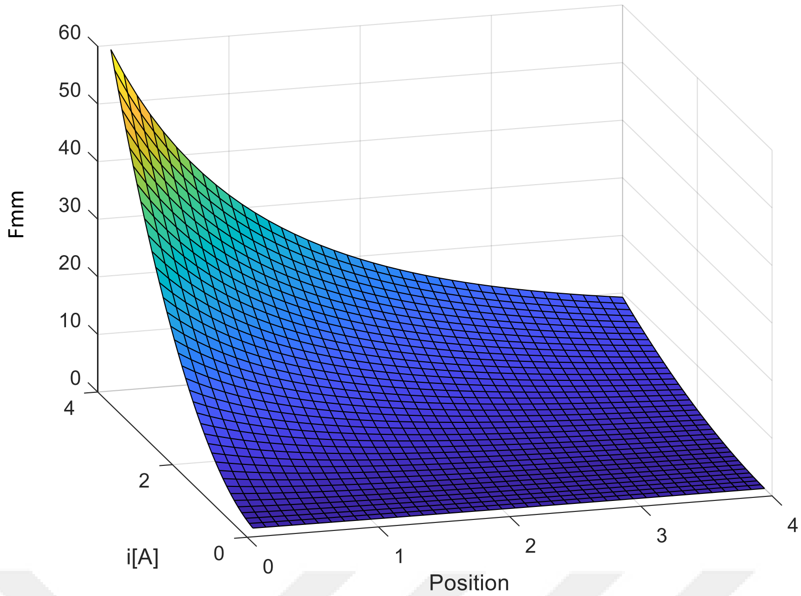

Figure 2.10. Graphic of the electromagnetic force

The electromagnetic force decreases significantly with distance, moreover it has an infinite range. And that particularly would present a problem of numerical simulation [23].

$$Fmm = K_1 \left(\frac{x_3}{x_1}\right)^2 \tag{2.27}$$

The expression of the electromagnetic force Figure 2.10 shows an approximation of the dynamic mathematical model, in which a, b and N are constants determined by numerical models or empirical methods [39]. The Equation (2.28) has got be approximated by constant parameters at the interest region, hence, due to the non-linearity of the magnetic field, those constants can vary when the force that passes through the system is large [40].

$$Fmm_u = \frac{u}{a(x_1+b)^N} \tag{2.28}$$

This model is approximate by a four-order polynomial according to the real behavior to which we are analyzing or implementing, thus the Fmm depends on the current and the position of the sphere (see Figure 2.12).

$$\text{Fmm} = \frac{x_3^2}{-5e\text{-}06x^4+0.0005x^3-0.0137x^2+0.1917x+0.011} \tag{2.29}$$

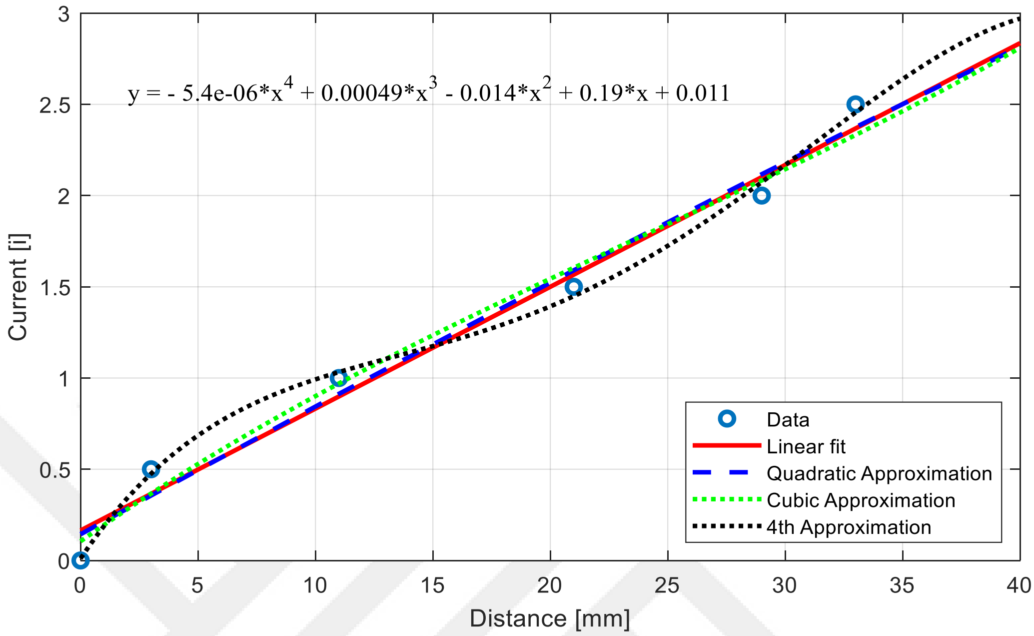

Figure 2.11. Electromagnetic force FMM using a 4th order polynomial

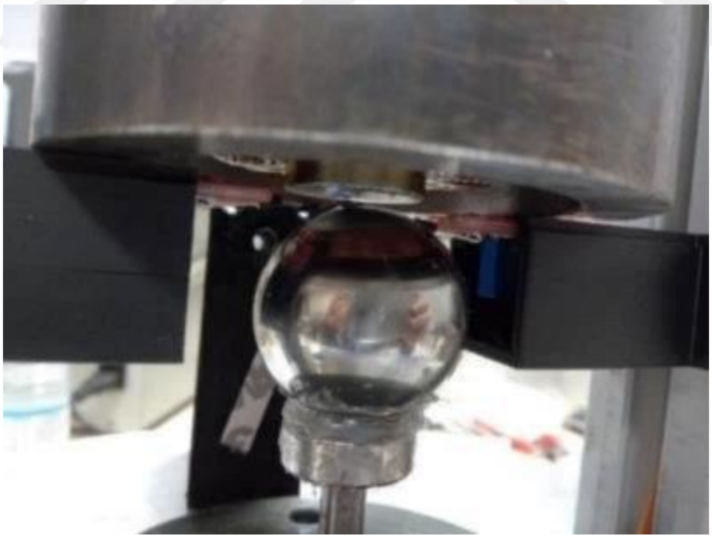

Figure 2.12. Setting the sphere and hall effect sensors before tests of current vs distance

2.6.1. FMM model simulation

According to the simulation carried out, see Figure 2.9, with the aim of measure the magnetic flux produced a 25 mm steel ball has been located below the electromagnet core, the initial airgap was set to 2 mm, from the simulation the linkage flux is observed as well. Likewise, the current supplied to the coil circuit was established at 4 ADC.

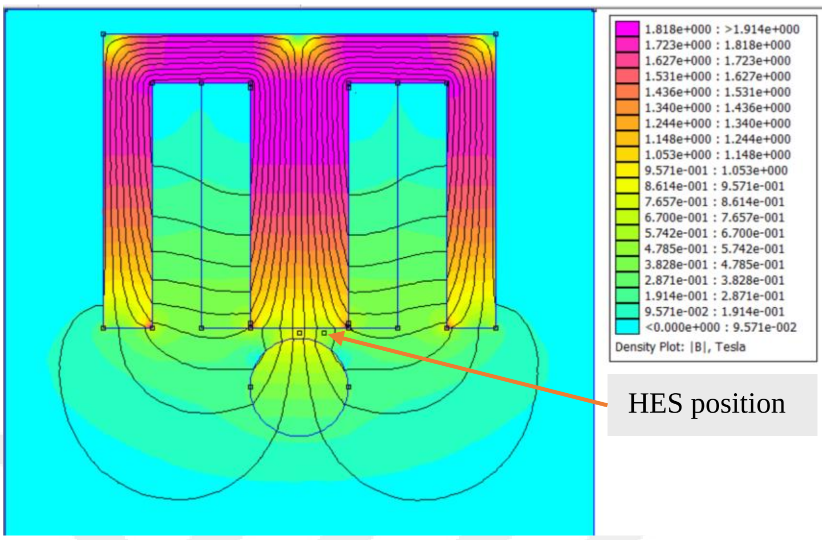

Figure 2.13. FMM-2D Model for magnetic flux density distribution

In Figure 2.13 the arrow indicates the fixed point established to perform the measurement of the magnetic flow, in each measurement in downward direction the ball was displaced on the Y axis 1mm at a time, the Table 2.6 shows the data obtained from the simulation where the airgap of the steel sphere has been varied in each test, as is to be expected, a decrease in the intensity of the magnetic field is observed as the measurement of the airgap increases.

Table 2.6. FMM simulation airgap outputs for the steel sphere

Distance (mm)	Magnetic flux (T)
1	0.95
2	0.90
3	0.67
4	0.57
5	0.51
6	0.45
7	0.42
8	0.39
9	0.37
10	0.36
15	0.32
20	0.28
25	0.29

The same process was carried out comparing the magnetic force in the absence of a ferromagnetic object see Figure 2.14. As expected, the result is lower (0.38 T) compared to the one obtained above, this is due to the reluctance that it presents by air in the airgap.

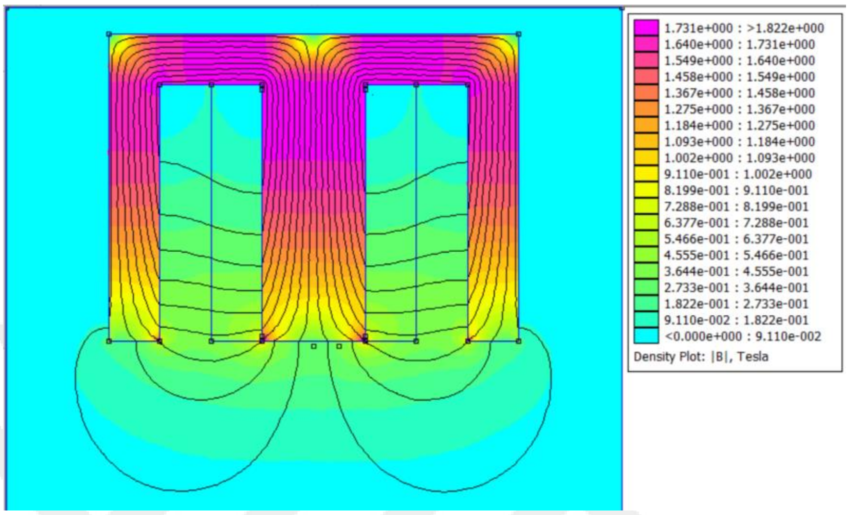

Figure 2.14. FMM-2D Model for magnetic flux density distribution in absence of the ball

Table 2.7. FMM simulation airgap outputs without steel sphere

Core Distance (mm)	Magnetic flux (T)
2	0.38

2.6.2. Mechanical model

The magnetic levitation system is a non-linear system, unstable and above all affected by the uncertainty principle due to the lack of estimation on some of its parameters such as magnetization, hysteresis, temperature, etc. Therefore, to design and establish control rules for the system is a very complex challenge, for this we define the following principles associated with the elements involved [37].

We get the magnetic levitation of the ball when the electromagnetic force cancels the gravitational force [33], and in that moment the steel ball's acceleration becomes 0 [32]. The system movement is described by the equation:

$$mg = C\left[\frac{I_0}{X_0}\right] \tag{2.30}$$

Using the fundamental principle of dynamics (Newton's second law), the dynamics of the ferromagnetic sphere is given by:

$$m\ddot{x} = mg\text{-}Fem \qquad (2.31)$$

Where Fem is the electromagnetic force that is generated by the electromagnetic effect in the system, m is the mass and g is the force of gravity that counteracts the electromagnetic force based on the definition of Newton's second law. Therefore, substituting the value of the calculated electromagnetic force in Equation (2.3), we substitute that value in Equation (2.19) and we obtain:

$$mg+m\ddot{x} = \frac{L_r}{2a} i^2 e^{-\frac{\infty}{a}} \qquad (2.32)$$

Finally, the mechanical model of the system remains as:

$$\ddot{x} = \frac{L_r}{2am} i^2 e^{-\frac{\infty}{a}} + g \qquad (2.33)$$

2.6.3. Magnetic Levitation

We know that our magnetic levitation system consists of the one degree of freedom see Figure 2.15.

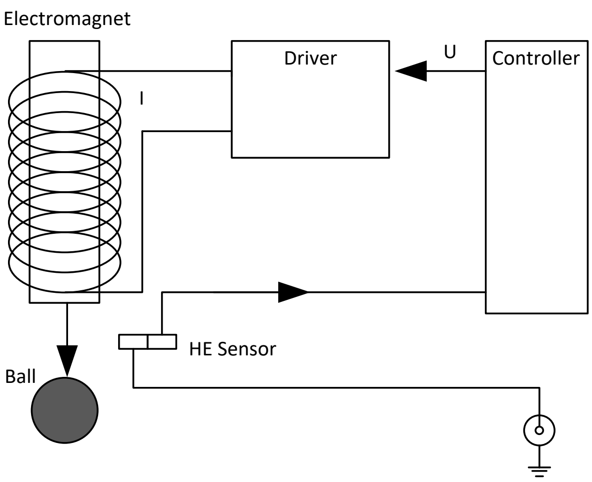

Figure 2.15. 1-DOF RL circuit for the magnetic levitation system

Considering that the above expressions are related by the current through the electromagnet. We can describe the dynamics of a generic magnetic levitation system by the following pair of differential equations.

$$\frac{d^2x}{dt^2} = g - \frac{1}{m}\frac{L_0 h_0}{2}\left(\frac{i}{x}\right)^2 = g - \frac{k}{m}\left(\frac{i}{x}\right)^2 \tag{2.34}$$

$$v = R.i + L_I\frac{di}{dt} \tag{2.35}$$

2.6.4. Dynamic equations of state space model

A complex system has many inputs and many outputs that are related to each other in a complicated way. To analyze such a system, it is essential to reduce the complexity of the relevant mathematical expressions, and from this point of view the approach of equations of states is the most convenient for the analysis of these systems.

We define the concept of state first, the state of a dynamic system is the smallest set of variables (called state variables), so that the knowledge of these variables in $t \geq t_0$, together with the knowledge of the input for $t \geq t_0$, completely determine the behavior of the system at any $t \geq t_0$.

It must be stated that state variables do not need to be physically measurable or observable quantities, such freedom in the choice of state variables is an advantage of the methods in the state space. However, in practice it is convenient to select for the state variables physically measurable quantities if possible, because the laws of control in the state space will require to feed back all the state variables with an appropriate weighting.

The equations of state, are the set of equations that describe the dynamics of a system by means of the relation between the input variables, the output variables and the state variables.

The modeling of dynamic systems in the state space allows to describe the behavior of all types of systems; SISO, MIMO, linear, non-linear, invariant, variants, so, the generic description for the state equations is:

$$\begin{aligned}
\dot{x}_1(t) &= f_1(x_1,x_2,\ldots,x_n;\ u_1,u_2,\ldots,u_r;t)\\
\dot{x}_2(t) &= f_2(x_1,x_2,\ldots,x_n;\ u_1,u_2,\ldots,u_r;t)\\
&\vdots\\
\dot{x}_n(t) &= f_n(x_1,x_2,\ldots,x_n;\ u_1,u_2,\ldots,u_r;t)
\end{aligned} \tag{2.36}$$

$$\begin{aligned}
\dot{y}_1(t) &= h_2(x_1,x_2,\ldots,x_n;\ u_1,u_2,\ldots,u_r;t)\\
\dot{y}_2(t) &= h_2(x_1,x_2,\ldots,x_n;\ u_1,u_2,\ldots,u_r;t)\\
&\vdots\\
\dot{y}_m(t) &= h_m(x_1,x_2,\ldots,x_n;\ u_1,u_2,\ldots,u_r;t)
\end{aligned} \tag{2.37}$$

If it is defined as shows below:

$$X(t) = \begin{bmatrix} x_1(t)\\ x_2(t)\\ \vdots\\ x_n(t) \end{bmatrix};\quad f(x,u,t) = \begin{bmatrix} f_1(x_1,x_2,\ldots,x_n;\ u_1,u_2,\ldots,u_r;t)\\ f_2(x_1,x_2,\ldots,x_n;\ u_1,u_2,\ldots,u_r;t)\\ \vdots\\ f_n(x_1,x_2,\ldots,x_n;\ u_1,u_2,\ldots,u_r;t) \end{bmatrix} \tag{2.38}$$

$$Y(t) = \begin{bmatrix} x_1(t)\\ x_2(t)\\ \vdots\\ x_n(t) \end{bmatrix};\quad h(x,u,t) = \begin{bmatrix} h_1(x_1,x_2,\ldots,x_n;\ u_1,u_2,\ldots,u_r;t)\\ h_2(x_1,x_2,\ldots,x_n;\ u_1,u_2,\ldots,u_r;t)\\ \vdots\\ h_m(x_1,x_2,\ldots,x_n;\ u_1,u_2,\ldots,u_r;t) \end{bmatrix} \tag{2.39}$$

$$u(t) = \begin{bmatrix} u_1(t)\\ u_2(t)\\ \vdots\\ u_n(t) \end{bmatrix} \tag{2.40}$$

Expressing the previous equations in matrix format we have:

$$\begin{aligned}
\dot{x}(t) &= f(x,u,t)\\
\dot{y}(t) &= h(x,u,t)
\end{aligned} \tag{2.41}$$

If we linearize the previous equations or write them in directly linear systems then the equations of state can be expressed as:

$$\begin{aligned}
\dot{X}(t) &= Ax(t)+Bu(t)\\
\dot{y}(t) &= Cx(t)+Du(t)
\end{aligned} \tag{2.42}$$

Where A(t) is called state matrix, B(t) input matrix, C(t) output matrix and D(t) direct transmission matrix.

2.6.5. State equations of a magnetic levitation system

Once obtained in Section 2.6.3 (the equations that model the dynamics of a magnetic levitation system) we can express these equations in the state space. To represent the system in the SE (State equations) we must know what the output variables, the input variables and the state variables are.

A magnetic levitation system of one degree of freedom is a SISO system, so it means that it only has one input variable and one output variable. The input variable will always be the input voltage to the circuit and the output variable will always be the height.

Now it would be necessary to define the state variables to have the representation of the system in the SE. The state variables were chosen according to the criterion of energy storage. Associated with the mass is the position x_1 (potential energy) and velocity x_2 (kinetic energy) as state variables. Associated with the inductance, the current x_3 (electromagnetic energy) defines the third state variable. In Equation (2.43) the state variables are shown.

$$x_1 = x; \quad x_2 = \frac{dx}{dt} = \dot{x}_1; \quad x_3 = i \tag{2.43}$$

Given the state variables, in this selection the state equations are described according to (2.44), (2.45) and (2.46).

$$\dot{x}_1 = x_2 = f_1(x,u) \tag{2.44}$$

$$\dot{x}_2 = g - \frac{K}{m}\left(\frac{x_3}{x_1+c}\right)^2 = f_2 = (x,u) \tag{2.45}$$

$$\dot{x}_3 = \frac{u}{L} - \frac{R}{L}x_3 = f_3 = (x,u) \tag{2.46}$$

3. SYSTEM IDENTIFICATION

A fundamental concept in science and technology is the concept of mathematical modelling. The system identification is conducted to obtain and verify if a suitable control law can be implemented to compensate the plant instability and improve its performance. The system identification of the magnetic levitation system is the process of developing the mathematical model using the response of the outputs and inputs of the system.

3.1. Magnetic Levitation System Dynamic Model

The coil acts as an electromagnet actuator, while a hall effect sensor helps to determine the steel ball's position by regulating the electric current in the circuit with a controller.

Analytical and experimental plant models were obtained by comparison and verification. Figure 3.1 shows the RL coil circuit that levitate the steel ball by electromagnetic force [41].

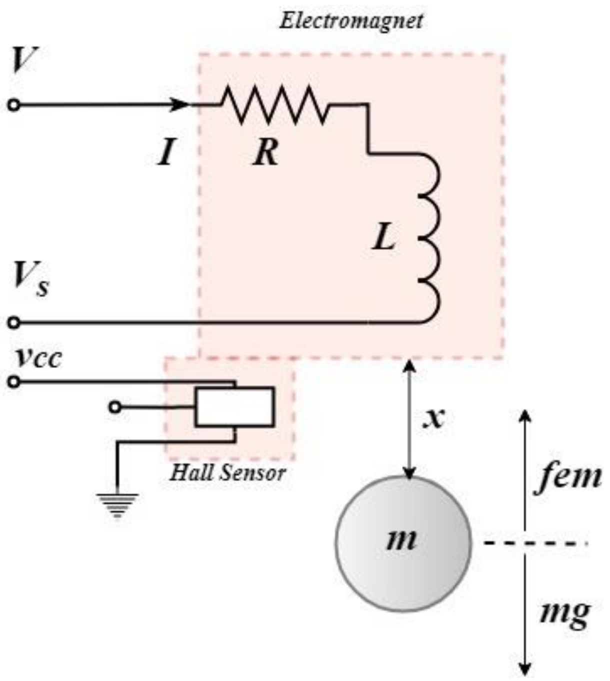

Figure 3.1. Illustration of DC magnetic levitation RL circuit

The electromagnetic force produced by current is given by Kirchhoff's Voltage law, we obtain the following tension-current relationship:

$$u(t) = V_R+V_L = iR+\frac{dL}{dt}i+L(x)\frac{di}{dt}$$
$$u = iR+L(x)\frac{di}{dt} \tag{3.1}$$

Where:

u: Voltage applied

i: Current in the coil

R: Coil resistance

L: Coil inductance

x: Sphere Position

x_0, L_0: Nominal Operating Constants

Assuming that we are close to the equilibrium position x_0 and that L_i is much greater than L_0 we can approximate the value of the inductance; here L(x) is a nonlinear function of x given as:

$$L(x) = Li+\frac{L_0x_0}{x_0} \tag{3.2}$$

Finally, we get voltage as shown following:

$$u = iR+L\frac{di}{dt}-\left(\frac{L_0x_0i}{x^2}\right)\frac{dx}{dt} \tag{3.3}$$

If $x_1 = x$, $x_2 = v$, $x_3 = i$ and $u = e$ (input voltage) then we obtain the following equations as:

$$\frac{dx_1}{dx} = x_2 \tag{3.4}$$

$$\frac{dx_2}{dt} = g-\frac{C}{m}\left(\frac{x_3}{x_1}\right)^2 \tag{3.5}$$

$$\frac{dx_3}{dt} = -\frac{Rx_3}{L}+\frac{2C\left(\frac{x_2x_3}{{x_1}^2}\right)}{L}+\frac{u}{L} \tag{3.6}$$

Free body diagram of steel ball suspended by balancing the electromagnet force $F_{em}(x, i)$ and gravitational force F_g is shown below.

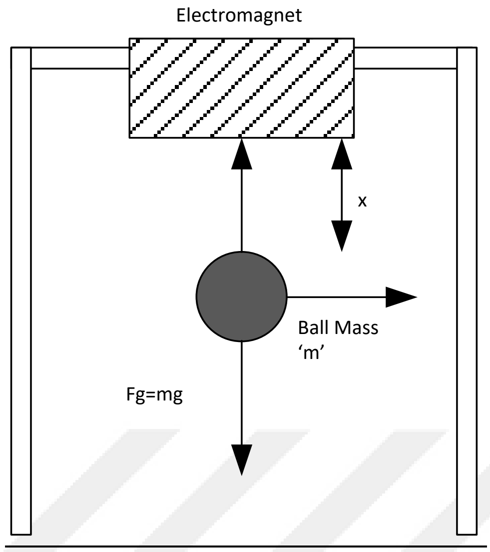

Figure 3.2. Free body diagram of DC Magnetic Levitation System.

Net force F_{net} acting on the ball is given by Newton's 3rd law of motion.

$$F_{net} = F_g - F_{em} \tag{3.7}$$

$$mx = mg - C\left(\frac{i}{x}\right)^2 \tag{3.8}$$

Where C and K are fixed parameters in the system identification

Table 3.1. Parameters considering for trials on Maglev System

Parameter	Description	Value
C	Magnetic constant	$1.477xE^{-4}$ Nm^2/A^2
m	Steel Sphere Mass	0.11 kg
g	Gravitational acceleration	9.82 m/s^2
K	Force constant	N
x	Ball position	4mm

Input voltage formula can be stated as:

$$e = Ri + \frac{d(Li)}{dt} \tag{3.9}$$

3.1.1. The temperature effects on maglev system

The magnetic levitation system consists of one model with a nucleus of material called Somaloy700 which is highly permeable and ideal for inducing magnetic fields. Around the nucleus the coil is found with 1090 turns.

According to the tests performed, at average room temperature the system usually can generate a magnetic field ranging from 0.06 to 1.3 Tesla, with a current flow of up to 5 A within a time interval of 10 to 120 s. The losses by temperature is a characteristic that stands out during the execution of tests carried out in the magnetic levitation system.

In the test carried out for the magnetic levitation system, current and time parameters have been taken into account as follows: current supplied 4 A, test time 190 s, an increase in temperature of 0.1 A per each 7 s. Figure 3.3, shows that the magnetic levitation system reaches a temperature of 160 °C when 190 s have elapsed, likewise, a magnetic field of approximately 1 Tesla has been generated, notice that, when the supplied current goes around 2 A, a slight curve begins to be generated, which means that the electromagnet begins to lose its magnetic force due to the increase of the temperature in the system.

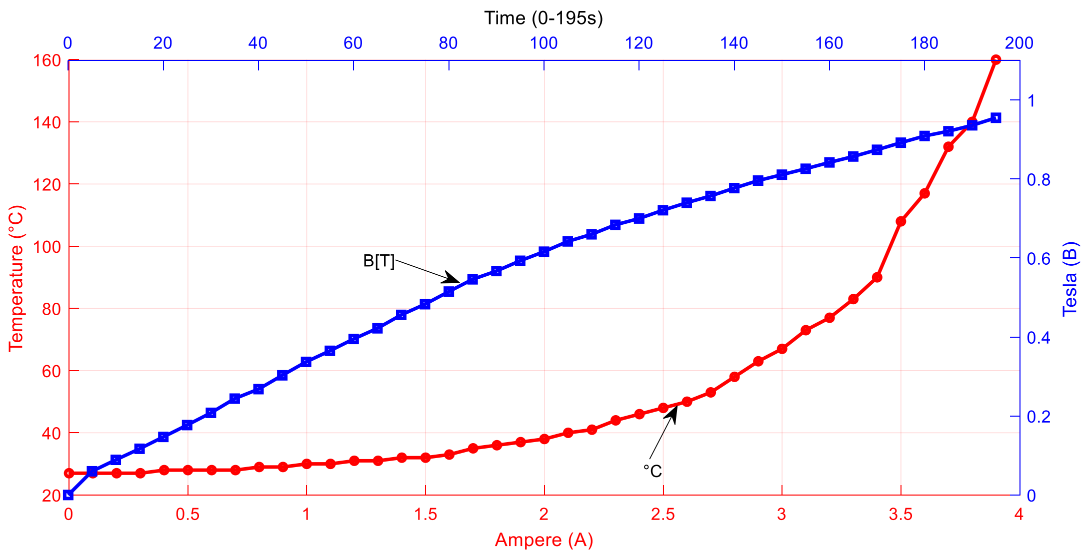

Figure 3.3. Effect of temperature on the magnetic field strength

Using the read values, the second graph was plotted in Matlab software obtaining a 3D model see Figure 3.4 where it is verified that the increase of the temperature begins to cause saturation in the magnetic field which is produced by the coil.

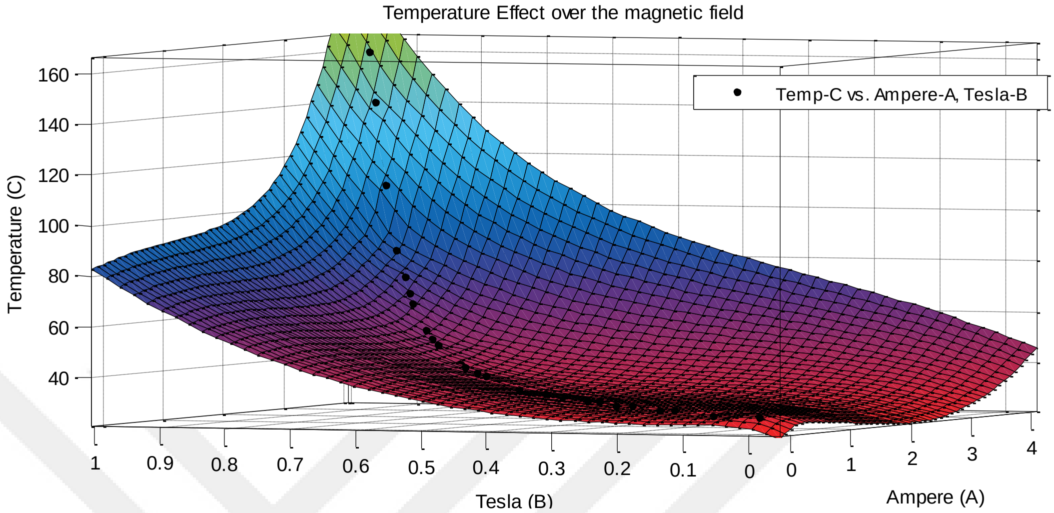

Figure 3.4. A 3D Plot concern to the measures which act on the Magnetic Levitation System

3.2. Magnetic Force

This section is focused on the development of the mathematical model of a magnetic levitation system with more than 1 degree of freedom, the type used to suspend a ferromagnetic object predetermined distances. The magnetic levitation system is constituted by a ferromagnetic ball suspended in a magnetic field controlled through the manipulation of the potential difference in the electric winding. The ferromagnetic ball has two degrees of freedom, the analysis focuses only on the movement of translation made in the vertical plane, ignoring the rotation of the ball around its axis.

The ferromagnetic ball is influenced by two forces:

- The gravitational force
- The electromagnetic upward force F_{mm} produced by the magnetic field in the coil.

Magnetic suspension systems are systems that have non-linear dynamics, which are unstable in an open loop, so feedback control is necessary to stabilize them [42]. In the proposed mathematical model, the state variables used are the position of the ball, the speed of the ball and the current that passes through the electromagnetic circuit. The mathematical model of the levitation system can be developed by employing the appropriate differential equations according to the mechanical and electrical principles.

3.2.1. Complete mathematical model

It is considered that the position x of the ball increases positively in the downward direction of the electro magnet. Using dynamic fundamental principles, the dynamics of the ferromagnetic ball expressed by Newton's law for the balance of forces has the following non-linear form.

$$m\frac{d^2x(t)}{dt^2} = mg - F_{em}(i,x,t) \tag{3.10}$$

Where:

- m = Mass of the levitated object
- g = Gravity force
- x(t) = Distance between the electromagnet and the sphere
- i(t) = Current through the coil

The expression for the energy balance within the system

$$dW_e = dW_{mec} + dW_t + dW_m \tag{3.11}$$

Where the terms represent the variation of the electric energy dW_e, the variation of the mechanical energy dW_{mec}, the variation of the thermal energy dW_t and the variation of the magnetic energy dW_m. The variation of the magnetic energy when the magnetic flux is changing and the bodies are moving within the magnetic field is given by:

$$dW_m = i\Phi - d_e dx \tag{3.12}$$

The electromagnetic levitation force can be determined using the generalized force theorems [43].

$$f_e = -\left[\frac{\partial W_m}{\partial_x}\right]_{i=current} \tag{3.13}$$

The specific magnetic energy of the coil is:

$$W_m = \frac{i\Phi(t)}{2} = \frac{L(x,t)i(t)^2}{2} \tag{3.14}$$

L(x,t) is the inductance of the electromagnet, where it is influenced by the levitated object, which can be determined by either direct calculation using reluctance or permeability. The bibliographic references used specify the fact that the air gap permeability (the region between the coil and the ferromagnetic core) corresponds exclusively to the area of the pole when the polar surface is much wider than the thickness.

Analytically determining the magnetic force for an experimental magnetic levitation system is extremely difficult since a combination of electromagnetic and ferromagnetic materials is used for the model [35], therefore we can take the inductance L(x) as a simplified non-linear function of the position x of the ferromagnetic ball [32].

$$L(x,t) = L + \frac{L_0 x_0}{x(t)} \tag{3.15}$$

Where:

- x_0 = Arbitrary reference position for the inductance measurement.
- L_0 = Incremental inductance produced by the steel ball corresponding to x_0.
- $x(t)$ = Effective distance between the ball and the electromagnet.
- L = Inductance of the electromagnet when the ball is far away so that its effect can be neglected.

Which is an approximation where it is assumed that this inductance varies inversely proportional to the position x of the ferromagnetic ball. Hence, deriving the expression (3.13) we obtain:

$$f_e(i,x,t) = \frac{\partial W(i,x,t)}{\partial x} = -\frac{i^2(t)dL(x,t)}{2dx} \tag{3.16}$$

Substituting and finding the C parameter we have:

$$f_e(i,x,t) = \frac{L_0 x_0}{2}\left[\frac{i(t)}{x(t)}\right]^2 = -\frac{i^2(t)dL(x,t)}{2dx} \quad (3.17)$$

$$C = \frac{L_0 x_0}{2} \quad (3.18)$$

Which is an electromagnetic parameter that depends on the reference point considered and that is characterized by x_0. Remaining finally:

$$m = \frac{d^2x(t)}{dt^2} = mg-C\left[\frac{i(t)}{x(t)}\right]^2 \quad (3.19)$$

The electrical part of the system we have the Kirchhoff law [26]:

$$e(t) = Ri(t)+\frac{d[L(x,t)i(t)]}{dt} \quad (3.20)$$

Where:

- R = Resistance of the circuit in Ohms
- e(t) = Difference of potential applied to the electrical circuit
- L(x) = Inductance as a function of the ball position

3.3. Linear Model

In this section the mathematical model of the system will be linearized. Linearization is necessary if the system is to be controlled using linear control theory.

Basically, the process consists of the Taylor series expansion of each of the system state equations around an operating point, cutting the series in the linear term using the Jacobian. The linear mathematic model in the state space of the magnetic levitation system is described according to the Equations (3.21) and (3.22).

$$\dot{x} = Ax+Bu \quad (3.21)$$

$$y = Cx \quad (3.22)$$

3.4. Linearization of the Model

It is based on the state equations described in Equations (2.44), (2.45) and (2.46). Assuming that the origin x = 0 (where magnetic and gravitational forces are equalized) [20]. It is an equilibrium point of the system, taken as the point of operation for the linearization since they are the points where the levitation can be controlled more easily.

The equilibrium point of the system is defined according to the chosen operating point, that is, the levitation position, the speed, the current required in the defined position, and the average voltage associated with such current. The equilibrium point is shown in (3.23) where $\dot{x}_1$, $\dot{x}_2$ and $\dot{x}_3$ are the values of each state variable at the equilibrium point and $\dot{u}$ is the input in the respective equilibrium.

$$\begin{aligned} \dot{x}_1 &= x_0 = 0.0112\text{m} \\ \dot{x}_2 &= \frac{0\text{m}}{\text{s}} \\ \dot{x}_3 &= \sqrt{\frac{mg}{K}}(x_0+c) = 0.9128\ \text{A} \\ \dot{u} &= R\sqrt{\frac{mg}{K}}(x_0+c) = 12.77\ \text{V} \end{aligned} \tag{3.23}$$

Experimentally, the values associated with the point of operation were obtained by determining the current for which the magnetic force and the gravitational force acting on the sphere are balanced at a specific voltage and position. For the linearization the Jacobian was used. The linearized system around the equilibrium point is a third order system with matrices A, B and C obtained according to (3.24).

$$\begin{aligned} A &= \frac{\partial f(x,u)}{\partial x}\bigg|_{\dot{x},\dot{u}} \\ B &= \frac{\partial f(x,u)}{\partial u}\bigg|_{\dot{x},\dot{u}} \\ C &= \frac{\partial f(x)}{\partial x}\bigg|_{\dot{x}} \end{aligned} \tag{3.24}$$

Now, linearizing the system, the matrices remain as shown in Equations (3.25), (3.26), and (3.27).

$$A = \begin{bmatrix} \frac{\partial f_1(x,u)}{\partial x_1} & \frac{\partial f_1(x,u)}{\partial x_2} & \frac{\partial f_1(x,u)}{\partial x_3} \\ \frac{\partial f_2(x,u)}{\partial x_1} & \frac{\partial f_2(x,u)}{\partial x_2} & \frac{\partial f_2(x,u)}{\partial x_3} \\ \frac{\partial f_3(x,u)}{\partial x_1} & \frac{\partial f_3(x,u)}{\partial x_2} & \frac{\partial f_3(x,u)}{\partial x_3} \end{bmatrix} = \begin{bmatrix} 0 & 1 & 0 \\ \frac{2K}{m}\frac{\dot{x}_3^2}{(\dot{x}_1+c)^3} & 0 & -\frac{2K}{m}\dot{x}_3(\dot{x}_1+c)^3 \\ 0 & 0 & -\frac{R}{L} \end{bmatrix} \quad (3.25)$$

$$B = \begin{bmatrix} \frac{\partial f_1(x,u)}{\partial x_1} \\ \frac{\partial f_2(x,u)}{\partial x_1} \\ \frac{\partial f_3(x,u)}{\partial x_1} \end{bmatrix}; B = \begin{bmatrix} 0 \\ 0 \\ \frac{1}{L} \end{bmatrix} \quad (3.26)$$

$$C = \begin{bmatrix} \frac{\partial h_1(x)}{\partial x_1} & \frac{\partial h_1(x)}{\partial x_2} & \frac{\partial h_1(x)}{\partial x_3} \end{bmatrix}; C = [1 \quad 0 \quad 0] \quad (3.27)$$

The L(x) variation respect to the ball position measurement of the inductance x_0 can be neglected. Since $L_x x_0/x$ is smaller than L [37]. The linearized system is then obtained in the manner described by Equations (3.28) and (3.29).

$$\dot{x}_\delta = A \cdot x_\delta + B \cdot u_\delta \quad (3.28)$$

$$y_\delta = C \cdot x_\delta \quad (3.29)$$

Where the sub-index δ refers to these as increment variables, that is, they describe the changes around the chosen operating point. The linearization of the experimental model of the levitation system was obtained calculating the matrices A, B, C and D corresponding to the linearization. The parameters used to define the real model are shown in Table 3.2, the values are given in units of the MKSA system.

Table 3.2. Initial parameters of system identification

Variable	Value
R	14 Ohm
L	0.15 H
K	0.0000241586 Nm^2/A^2
C	0.002438 N

Table 3.3 shows the found values to establish the start setpoint for the magnetic levitation system.

Table 3.3. Parameters of magnetic levitation system

Variable	Value
$\dot{x}_3$ (Current)	0.9128 A
$\dot{x}_2$ (Velocity)	0 m/s
$\dot{x}_1$ (Position)	0.0112 m
m (mass)	0.0110 Kg
$\dot{u}$ (Voltage)	12.77 v

On one side, using the parameters of the system the corresponding calculations were made and the output matrices of the model of the maglev system were obtained, these are shown in (3.30), (3.31) and (3.32).

$$A = \begin{bmatrix} 0 & 1 & 0 \\ 1442.81 & 0 & -1.01701e^{-8} \\ 0 & 0 & -93.33 \end{bmatrix} \tag{3.30}$$

$$B = \begin{bmatrix} 0 \\ 0 \\ 6.6 \end{bmatrix} \tag{3.31}$$

$$C = [1 \quad 0 \quad 0] \tag{3.32}$$

On the other hand, the obtaining of results using Matlab was also carried out. For this, taking as a starting point the non-linear model of the magnetic levitation system designed in Simulink, the follow parameters [0.0112 0.9128 12.77] was used to set the state space equation.

The results obtained by both methods were identical (neglecting the significant figures of smaller order 10^{-4}), showing the validity of the non-linear model created in Simulink. After having the linearized model, a comparison was made about the behavior of the latter with respect to the non-linear model. In Figure 3.5 the plot using Simulink to make the comparison is shown.

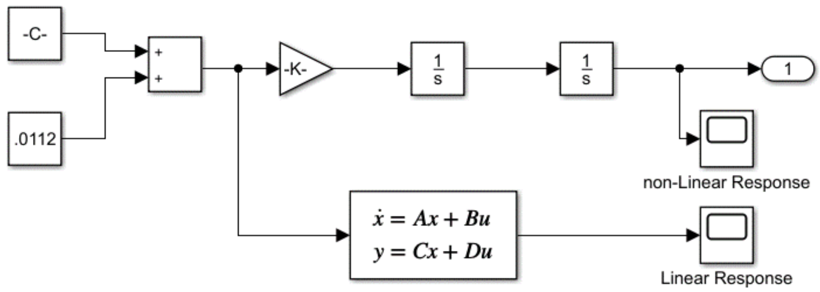

Figure 3.5. Simulink model for comparison of the linear and non-linear response

Linearization is an approximation of the non-linear model at the point of operation, for which the point of equilibrium of gravitational and magnetic forces was selected. It is expected then that as long as the characteristics of the nonlinear model (in representation of reality) do not depart much from that point of operation (that is, remain within the range of operation), the linearization will adequately represent the system. This is where the success of the use of linear techniques in magnetic levitation is visualized.

The response of the non-linear and linear system at the chosen operating point is illustrated in Figure 3.6 and Figure 3.7. Basically, while guaranteeing that the real system is around the chosen operating point, any approximation made with the linearized model will be useful to represent the non-linear system. From the graph it is observed that when both the non-linear and the linearized systems have similar characteristics of position and velocity (near the point of operation), they give a solution very similar to each other (in the time interval [0 0.03]). However, when both the position and speed (slope of the position curve) move away from the operation point $\dot{x}_1 = 0.0112$ m and $\dot{x}_2 = 0$ m/s, the curves associated with the response of each model are more disparate.

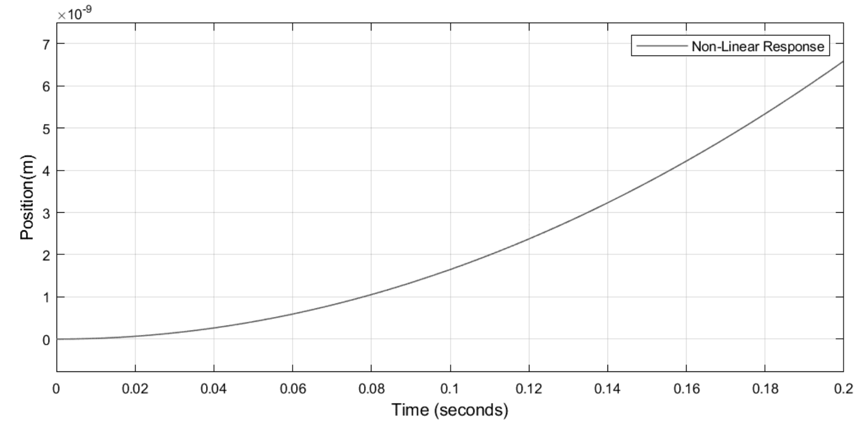

Figure 3.6. Non-Linear response

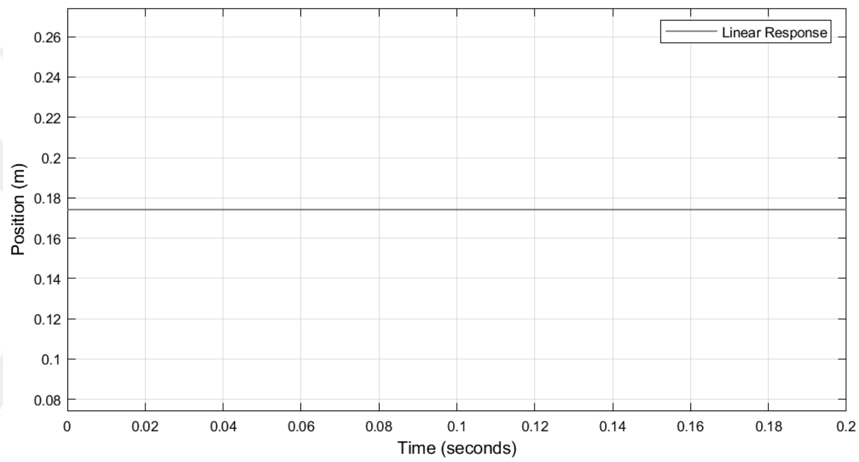

Figure 3.7. Linear response

3.5. Plant Transfer Function

The transfer function of the plant can be obtained from the state Equations (3.21) and (3.22). To do this we must obtain $\Phi(s) = (sI-A)^{-1}$, which is the Laplace transform of the state transition matrix $\Phi(t)$. This matrix is shown in (3.33).

$$\Phi(s) = (sI-A)^{-1} = \begin{pmatrix} s & -1 & 0 \\ -1442.81 & 0 & 1.01701e^{-8} \\ 0 & 0 & s+93.33 \end{pmatrix}^{-1} \tag{3.33}$$

The transfer function is given by Equation (3.34)

$$G(s) = C\Phi(s)B \tag{3.34}$$

Therefore, the transfer function is:

$$G(s) = (1 \quad 0 \quad 0)\begin{pmatrix} s & -1 & 0 \\ -1442.81 & 0 & 1.01701e^{-8} \\ 0 & 0 & s+93.33 \end{pmatrix}^{-1}\begin{pmatrix} 0 \\ 0 \\ 6.6 \end{pmatrix} \tag{3.35}$$

Using the command line (sys = ss[A, B, C, D]) and tf(sys) in Matlab we get the transfer function as shown in (3.36), with poles 37.98, -37.98 and -93.33.

$$G(s) = \frac{-6{,}712e\text{-}08}{s^3 + 93.33\, s^2 - 1443\, s - 1.347e05} \tag{3.36}$$

From this transfer function in Figure 3.8 it is observed that the system is of third order. Additionally, the system is unstable because it has a pole in the right semi plane of the plane S. Furthermore, it should always be positive, so if any of the coefficients are zero or negative in the presence of at least one positive coefficient in the characteristic polynomial, it implies that there is an imaginary pole or poles that have a positive real part, in this case the system is not stable [44]. From the above it is shown that in the magnetic levitation system:

1. Exist continuous equilibrium points.
2. The equilibrium points are unstable.

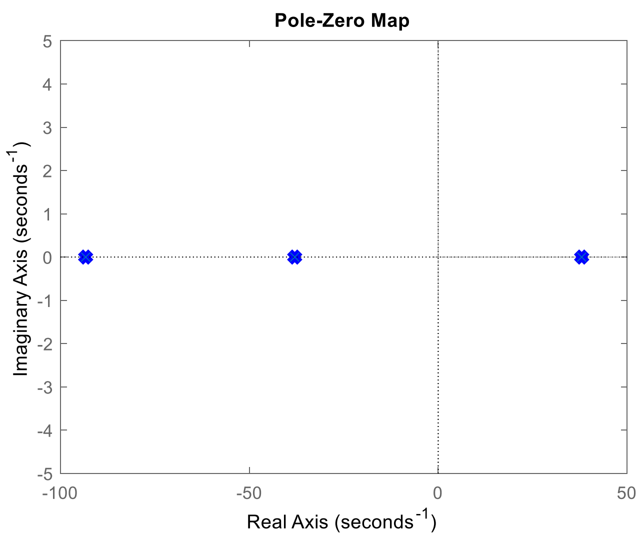

Figure 3.8. Poles of the Transfer Function

3.5.1. Power gain

To establish a dynamic model of the entire system, it is important to know the relationship between the control signal from the controller and the average voltage in the coil. In Figure 3.9 the block diagram that relates various variables through transfer functions is shown.

Basically, in the microcontroller the control signal u(t) is calculated. this value is then transformed into the equivalent in the form of a square wave which is modulated by a pulse width (PWM) when performing the conversion $D_{pwm}=u(t)\frac{1000}{4950}$, where D_{pwm} is the duty cycle of the PWM signal, and 1000/4950 is the control signal conversion factor u(t) of the duty of the PWM signal, D_{pwm} (1000 equals to 100% duty cycle in the microcontroller, and 4950 equals the maximum voltage control).

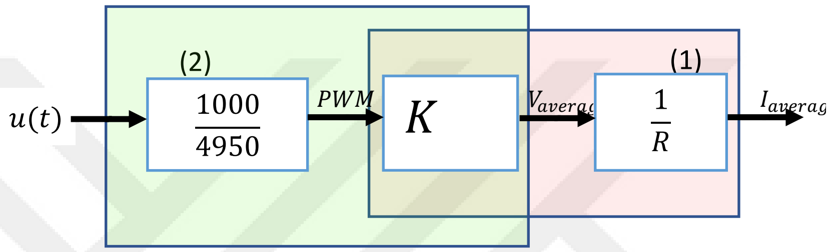

Figure 3.9. Block diagram for various system signals, (2) The relation between PWM and average current, (1) The relation between controller output and average voltage.

Now, the duty changes of the PWM signal at average current are modulated by the product of the transfer functions within the box (1), that is, K and 1/R, where K is the transfer function that models the change of duty cycle to an average voltage, and 1/R models the change of average voltage to average current.

The value 1/R (Ohm's law) has been taken as a transfer function between average current and average voltage for two reasons: these are measured values in a steady state (for a fixed duty cycle), so the measurement already includes the effect inductive, and, since $\tau = RL \gg T_{pwm}$ (that is, the time constant RL is much greater than the switching period of the PWM signal), it is possible to model the electrical circuit of the magnetic levitation system with a linear average model to analyze the temporary response of the system [45].

Additionally, the Ohmic relationship has been experimentally verified. From Figure 2.8 it is known that the transfer function that describes the changes of average current, before changes in the duty cycle, is $G_1 = 0.0668\frac{A}{D_{pwm}}$, and expressing the percentage in real form is $G_1 = 6.8\frac{A}{D_{pwm}}$. In this way, the equivalence given in Equation (3.37) is obtained.

$$K\frac{1}{R}=6.68 \tag{3.37}$$

Given the resistance R=14 Ohm for the solenoid, the constant K is found according to Equation (3.37) as follow K=6.68 R; K = 18.88.

Therefore, the power gain (that is, the relation between changes in the control signal and changes in the control voltage), is given by the product of the transfer functions that describe the change of control signal to duty cycle PWM, and from the latter to control voltage, as shown in Equation (3.38).

$$G_v=\frac{1000}{4950}K=\frac{1000}{4950}18.88 = 3.814 \tag{3.38}$$

3.6. Dynamic System

The block diagram representing the dynamic magnetic levitation system is shown in Figure 3.10.

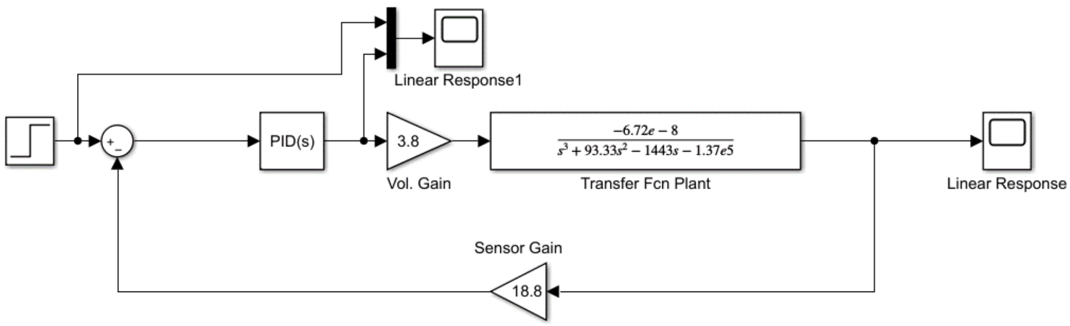

Figure 3.10. Block diagram representing the magnetic levitation system

The current position of the object is read by a distance sensor and converted to a voltage signal, directly related to the actual position of the object. The sensor transfer function is $\frac{v_s(s)}{X(s)} = -2500\frac{V}{m}$ for a position of 11.2 mm approximately. This position signal in the form of a voltage is subtracted from a reference voltage value, which is the n-shaped representation of the chosen linearization position (11.2 mm). In this way the error signal is obtained, which enters the PID controller (Proportional-Integral-

Derivative) that will be explained in detail in the next chapter. A control signal u(t) is the output from the controller, this signal is amplified by a power gain, and represents the transfer function that is related to the changes in the solenoid voltage and the changes in the control signal $G_V=\frac{V(s)}{u(s)}=6.68$, obtained in Section 3.5.1. This amplified signal is the control voltage of the magnetic levitation system.

This control voltage is the input signal of the plant, which was described in detail in Sections 3.1, 3.2, and 3.3. The output of the plant is the real position of the object x(t). This position is sensed again and converted to an equivalent voltage, repeating the control cycle in order to obtain stability. Thus, it has a feedback control system whose purpose is to keep levitating in the air an object of ferromagnetic material in a desired position.

3.7. Model of Laboratory Magnetic Levitation System

In the magnetic levitation system, a steel ball with a diameter of 20 mm and a mass of 28.3 g was used. This ball is under the influence of three forces: the magnetic force, the gravitational force acting downwards and the damping force which acts in a direction opposite to the velocity at any instance of time. The control of these three forces results in a vertical damping movement and variable in time, which allows the ball to enter the state of suspension in the air.

Preliminary tests were carried out in the laboratory in order to determine the magnetic field (T) produced by the electromagnet in relation to the current that flows through the maglev system, in the test, the airgap represents an important factor in tracing the path of the magnetic flux while there are variations in distance, temperature and time.

The airgap was taken into account because it permits to observe the variation of the electromagnetic force related to the movement of the ball to be levitated. For the data capture, 5 current levels were defined from 1 to 5 A, for each current level the ball was moved from the setpoint test defined downwards on the Y axis 1 mm at a time until completing 10 mm.

In order to capture the data optimally two tests were executed one of them at 25 °C and the another one at 100 °C, at the beginning of each test the conditions should be maintained the same values regarding temperature, the position and hall effect sensors. In order to validate the data captured by the HES in the magnetic levitation system, ANSYS Maxwell software was used to carry out simulations under the same parameters used in the plant model.

The Gap and current relationship given in millimeters [mm] and amperes [A] respectively; temperature, an interval of 2 to 10 mm for the gap and a current of 1 to 5 A are the parameters defined in the tests. The first test corresponds to the plant model, Table 3.4 and Table 3.5 show the data obtained by performing the test at a temperature of 25 °C and 100 °C.

Table 3.4. Experimental data at room temperature (25°C)

Gap/Current	2mm	4mm	5mm	8mm	10mm
1	0.394	0.226	0.209	0.145	0.119
2	0.658	0.4	0.367	0.26	0.216
3	0.79	0.5	0.454	0.333	0.28
4	0.887	0.575	0.527	0.388	0.328
5	0.995	0.628	0.577	0.427	0.367

Table 3.5. Experimental data at room temperature (100°C)

Gap/Current	2mm	4mm	5mm	8mm	10mm
1	0.392	0.220	0.19	0.119	0.089
2	0.638	0.384	0.326	0.215	0.168
3	0.763	0.480	0.415	0.279	0.224
4	0.852	0.553	0.477	0.325	0.263

In Figure 3.11 and Figure 3.12 the performance of the magnetic field produced by the electromagnet is shown when the current and the distance of the ball increase.

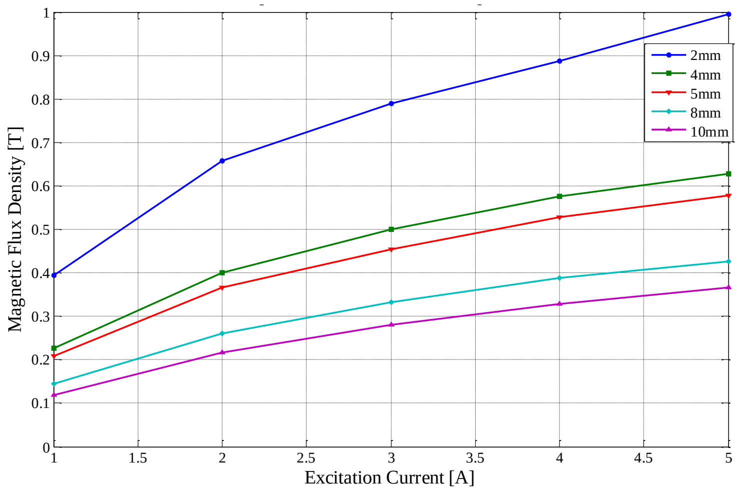

Figure 3.11. Graph of experimental data from maglev system at room temperature (25°C)

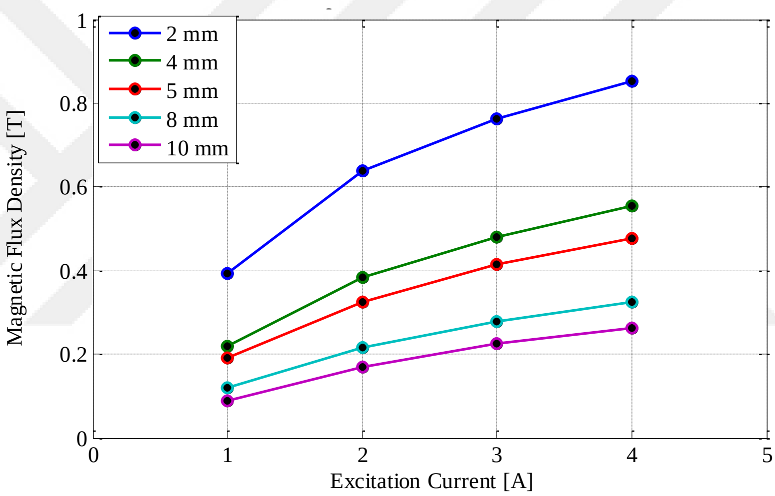

Figure 3.12. Graph of experimental data from maglev system at room temperature (100°C)

The second test was run using ANSYS Maxwell electromagnet simulation software, for a temperature of 25 °C and 100 °C, the Table 3.6 and Table 3.7 shows the data obtained through the simulation, the other parameters are left unchanged.

Table 3.6. ANSYS Maxwell simulated data at 25°C

Gap/Current	2mm	4mm	5mm	8mm	10mm
1	0.492	0.253	0.203	0.127	0.102
2	0.784	0.472	0.387	0.248	0.2
3	0.915	0.575	0.482	0.324	0.265
4	1	0.649	0.549	0.374	0.309
5	1.08	0.707	0.599	0.414	0.342

Table 3.7. ANSYS Maxwell simulated data at 100°C

Gap/Current	2mm	4mm	5mm	8mm	10mm
1	0.490	0.246	0.185	0.104	0.076
2	0.760	0.453	0.344	0.205	0.156
3	0.884	0.552	0.441	0.271	0.212
4	0.961	0.624	0.497	0.313	0.248

In Figure 3.13 and Figure 3.14 the behavior of the magnetic field of the simulation performed in ANSYS Maxwell software is shown.

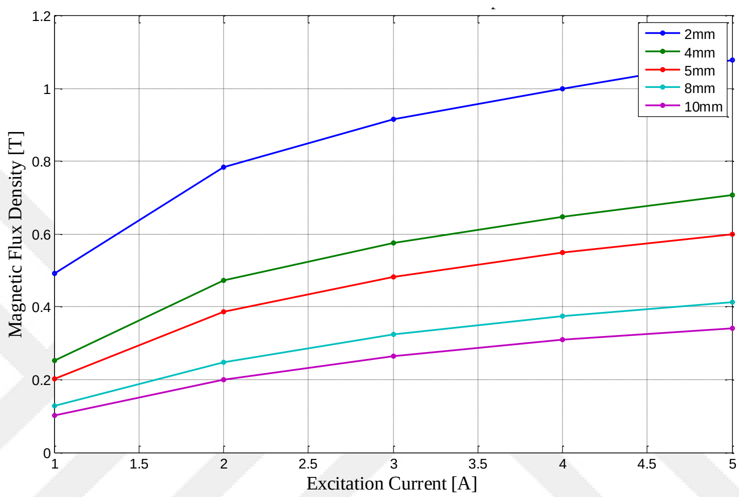

Figure 3.13. Graph of ANSYS Maxwell simulated data at 25 °C

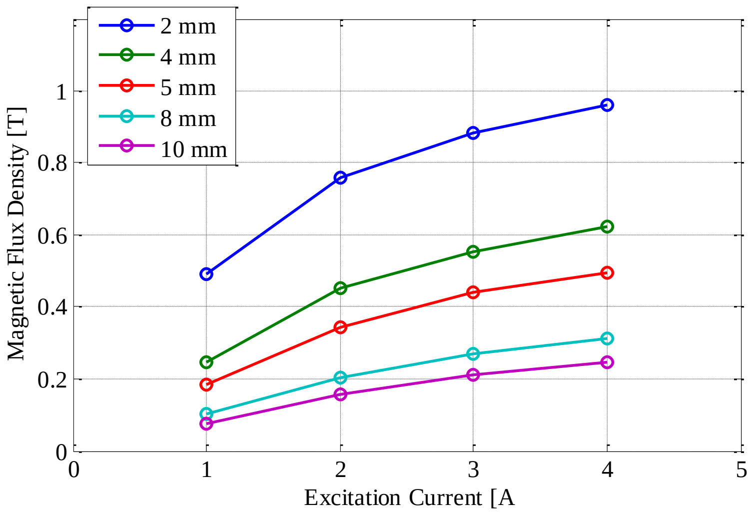

Figure 3.14. Graph of ANSYS Maxwell simulated data at 100 °C

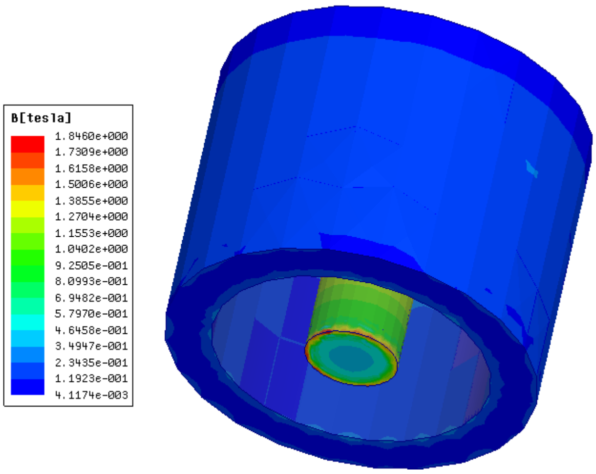

Figure 3.15. 3D-FEA model of core magnetization

If we make a comparison of the data obtained from the simulation as well as in the magnetic levitation system, for example at room temperature when the ball is located at 2mm from the core and there is a current of 4A, the magnetic field produced by the electromagnet is of 0.887 T, in comparison with the data of the simulation under the same characteristics, the magnetic field produced is 1T.

This means that the results of the performance in the magnetic levitation system is slightly lower than what the simulation results show, however, to adjust the accuracy the position of the sensors is improved as well as their calibration.

3.7.1. Hall effect sensors on maglev system

Figure 3.16 shows the set of sensors used in the magnetic levitation system. In the maglev plant we have two of the three hall effect sensors called A0 and A1, as well as a transducer current sensor to sense the quantity of flow current through the system and thermocouples which are going to detect the temperature when the plant is working.

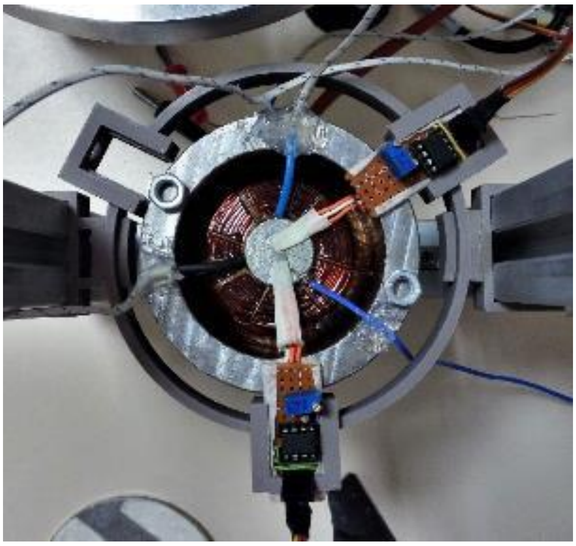

Figure 3.16. Hall effect sensors on Maglev system

For every sensor excluding the current transducer sensor, an electronic circuit (PCB) was designed with the aim to collect all the data delivered by these set of sensors located on the plant afterwards those data will be stored and processed. A DAQ USB-6009 Multifunction I/O Device from National Instruments was used as a physical interface for data recording between the maglev system and the PC.

The current sensor is of the transducer type (LTS 6-NP) see Figure 3.17, which has important features such as high accuracy, sensitivity, optimized response time and high immunity to external interference; With a current working capacity of up to 6A It has its own embedded circuit for the transduction of the sensed signal and a digital output that can be connected directly to the DAQ card, which makes it ideal for use in the project.

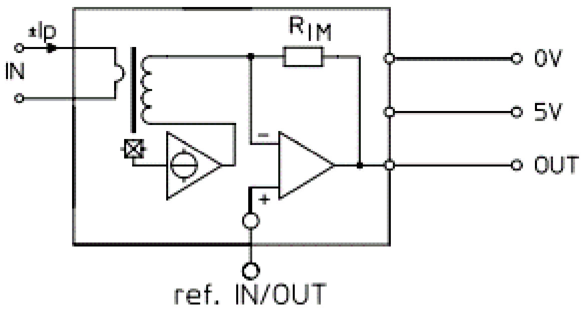

Figure 3.17. Current Transducer LTS 6-NP

In the case of hall effect sensors, an amplifier circuit was built, see Figure 3.18, which allows obtaining a measurable signal with a maximum input-output ratio gain of 20x.

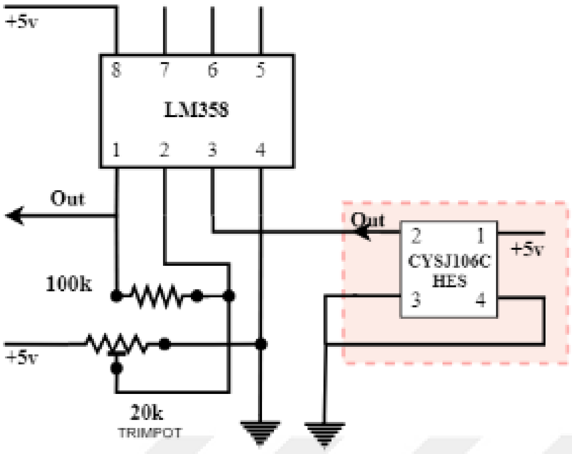

Figure 3.18. Diagram of amplifier circuit for hall effect sensor

In Figure 3.19 shows the built-in PCB circuit. To accommodate these sensors near the core, a special socket designed and printed in 3D was developed.

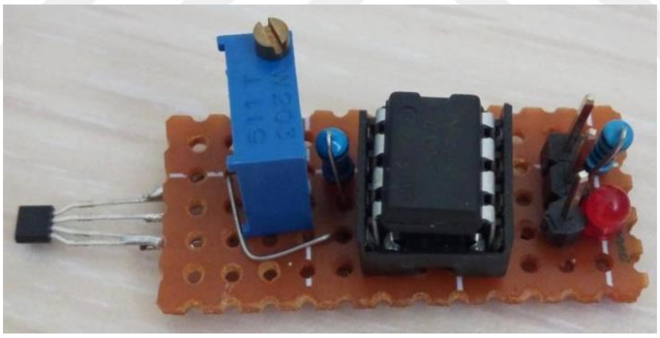

Figure 3.19. PCB amplifier circuit module of hall effect sensor

K-type thermocouples were used to measure core temperature variation, mainly because they offer a rapid response in terms of the variation of environmental conditions where they are located, unlike the LM35 integrated circuit, which has a high response time of offset. For this an operational amplifier circuit was designed using an OPAM LM358 (Figure 3.20 and Figure 3.21) to operate the voltage signal coming from the thermocouple.

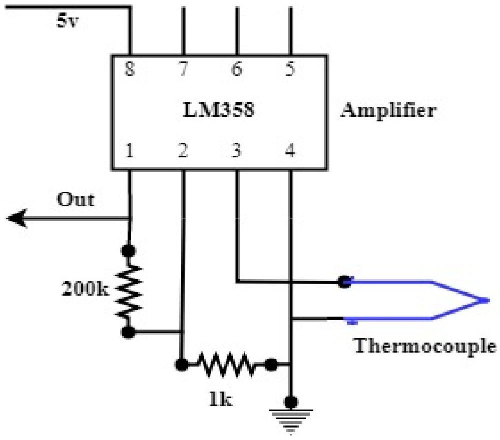

Figure 3.20. Scheme of the OPAM LM358 for thermocouple signal

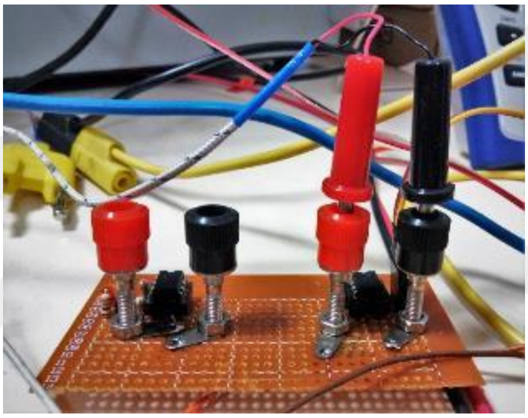

Figure 3.21. PCB circuit of the OPAM LM358 for thermocouple

Once all the sensors were located in their corresponding socket in the plant, their interfaces for the acquisition of the data were connected, and the data were obtained; Figure 3.23 shows the results captured from two hall effect sensors called A0 and A1. In this test the electromagnet was configured with 1A of current and an airgap interval of 10mm on the Y axis, the movement up and down of the ball was made by a mechanism which has a micrometer to fix the airgap from the electromagnet, this mechanism can be assembled on the structural basis of the maglev system to perform the tests (see Figure 3.22).

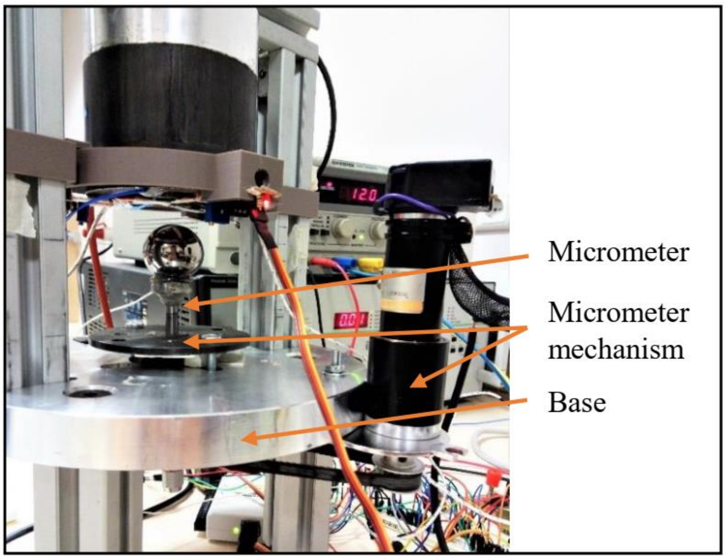

Figure 3.22. Micrometer and movement mechanism

A frequency of 0.02 Hz was used in the tests; furthermore. As expected, during the time that the test is conducted (around of 7 minutes), the current flowing through the plant causes an increase in temperature in the coil of the electromagnet by 6 °C, which is not a big increase because the working current is only 1 A and this does not cause thermal fatigue in the system.

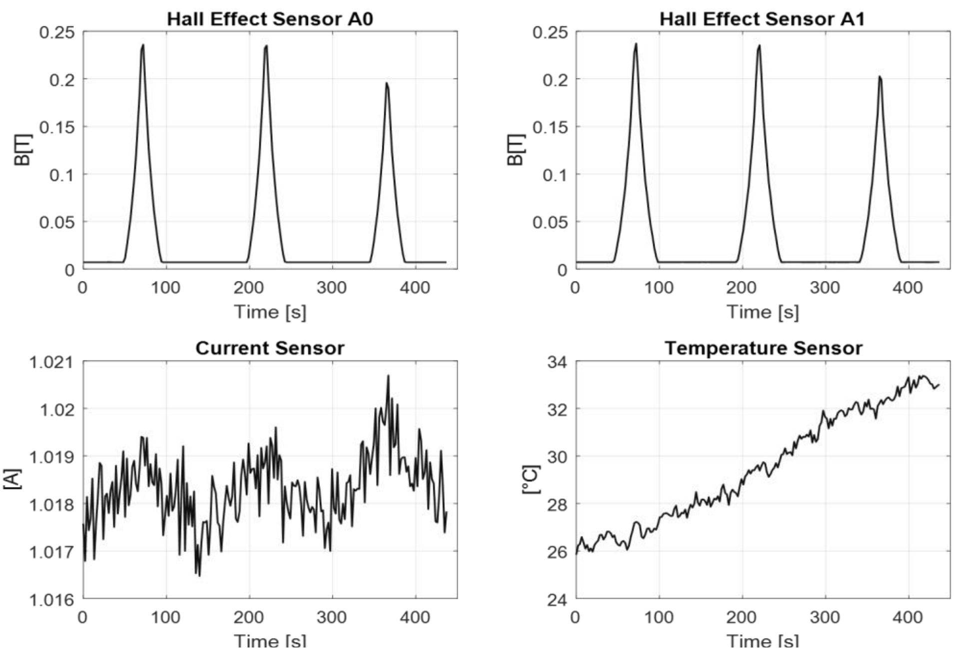

Figure 3.23. Data obtained in the response test at 0.02 HZ frequency and 10mm airgap

3.7.2. Variation in temperature

The maglev system has been configured with all necessary elements as shown in Figure 3.24, which has 3 hall effect sensors, a thermocouple to detect the increase in temperature, and a transducer to measure the current that passes through the system.

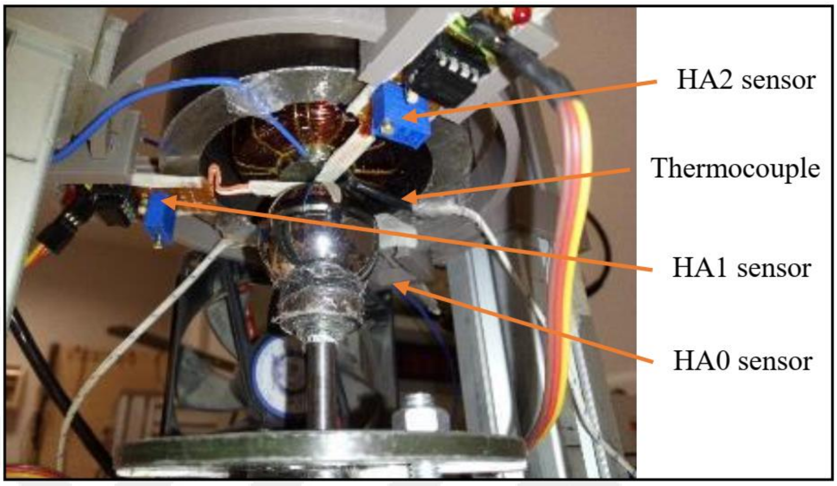

Figure 3.24. Configuration of hall effect and thermocouple sensors on maglev system

As defined variables, the coil of the electromagnet is provided with a maximum voltage of 30 vdc and a current up to a maximum of 4 A in order to obtain a satisfactory performance, taking into account the harmful effect that the increase in temperature can have on the electromagnet. The current intensity was varied in steps of 0.5A per each interval of time, the data obtained are as seen in Table 3.8.

Table 3.8. Data obtained through the sensors located in the maglev system

Dist,[mm]	Time[s]	Amp[A]	HA0[T]	HA1[T]	HA2[T]	Temp[°C]	Vol [v]
25	0.033	1.5	0.13	0.05	0.16	30.91	8.29
25	0.067	1.55	0.24	0.10	0.24	30.91	8.79
25	0.1	1.6	0.30	0.15	0.28	31.08	9.08
25	0.133	1.65	0.36	0.20	0.31	31.08	9.37
25	0.167	1.7	0.45	0.27	0.37	31.82	9.71
25	0.2	1.75	0.50	0.31	0.41	31.98	10.02
25	0.233	1.8	0.56	0.36	0.45	31.26	10.35
25	0.267	1.85	0.61	0.40	0.49	31.19	10.67
25	0.3	1.9	0.67	0.44	0.52	31.37	11
25	0.333	1.95	0.72	0.48	0.56	31.80	11.3
25	0.367	2	0.77	0.53	0.59	32.49	11.6

Table 3.8. (Continue) Data obtained through the sensors located in the maglev system

Dist. [mm]	Time[s]	Amp[A]	HA0[T]	HA1[T]	HA2[T]	Temp[°C]	Vol. [v]
25	0.4	2.05	0.82	0.57	0.63	32.77	11.96
25	0.433	2.1	0.87	0.61	0.66	33.10	12.3
25	0.467	2.15	0.92	0.65	0.69	33.36	12.66
25	0.5	2.2	0.97	0.69	0.72	33.37	13.04
25	0.533	2.25	1.01	0.72	0.76	34.12	13.39
25	0.567	2.3	1.05	0.74	0.79	34.89	13.76
25	0.6	2.35	1.09	0.77	0.82	35.43	14.14
25	0.633	2.4	1.14	0.81	0.85	36.02	14.48
25	0.667	2.45	1.18	0.84	0.87	36.56	15.3
25	0.7	2.5	1.22	0.88	0.90	37.12	15.7
25	0.733	2.55	1.26	0.92	0.93	37.72	16.12
25	0.767	2.6	1.28	0.95	0.96	38.46	16.25
25	0.8	2.65	1.30	0.98	0.99	38.84	16.44
25	0.833	2.7	1.32	1.01	1.01	39.22	17.12
25	0.867	2.75	1.33	1.04	1.04	39.60	17.61
25	0.9	2.8	1.35	1.06	1.06	40.45	18.1
25	0.933	2.85	1.37	1.09	1.09	41.19	18.57
25	0.967	2.9	1.39	1.12	1.11	41.78	18.85
25	1	2.95	1.40	1.14	1.14	42.93	19.3
25	1.033	3	1.42	1.17	1.16	43.43	19.9
25	1.067	3.05	1.44	1.20	1.19	44.20	20.41
25	1.1	3.1	1.45	1.22	1.21	45.32	20.95
25	1.133	3.15	1.47	1.24	1.23	46.53	21.5
25	1.167	3.2	1.48	1.26	1.26	47.42	22.07
25	1.2	3.25	1.50	1.28	1.28	48.47	22.66
25	1.233	3.3	1.51	1.30	1.30	49.89	23.4
25	1.267	3.35	1.53	1.33	1.32	51.45	24
25	1.3	3.4	1.54	1.34	1.34	52.95	24.71
25	1.333	3.45	1.55	1.36	1.36	54.56	25.3
25	1.367	3.5	1.57	1.38	1.38	56.03	26.3
25	1.4	3.55	1.59	1.42	1.42	57.56	27.01
25	1.433	3.6	1.60	1.44	1.44	59.15	27.7
25	1.467	3.65	1.61	1.45	1.46	60.69	28.83
25	1.5	3.7	1.64	1.49	1.50	62.50	29.53
25	1.533	3.75	1.66	1.53	1.53	64.87	29.96
25	1.567	3.8	1.66	1.54	1.52	66.53	29.96
25	1.6	3.85	1.67	1.55	1.52	68.18	29.96
25	1.633	3.9	1.65	1.53	1.50	69.33	29.96

Once the data is obtained, we can observe the results plotted in Figure 3.25; In this case the steel sphere remains in static position at 25 mm from the end of the electromagnetic core, as the current increases gradually the magnetic flux also increases. In optimal conditions, where there are no losses by hysteresis or temperature, an average magnetic flux of 1.6 T is reached at a maximum current of 3.9 A. It should be noted that the effect caused by the high temperature generates an increase in the reluctance of the coil causing the power of attraction to be decreased.

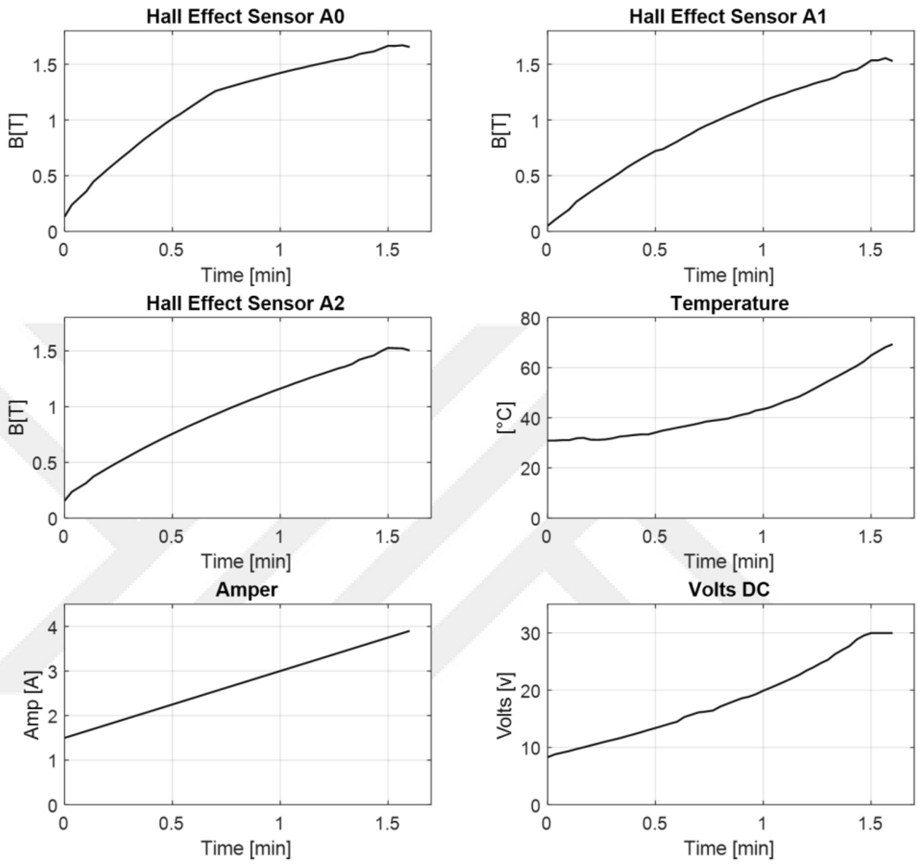

Figure 3.25. Temperature effects over the magnetic strength of the maglev system

3.8. Behavior of the Magnetic Levitation System

Magnetic levitation systems present a problem of non-linearity due to multiple variables that affect them such as temperature, distance (Airgap), and the geometry of objects to be levitated, and according to the position of the objects the inductance in the coil is also affected; Figure 3.26 shows the best performance of the system in terms of stability, linearity for magnetic force values (B), acceptable temperature, and lower temperature losses.

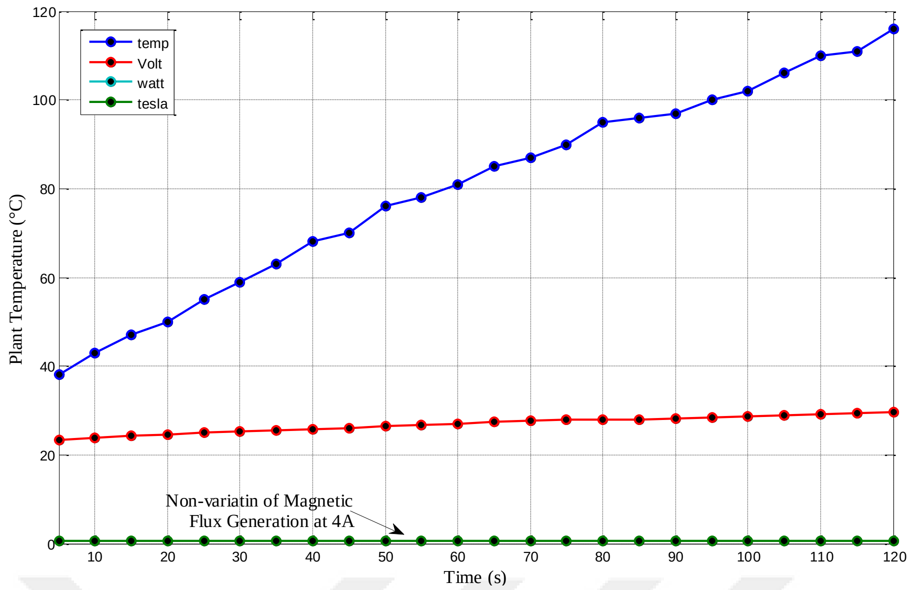

Figure 3.26. Magnetic Flux behavior according to temperature, current and tesla parameters

3.8.1. Determining the best conditions

This test system has been evaluated for a given period of 2 minutes, with the constant current values 4 A and a distance of 0.4 mm from the end of the main tooth to the position of a steel sphere of 30 mm in diameter. With these values an average of 0.506 T of magnetic flux was obtained. During the test, its maximum temperature was 116 °C, and the quantity of watts reached has been taken into account in the following values:

Table 3.9. Measurement result at 4A and 4mm from the electromagnet center

Time (Min)	Max Temp °C	Average Mag. Flux (T)	Watt
2	116	0.506	119

4A to 4mm from the center of core

3.8.2. Evaluation of obtained data

At this point the tests were carried out using a stainless-steel sphere positioned to 1mm below the electromagnet core, it was configured so that in each test the data related to the distance from the initial position of 1mm, and the successive displacements are captured After 5 mm each, for each displacement parameter the amount of magnetic flow (T) and temperature °C was captured.

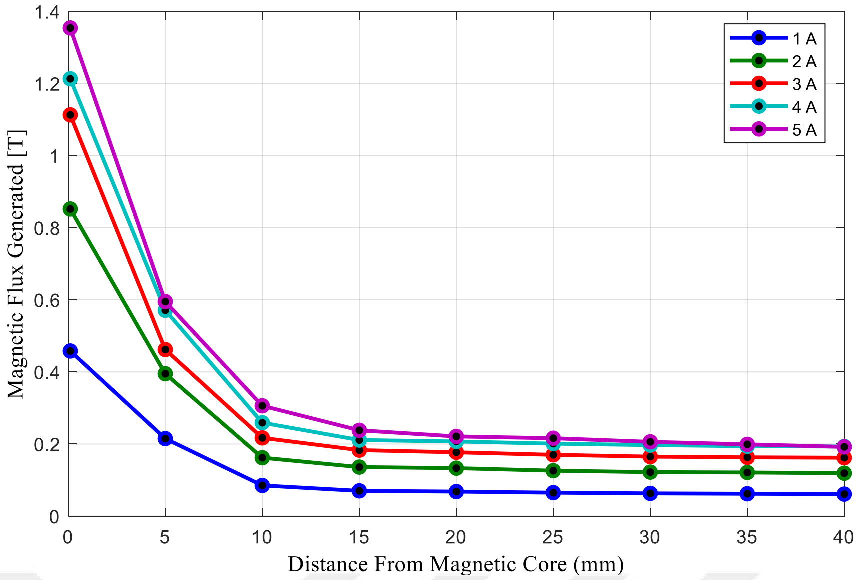

Figure 3.27. Variation of magnetic flux vs distance

Figure 3.28 a) shows the magnetic flux produced in a 4 mm airgap. This test is interesting because it allows to define that maximum 4 A is the appropriate measure for the magnetic levitation system to operate without experiencing variation or loss of magnetic force [B]. It should be noted the increase in temperature in the coil, which as shown in Figure 3.28 b) because of the time and current flow the electromagnet dramatically increases its temperature.

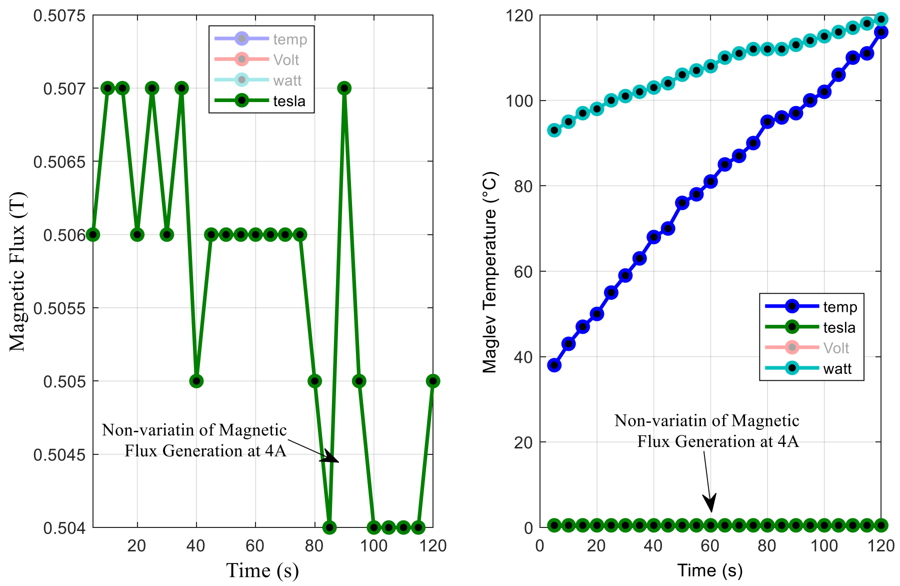

(a) (b)

Figure 3.28. a) Magnetic Flux Close up laid with 4A and 4mm airgap, b) The temperature and power consumption effect on maglev system

The test was carried out again, but in this case, it was configured with 5 A of current and a 4mm airgap, obtaining unfavorable results, see Figure 3.29 a). This is due to an abrupt increase in temperature, and in a short period of time it causes an increase of the reluctance in the coil and therefore lower work efficiency related to the magnetic flux in the system, see Figure 3.29 b).

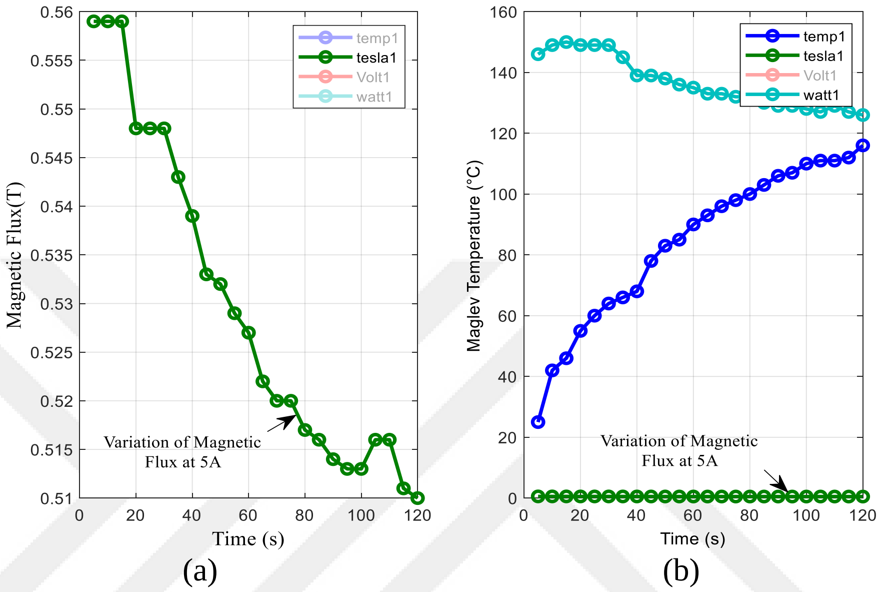

Figure 3.29. a) Magnetic flux close up laid with 5A and 4mm airgap, b) Temperature increases and power drop on the maglev system

3.8.3. Air gap variations

In order to evaluate the behavior of the sphere by performing vertical movements in a distance (Airgap) of 10 mm different frequencies have been used. The sphere has been attached to the rod of a micrometer in order to achieve the vertical displacement, Moreover, the micrometer movement being performed ball bottom up and vice versa in a range of 25 mm.

Tests have been carried out in the system using different current intensities. Figure 3.30 shows the density of the magnetic field measured in Tesla (T) on the Y-axis and the elapsed time on the X-axis, for this test 1.75A has been used, the closest approach reached by the sphere to the core of the electromagnet is 3mm, arriving at this point, we obtain the greatest attractive force 0.34T produced the magnetic field strength.

The generated displacement is within a range of 10 mm on the vertical axis; in the test, an DC motor and an encoder provided the necessary data to perform the displacement and locate the position of the ball in relation to time, the steel ball was linked to a micrometer to perform upward and downward movements. The intensity of the magnetic field is measured by hall effect sensors, two units named HES_A0 and HES_A1, Figure 3.30 shows the magnetic field strength obtained during vertical movement for 4 types of frequencies over a period of time.

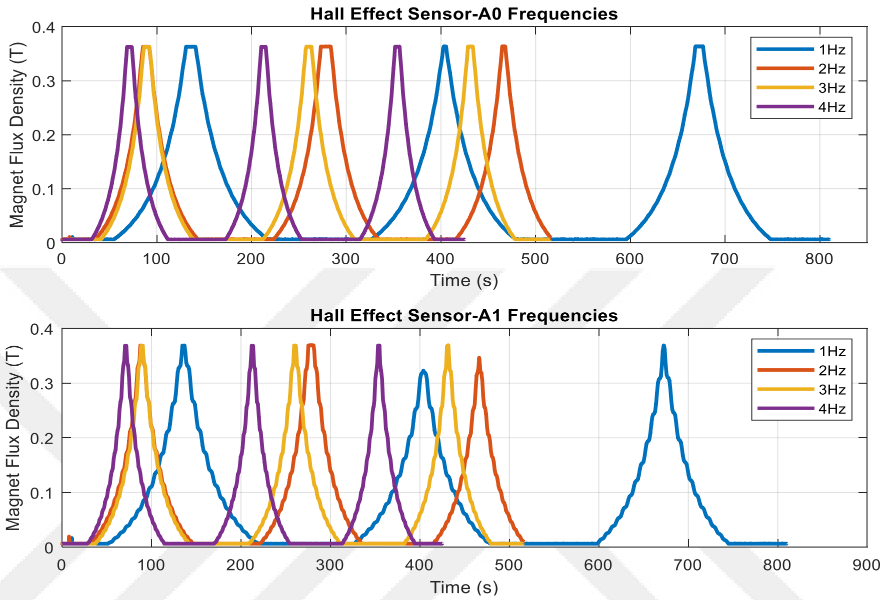

Figure 3.30. Hall effect sensor HES_A0 and HES_A1 responses at different frequencies

3.8.4. Power stage

The power stage that provides the necessary energy to the actuator has a control by pulse width modulation (PWM). For this a discrete MOSFET H-Bridge driver is used that allows us to perform the frequency control by varying the pulse and thus that way the sphere runs up and down. Its maximum working voltage is + 30V to 15A.

Figure 3.31. Top view of the MOSFET H-Bridge High-Power Driver 30v15

3.8.5. Frequency variation using a pneumatic system

To verify if the hall effect sensor responds to different frequencies which are relative to the vertical movement cycle of the steel sphere, it was necessary to configure an alternate pneumatic system see Figure 3.32 the aim of the system is to generate frequencies in a range from 1 hz to 18 hz.

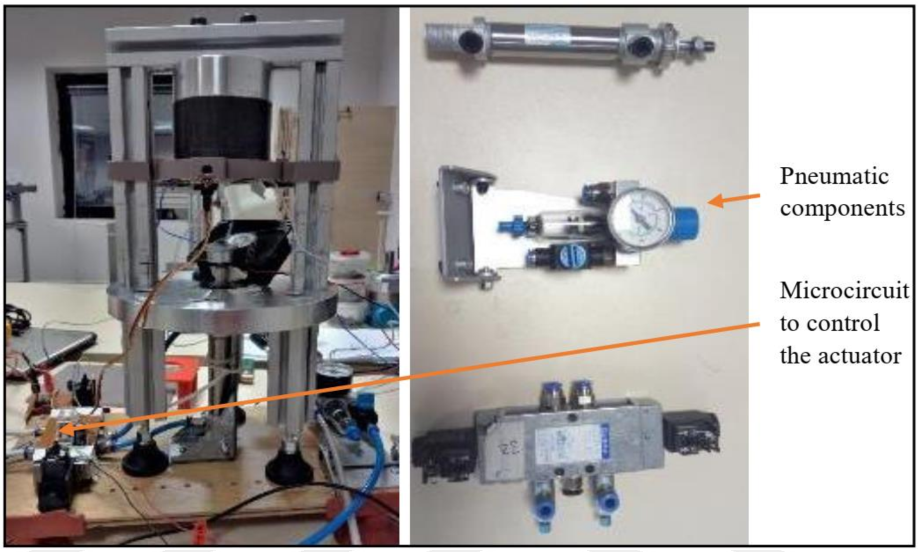

(a) (b)

Figure 3.32. a) Alternate pneumatic system, work frequency interval at 1-18hz, b) Main pneumatic components

Due to the work cycles being too short and the level of precision the switching operation required, an alternate pneumatic system was implemented with a 5-way pneumatic solenoid valve and was used to generate the up/down cycle for the piston of the pneumatic cylinder. The steel sphere was attached to the end of the piston, and the outlet pressure of the reservoir unit was set at 4 bar, which ensured a fluid movement according to the required frequency. In this way, the alternate pneumatic system was used utilized to precisely control the movement of the ball, while the data of the magnetic flux and the time response was obtained.

The solenoids of the pneumatic valve are connected and fed directly to the 24vdc outputs of the relay coils. To operate the system, initially a + 5vdc and 0vdc signal called status signal is sent from the control card (see Figure 3.33 a)) to each of the control pins of the relay coils that is located in the microcircuit (see Figure 3.33 b)). This configures each of its coils with + 24Vdc (Right-ON) and 0V (Left-OFF). When this happens, the pneumatic valve allows the flow of air in the forward direction, and according to the frequency programmed in the control card, the switching cycle (ON / OFF) on the relay will change the status signal on the control card from + 5vdc to 0vdc in thousandths of a second.

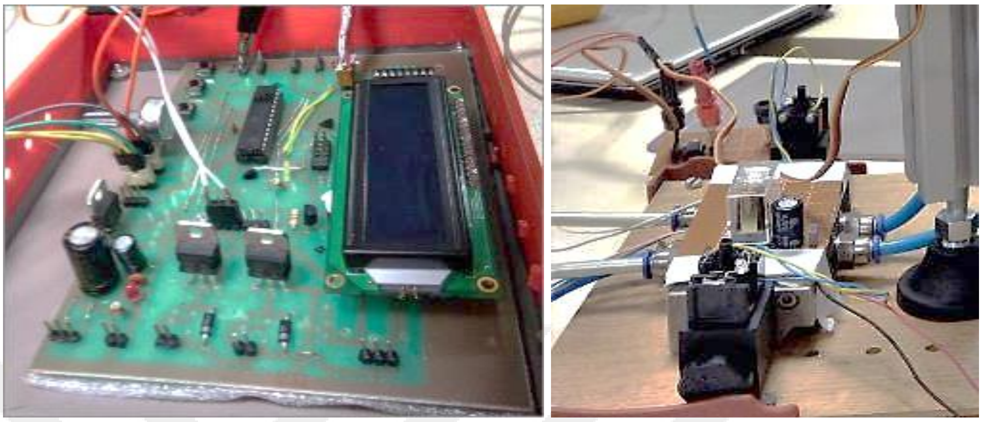

(a) (b)

Figure 3.33. a) Data acquisition card (DAQ), b) Microcircuit to commute the electropneumatic valve

3.8.6. Outputs of the alternate pneumatic system

The first data were obtained in a frequency of 6 and 8 hz, Figure 3.34 allows to see how the cycle of movement up and down in the y-axis was generated by the pneumatic system, in these frequencies the displacement of the object to be levitated is around 1.8 mm for 8 hz and 0.4 mm for 6 hz in a time interval of 6.5 s

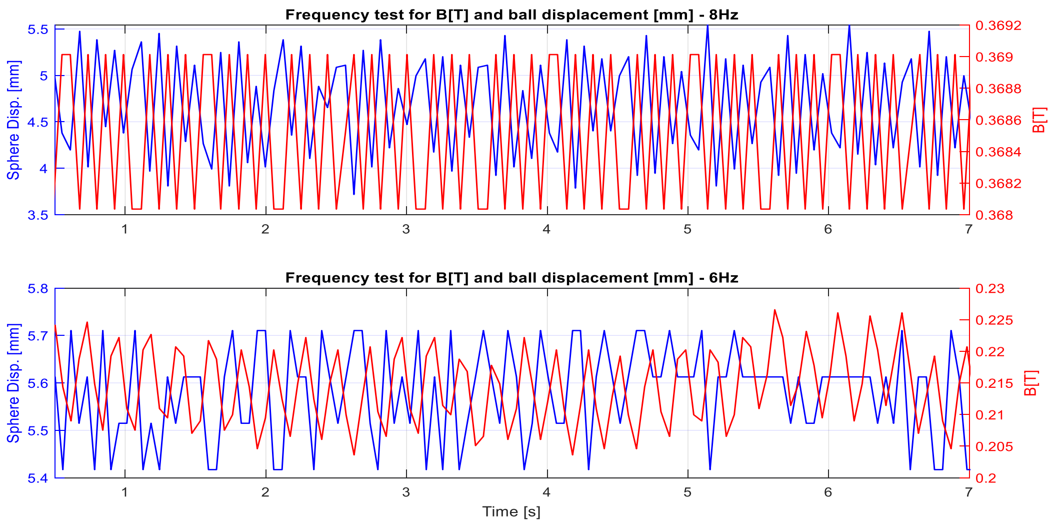

Figure 3.34. Frequency test in 6hz and 8hz data obtained by the alternate pneumatic system

The signal that is used to control the solenoids of the pneumatic system is generated by means of a special electronic control card which has an interface to the PC which allows us to reprogram instructions for the microcontroller to run through the output ports. A microcircuit is also used to activate the solenoids of the pneumatic valve with a status signal.

3.8.7. Frequencies variations using servomotor system

Another alternative system used in the MagLev system is that which is constituted of mechanical mechanisms and is used to control the work cycle (up/down) for the movement of the steel ball. The performance of the hall effect sensor was also verified in conditions related to the variation of reluctance, magnetic flux and temperature, which increases gradually due to the flow of current through the electromagnet coil and the reciprocating movement of the object to be levitated on the Y axis. Figure 3.35 shows the mechanism assembled and in operation with the maglev system. For the respective tests, the mechanical system was built using the following elements: a micrometer, a cogwheel designed and printed on the laboratory's 3D printer, a servomotor-encoder and a toothed belt to transmit the sinusoidal movement from the motor to the mechanism of the micrometer.

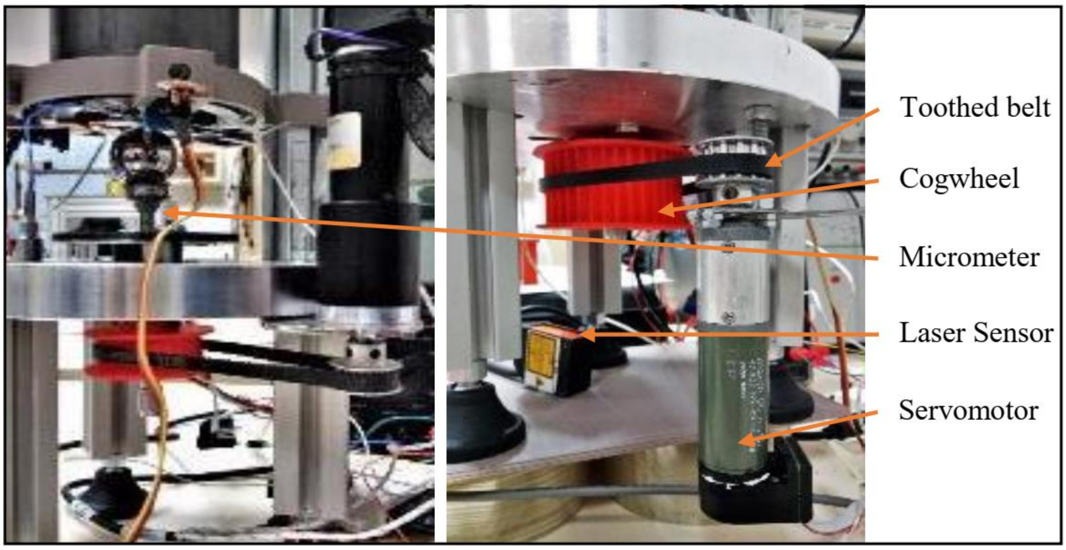

Figure 3.35. Servomotor mechanism attached to the maglev system to generate the up/down movement

The servo motor obtains the signal pulse through a double-channel encoder with a resolution of between 96 and 1024 counts per revolution. A pulse width modulation

(PWM) signal, a 5 V supply voltage and a pin to apply a pulse train are generated. We use the micrometer fixture to both position the steel sphere and for calibration and force-current relationship measurements.

3.8.8. Outputs of the alternate servomotor system

As show in Figure 3.36, The results obtained using the servomotor mechanism provide adequate data for the displacement of the ball and to measure the variation that occurs in the magnetic field with respect to its movement. A disadvantage found when using this mechanism is the frequency of the work cycle which is not higher than 1 Hz, however it is useful to verify the response of the hall effect sensors when the ball is moved up / down in the magnetic levitation system.

The work cycle configuration takes place within a time range of 100 s at frequencies of 0.25, 0.33 and 0.5 Hz, dependent on the frequency of the cycle, a displacement of ball of about 4, 2.3, and 1.8 mm respectively is generated; besides, as the ball approaches the nucleus of the electromagnet, the magnetic field increases. The same happens with the force of magnetic attraction on the ball; the system current for this data was set at around 1.5A, producing a magnetic flux of 0.17, 0.22 and 0.1T respectively. At the point closest to the core, the airgap between the ball and the end of the core was 3 mm.

According to the data obtained from the tests, there is no offset displacement on the part of the sensor with respect to the frequency cycle of the ball, which represents an adequate selection of the hall effect sensor to operate in the maglev system.

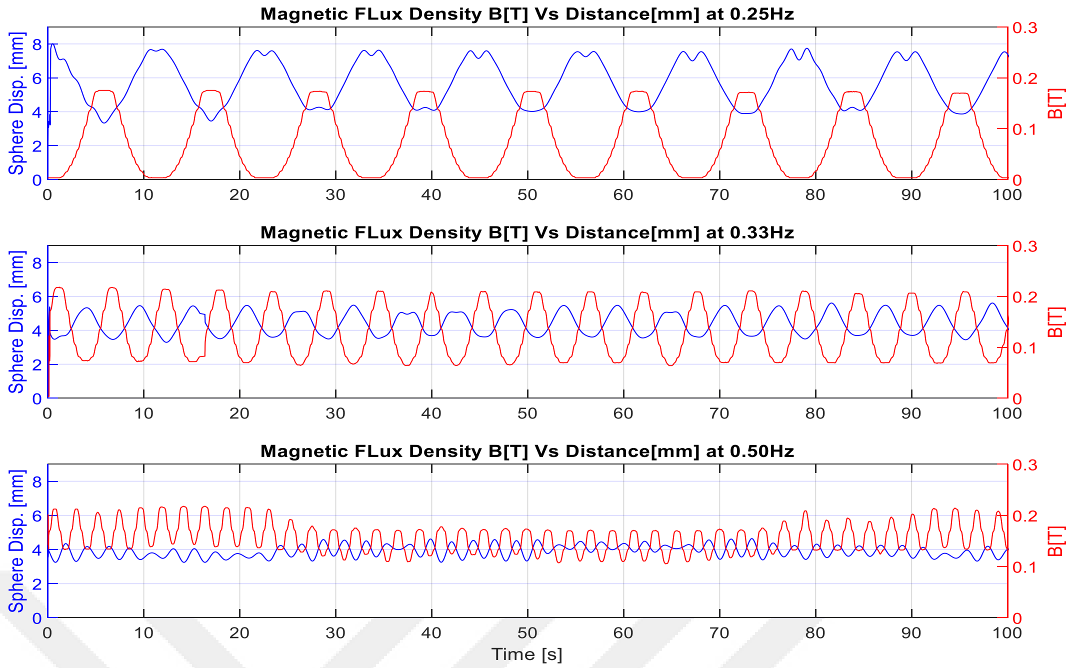

Figure 3.36. Experimental results to different frequencies for the downward-upward sphere movement using HES to capture the magnetic flux variation related to the movement

Once the experimental tests were carried out and the data from the magnetic levitation system were obtained, the hysteresis gap of the magnetic flux produced in the electromagnet was verified. Figure 3.37 a) shows a section of the data obtained in the tests, this section represents the complete cycle (up / down) performed by the ball within the magnetic field produced by the electromagnet, all parameters used are shown as follows: steel ball diameter of 25 mm, current density 2 A, residual magnetic field [B] of 0.2 T, displacement range on the Y axis 4mm, frequency of 0.25 Hz and the initial temperature of the maglev system of 27 °C.

Under these parameters, as is to be expected, the hysteresis phenomenon occurs during the operation cycle of the system, in Figure 3.37 b) it is observed that when using Somaloy700 it is almost negligible the delay in time to demagnetize the electromagnet in the absence of ball, this represents an advantage because it indicates that both the sensors and the electromagnet have good agreement in the experimental results.

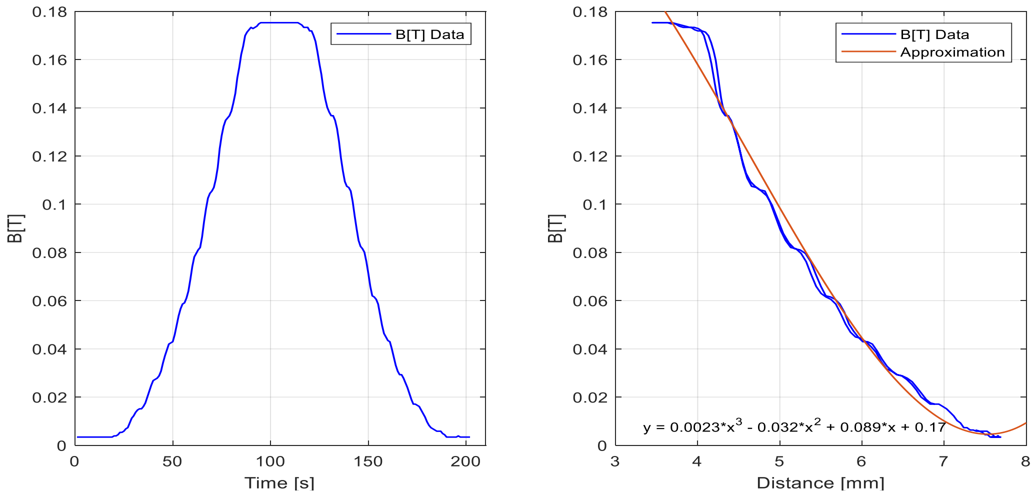

(a) (b)

Figure 3.37. a) Experimental data of magnetic flux, b) Hysteresis curve of the magnetic levitation system

3.8.9. HES signal for sinusoidal ball position

An important aspect is to verify the response behavior of the hall effect sensor called HES_A1 against the periodic signal. This signal must be registered by the set of Hall effect sensors without presenting delay or offset. In the execution of the test (see Figure 3.38), through the driver, a pulse signal is sent to the ball mechanism so that it oscillates on the Y axis at a frequency of 0.5 Hz. Also, the current of magnetic system was configured to 2 A, a 4 mm airgap and a test run time of 110 s. As result, it is observed that the HES_A1 sensor has responded accurately detecting the given periodic signal,

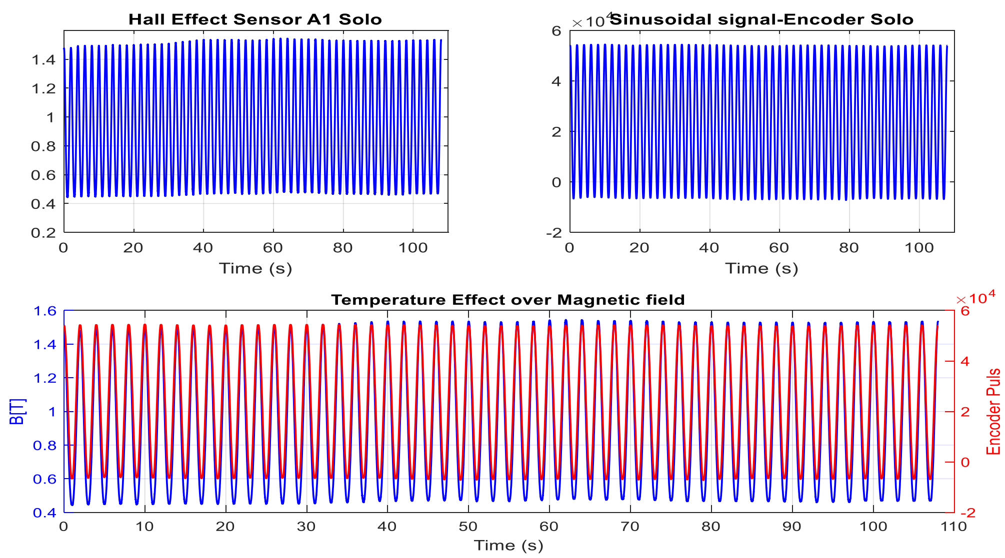

Figure 3.38. HES signal for sinusoidal ball position

3.8.10. Plant configuration

The first controlled attempt to keep the capsule suspended in the air was made by configuring the distance sensor. Depending on the distance recorded, a signal in volts is sent to the multifunction card. There, the PWM signal together with the driver device allow it to handle the current that the electromagnet needs to generate the magnetic field when the capsule is at a distance of 5 cm, and disable the flow of it when the capsule is near the core of the electromagnet. As a result, an oscillatory movement of the element to be levitated is obtained.

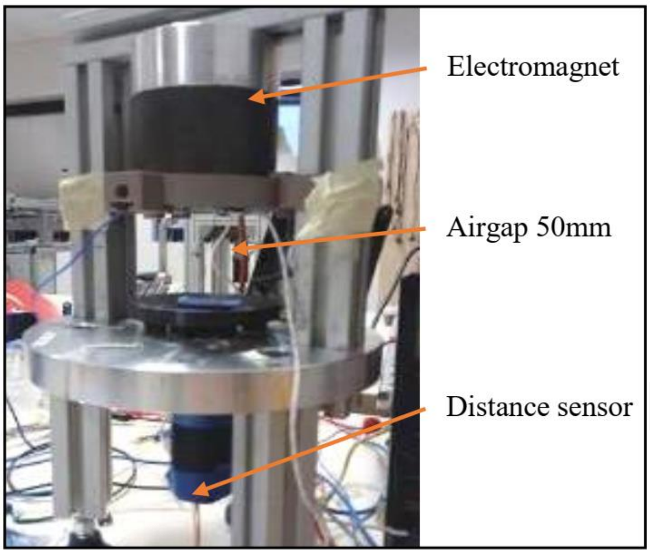

Figure 3.39. Setting Maglev system for control test

The system is operated on different frequencies in order to determine which is the most suitable, 1KHz is the operating frequency of the magnetic levitation system and the current supplied to the plant is defined in a range of 1A to 4A.

4. CONTROLLERS DESIGN

In the previous chapter, the mathematical model of the system was obtained and the block diagram representing the linear dynamic system was described. In this section, the design of a PID controller as well as a fuzzy controller are made, which meet design requirements and also allow the stabilization of the magnetic levitation system. Thus, the dynamics of the system will be analyzed and simulated to demonstrate the response of the system.

The magnetic levitation system is a nonlinear and unstable dynamic system with one input and one output [45]. The input voltage is applied to a coil that creates the electromagnetic field. The output voltage is measured by a distance sensor which represents the object position in the magnetic field. The diagram in Figure 4.1 outlines this system.

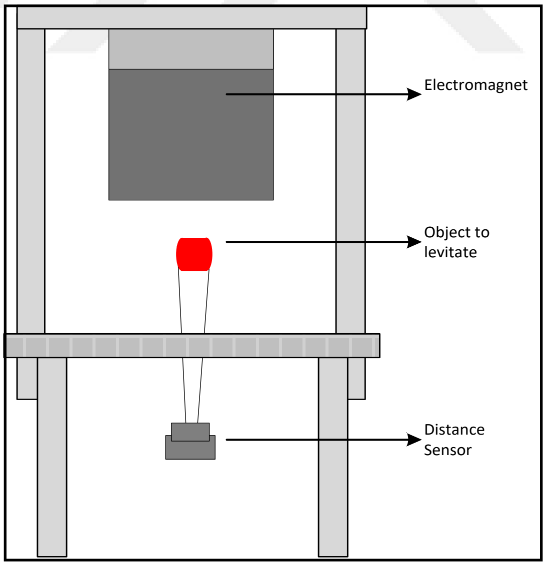

Figure 4.1. Scheme of the magnetic levitation system

The plant model (coil/ball) is controlled by two methods a Fuzzy Logic Controller (FLC) and a PID controller with feedforward with the aim to handle the non-linearity of the magnetic levitation system. The position of the ball responds to the changing value of the setpoint. Notably, in this change, the position of the capsule represents the real dynamics of the system. The physical system consists of a capsule (with mass 0,110 kg) which is under the influence of three forces: The electromagnetic force produced by the electromagnet, the gravitational force acting downwards and a damping force which acts in a direction opposite to the velocity at any point in time. The magnetic field produced by the electromagnet depends on the square of the current, the airgap between the coil and the ball to levitate, and the physical properties of the ball to levitate. By controlling these three forces the oscillating movement of the ball ends stabilizing at a given setpoint.

4.1. PID Controller

The PID controller carries out a signal which depends on the error value calculated as difference between the desired and real output system signal. If the output signal of the system is far from the reference signal, then the action control must be proportional to the error value, this action corresponds to the proportional part, which explains the $P = K_p e(t)$ operation. A control action is also required that acts upon the accumulation of the error (that is, even when the error signal becomes constant), which makes the control signal act to improve the response of the system in a steady state with tendency to the reference signal (null error), which is equivalent to the integral control action or memory action $I = K_i \int_0^t e(t)\,dt$. Finally, the derivative control action acts against changes in the output of the system over time, trying to anticipate these changes, in what is known as a predictive action $D = K_d \frac{d}{dt} e(t)$. The general form of the PID action is shown in Equation (4.1), as well as its transfer function in Equation (4.2).

$$u(t) = K_p e(t) + K_i \int_0^t e(t)dt + K_d \frac{d}{dt} e(t) \tag{4.1}$$

$$\frac{U(s)}{E(s)} = K_p + \frac{K_i}{s} + K_d s \tag{4.2}$$

The constants K_p, K_i and K_d can be interpreted as a weight that assigns a scaling to the control action according to the variation in each component of the PID controller. Also, the parameters to set the model which is executed in Simulink can be found in Annex A. As shown in Figure 4.2, the magnetic levitation system is modeled and simulated by Simulink.

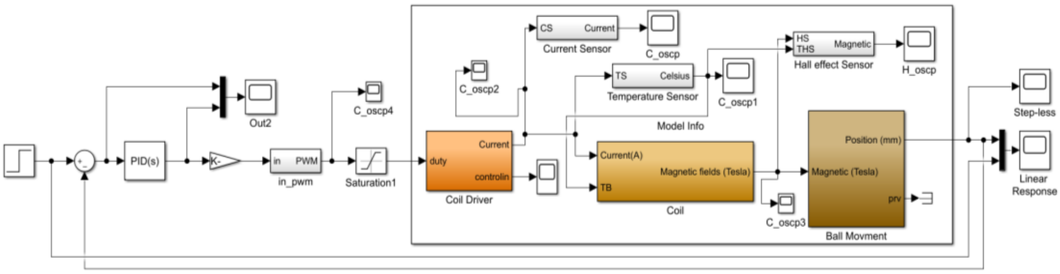

Figure 4.2. Simulink PID diagram of maglev system

4.1.1. Tuning of the PID

A proportional-integral-derivative controller (PID controller) is a generic control loop feedback mechanism widely used in industrial control systems. It attempts to correct the error between a measured process variable and a desired set point by calculating and then implementing a corrective action. The PID controller involves three separate parameters; the Proportional, the Integral and Derivative values. The Proportional term produces a response that is proportional to the error signal, the Integral term examines the set point's offset over time and corrects it when and if necessary, while the Derivative term produces an output that is proportional to the rate of change of error. The sum of these three actions is collectively termed as PID control.

Several methods can be used to tune the PID controller. Among these are the heuristic criteria of Ziegler-Nichols; The values obtained by this method have been used as an initial tuning criterion in magnetic levitation systems [46]. The tuning can also be achieved by trial and error, however, the time and effort required to achieve it by someone not experienced is unknown, in the sense that the constants Kp, Ki and Kd form a constant space in which each Point is a possible option.

Using autotuning provided by Matlab it was found that the values Kp = 1, Kd = 0.015 and Ki = 4 make the system stable. The space of valid constants is shown in Figure 4.3, product of the intersection of these three inequalities in a constant space where each axis represents the constants of the PID controller.

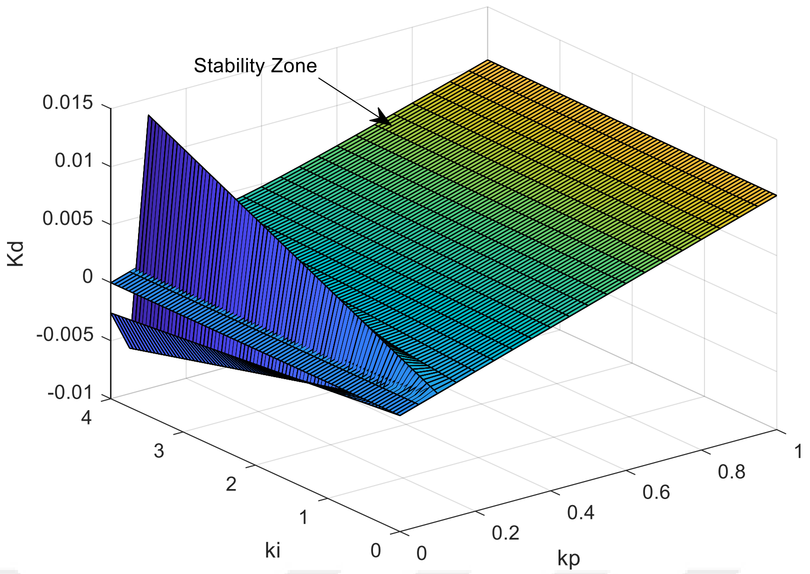

Figure 4.3. Region of stability in the space of PID constants

The upper region corresponds to the stability zone, the triplet Kp, Ki, Kd stabilize the system. The graph has been generated as the intersection of the three stability conditions, for Kp values between 0 and 1, and Ki values between 0 and 5,87, using Kd as a dependent variable. At the entrance step of 7 mm of amplitude these requirements were fulfilled for the triplet of values as given follow: $K_p = 0.15$, $K_d = 5.87$, $K_i = 0.019$

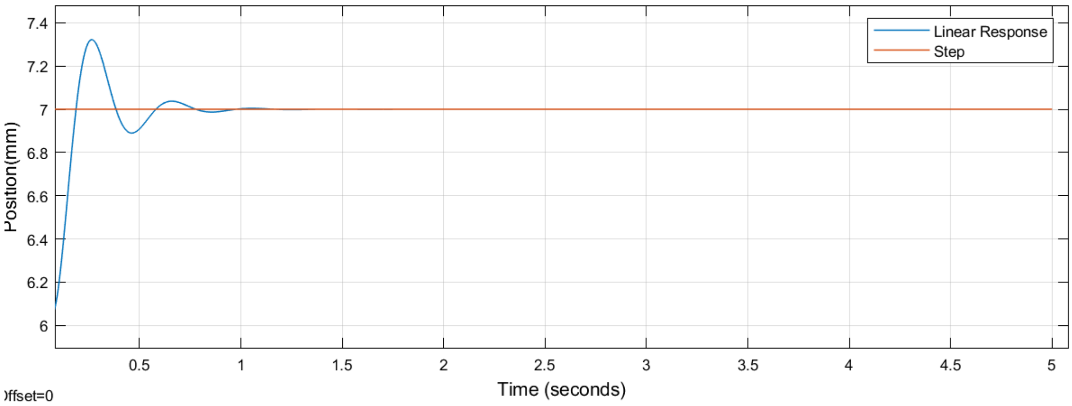

Figure 4.4. System response for a 5 mm step input

From the result in the graph, the rise time is approximately 1.25 s. The peak time is 0.24s.

4.1.2. GOOGOLTECH industrial PC

Googoltech is a terminal board that has a highly integrated motion controller that comes with computer functions, controller, signal generator, etc. Is used to serve as an interface and on it carry out the control of the magnetic levitation system, also, is used for connecting the PC to real world signals (maglev system signals). The interface contains channels, digital input/output ports, PWM A/B output, etc. Googoltech is designed to allow standard data acquisition and control of applications, in addition, it is optimized for use in a PC-Interface in Real-Time by Simulink or MS Visual Studio.

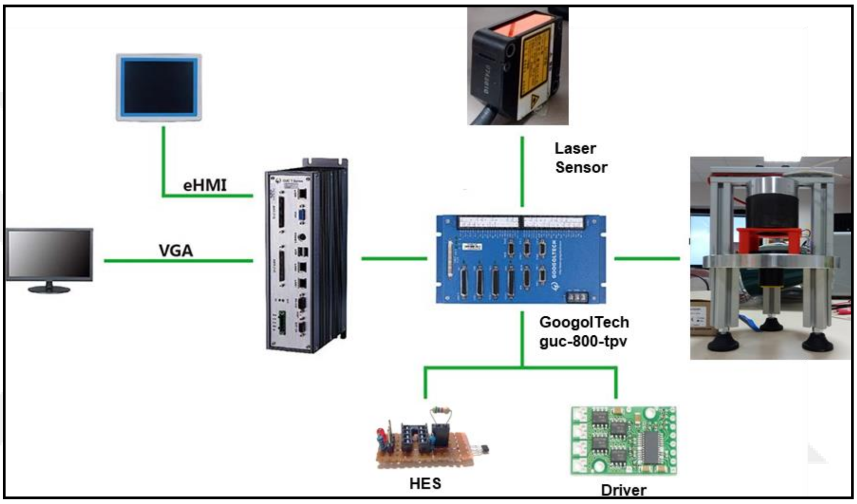

Figure 4.5. Industrial GoogolTech interface

To achieve control of the sphere in the stable levitation position, it is necessary to have a feedback system as shown in Figure 4.6. The operation of the system can be explained as follows: In the controller exists a reference position of the sphere, with which its objective will be to ensure the real position is as close to the reference position as possible. The controller will continuously receive information about the actual position in which the ball is located, this signal will be provided by the hall effect sensors and laser sensor.

Depending on whether the position is greater or less than desired, the current applied to the electromagnet will be reduced or increased.

The electronic actuator (driver) is in charge of supplying the necessary electric energy to the electromagnet, so that it establishes the magnetic force on the metallic sphere, therefore, certain important considerations for its design must be considered. The operation of this device is described by a block diagram.

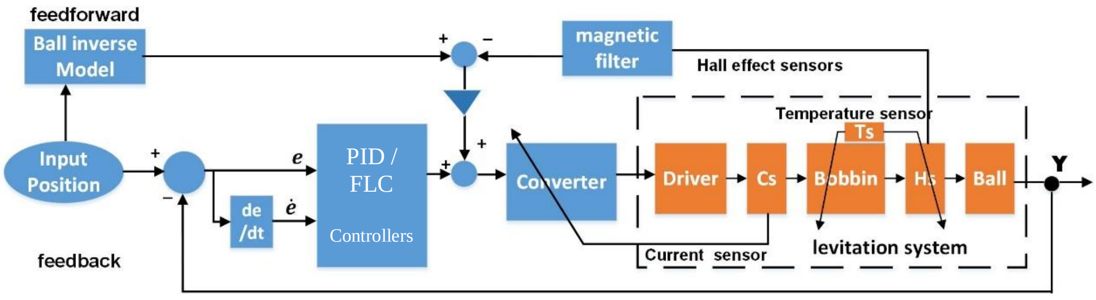

Figure 4.6. Control Block Diagram of maglev system

4.2. Fuzzy Logic Controller Design

Fuzzy controllers based on fuzzy logic provides a means of converting a linguistic control strategy based on expert knowledge into an automatic control strategy. Fuzzy logic controllers are an interesting alternative to classical controllers that are used for the design of non-linear control systems [47]. Fuzzy logic control is useful when the processes to be controlled are very complex for analysis with conventional techniques or when the available sources of information are inaccurate or in the presence of uncertainties.

4.2.1. Fundamental principles of FLC

This part highlights the fundamental principle of the FLC. In order to visualize the related issues, Figure 4.7 shows the basic configuration of an FLC, which is composed of four main components: a fuzzification interface, a knowledge base, decision making logic, and a defuzzification interface [48].

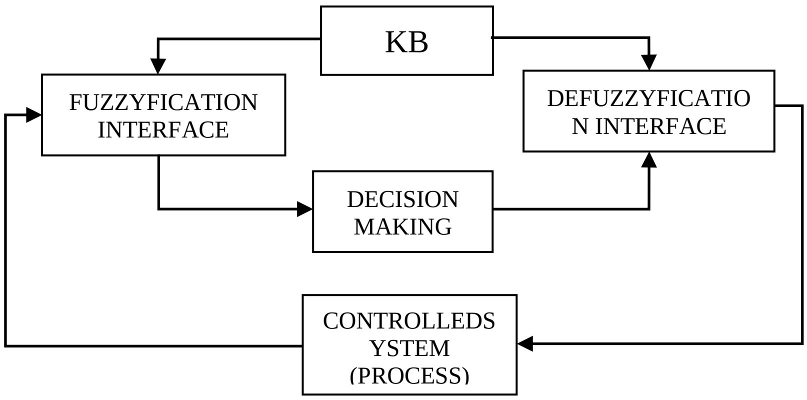

Figure 4.7. Basic fuzzy logic controller (FLC) configuration

The fuzzification interface functions like so: a) the values of the input variables are measured, b) a scale mapping is carried out that transfers the range of values of the input variables to corresponding universes of the discourse, c) the fuzzification function is performed, which converts the input data into suitable linguistic values that can be seen as fuzzy set tags.

The knowledge base includes knowledge of the domain of the application and the control objectives of the assistant. It consists of a "database" and a "base of linguistic (fuzzy) control rules". a) the database provides the necessary definitions, which are used to define rules of linguistic control and manipulation of fuzzy data in an FLC, b) the rule base characterizes the control objectives and control policy of domain experts through a set of linguistic control rules.

The logic of decision making is the core of an FLC; it has the ability to simulate human decision-making based on fuzzy concepts and to infer fuzzy control actions using fuzzy implications and rules of inference in fuzzy logic.

The defuzzification interface converts the fuzzy result to a number that can be sent to the process as a control signal [49]. The defuzzification interface performs the following functions: a) a scale mapping, which converts the range of values of the output variables in corresponding universes of the discourse. b) defuzzification, which produces a non-fuzzy control action from an inferred fuzzy control action.

The conditional declarations and the diffuse control rules in an FLC, establish the dynamic behavior of the system. This is characterized by a set of rules of linguistic description based on expert knowledge. This expert knowledge is usually of the form:

IF (a set of conditions are met) THEN (a set of consequences can be inferred).

In first phase of the fuzzy controller, rules have been designed for error and rate of error to get FLC response for desire set point of steel sphere which will be able to control the one degree of freedom system (see Figure 4.8).

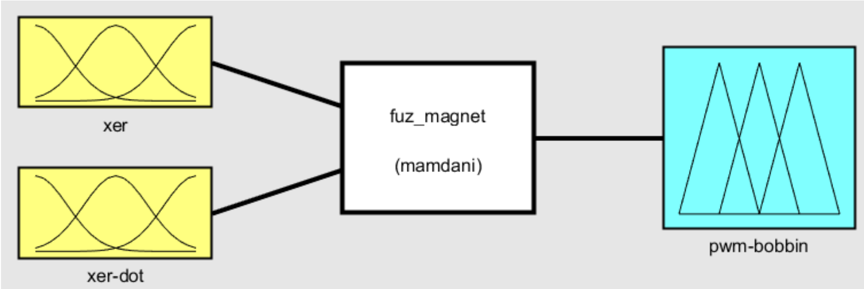

Figure 4.8. Definition of input - output variables for Fuzzy Logic Controller (FLC)

In Figure 4.9, d1 is controlled by the electromagnet on the vertical axis. The electromagnet provides the force that pulls up. Hence, d1 is positive below horizontal zero and negative above horizontal zero.

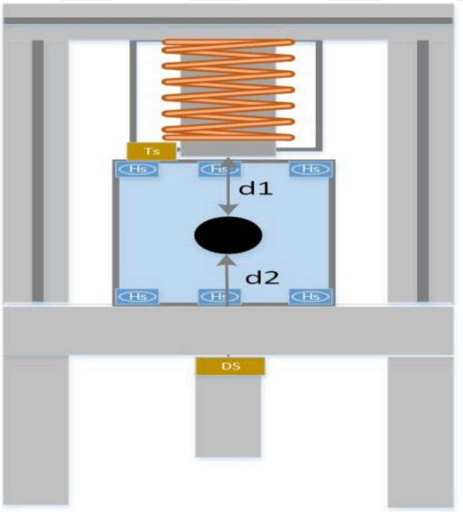

Figure 4.9. Airgap between electromagnet and HES

Once the electromagnet moves the ball upward, in the laser sensor, the distance increases gradually and the position error decreases; In the same way, when the actuator goes down, the distance of the sensor decreases. The actuator needs to operate on different duty cycle to get the desired net force for a one-degree horizontal change.

4.3. FLC Implementation

FLC is employed to control the magnetic system position with a negligible time delay. It is worth mentioning that, in experimental design, FLC is preferred to the PID controller. The rationale for preferring the FLC is that the time constant of the experimental system including PID controller is greater than the Industrial PC

“GoogolTech” period. Hence the system would fluctuate around an unwanted operating point continuously without taking into account the predefined reference. Figure 4.10 show the implementation of the FLC in the maglev system. The FLC regulates mass flow using the PWM signals to the converter. To control the variation of the position of the ball, the FLC determines the appropriate duty cycle for the PWM. signals. The inputs of FLC are error and error rate. The error is defined as the difference between the desired and measured sphere position as:

$$e = y_d - y_a \tag{4.3}$$

where y_a and y_d are the actual position and desired position, respectively. Figure 4.10 shows the schematic of the FLC with inputs and output are membership functions.

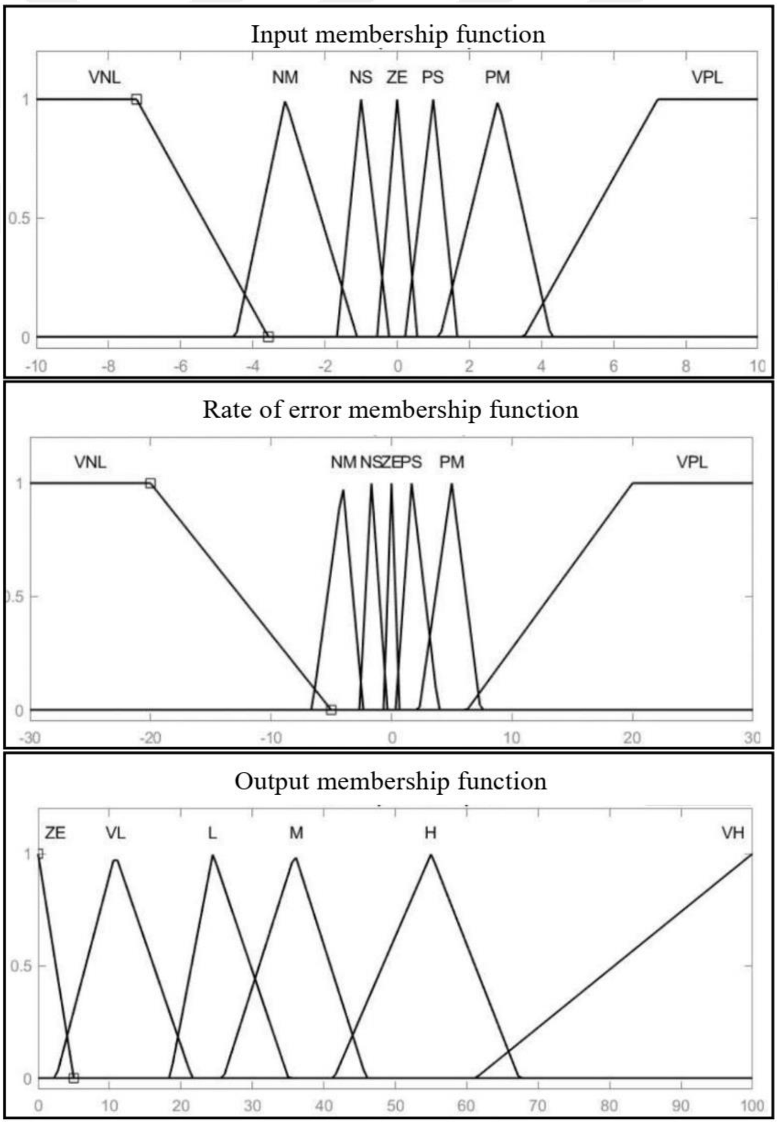

Figure 4.10. FLC membership functions of FLC

The next step for the controller design defines the partitions corresponding to the input and output variables, assigning each partition a linguistic value. For this, three partitions with a triangular function are considered, where the central point is the desired value and the rank of belonging is between 0 and 1. The top vertex of the triangle corresponds to the measure of the registered value and the width of its base to the standard deviation. Distance range: $-10 \leq x \leq 10$

4.3.1. Rule base

The next step is to select the set of rules that will be used in the controller using Mamdani's method, so as to express the rules according to the experience and knowledge of an expert [50].

In this thesis the FLC is a Mamdani type fuzzy system [51-53]. Linguistic variables for the input and output are listed in Table 4.1. The triangular input and output membership functions of the FLC are presented and the Fuzzy rules are presented in Table 4.1. The following example explains two rules.

When the error is zero and the error rate is zero too, it can be deduced that the system is placed at the desired position and the system is stationary, therefore, the duty cycle must be set at zero in order to keep the current position of the system.

Table 4.1. Linguistic variables set for FLC

Symbol	Definition	Function
VNL, VPL	Very Negative Large, Very Positive Large	Input
NM, PM	Negative Medium, Positive Medium	Input
NS, PS	Negative Small, Positive Small	Input
ZE	Zero	Input
VL	Very Large	Output
L	Large	Output
M	Medium	Output
H	Hight	Output
VH	Very Hight	Output

In Table 4.2 the base of rules obtained empirically is defined as a fuzzy associative memory that is a matrix that represents the consequences of each rule according to the entries. The graphical analysis of the rules bases is observed in Figure 4.11.

Table 4.2. FLC rule base

e/ė	VNL	NM	NS	ZE	PS	PM	VPL
VNL	L	VL	VL	ZE	VL	ZE	ZE
NM	VL	VL	ZE	ZE	VL	ZE	ZE
NS	VL	ZE	ZE	ZE	ZE	ZE	ZE
ZE	L	VL	ZE	ZE	ZE	ZE	ZE
PS	M	VL	VL	VL	VL	L	M
PM	VL	L	L	L	L	L	M
VPL	VH	H	H	M	H	H	M

Here, the rate of error dEr/dt = 0 has two states.

1. When the link is on or crossing horizontal zero.
2. When the link is at the extreme point during oscillation about desired setpoint.

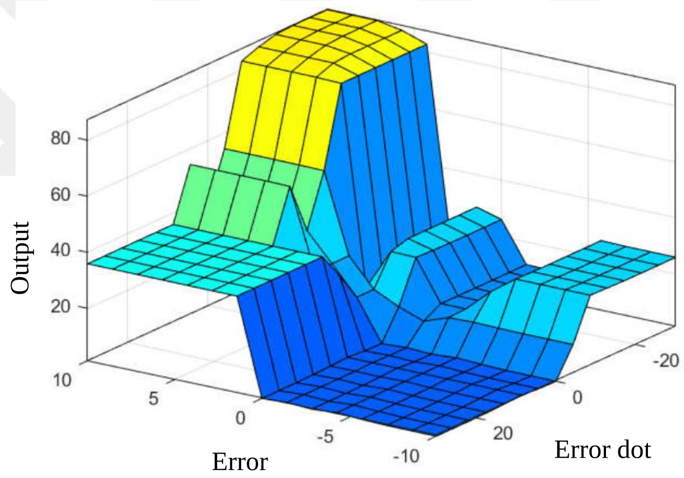

Figure 4.11. FLC Fuzzy Rule Base Analysis surface

5. RESULTS AND DISCUSSIONS

5.1. Hall Effect Sensor Bode Diagram

Once we have collected the distance and the magnetics flux response for many frequencies, we can display it in one of the most intuitive ways which is to plot the magnetic flux vs. frequency and put it in one plot (see Figure 5.1). The below diagram shows the frequency response of the magnetic flux sensor.

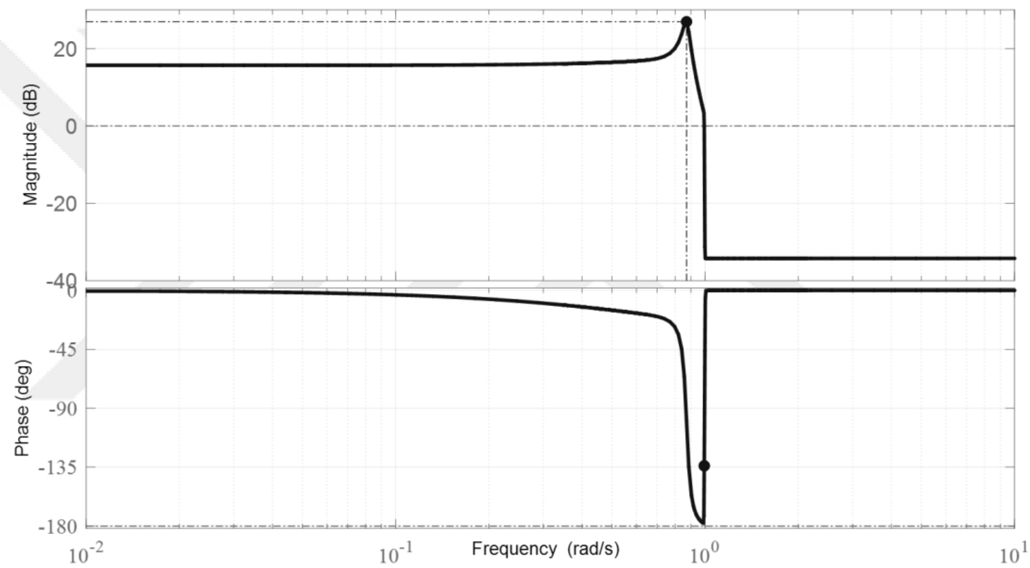

Figure 5.1. Bode diagram of hall effect sensor

First, we observe the frequency response at frequencies less than 10hz. The response is close to 0.8 dB (20LOG(dB/10)) where T is the amount in Tesla measured by magnetic flux sensor, this means that the ball's movement output will look like the ball's input. If the input is set at 10hz the control system can follow it with close to identical amplitude. Looking at the magnetic flux measured trajectory, this is near 0 degrees, which means that the output will not lag behind the input. 0.8 dB at 0 degrees implies perfect agreement between the output and the input to the system. This is what we are aiming for. Second, taking a look at the readings for 15 Hz. The measure is around 0.9 dB, -60 degrees. This means that the output will be 20 ^ LOG(0,9dB/10) = 1.2 times as large as the output and 60 degrees behind the input at 15 Hz. This isn't what we want. We want the system to move as far as specified.

Lastly, let's look at the frequency response at the approximation 100hz. The amplitude response is 0.3 dB, and similar to -60 degrees, this means that the output amplitude is 20^LOG(0,3dB/10) = 1 times the input amplitude and 60 degrees behind the input.

5.2. System Signal Analysis

For start of the tests, the HES was located at a distance of 4 mm from the core of the electromagnet, considering 1 mm of the thickness of the HES, the initial airgap is defined in 3 mm, the ball displacement is formed by steps of 1 mm in each case and, in downwards direction; moreover, Figure 5.2 shows each sensor's trajectory. The amount of current is represented by relation distance (mm) vs magnetic field (T), a dataset of interest is the yellow line, which represents a signal filter of all sensors connected to the system, this means that we have the average of all the signals that come from all the hall effect sensors.

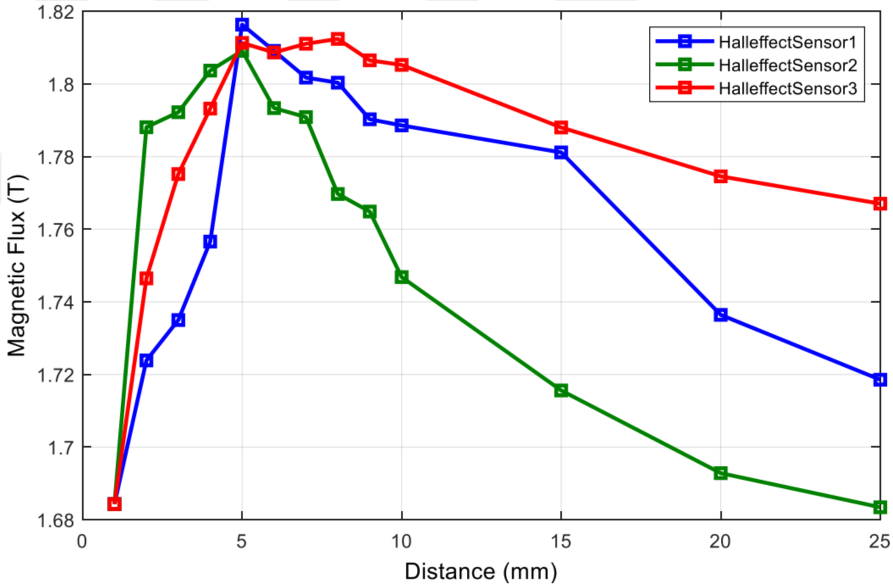

Figure 5.2. Magnetic flux vs. distance obtained in the maglev system

In order to achieve a more precise hall effect sensor signal, a medium filter was applied by means of a program compiled in Matlab software. In Figure 5.3 the result is shown.

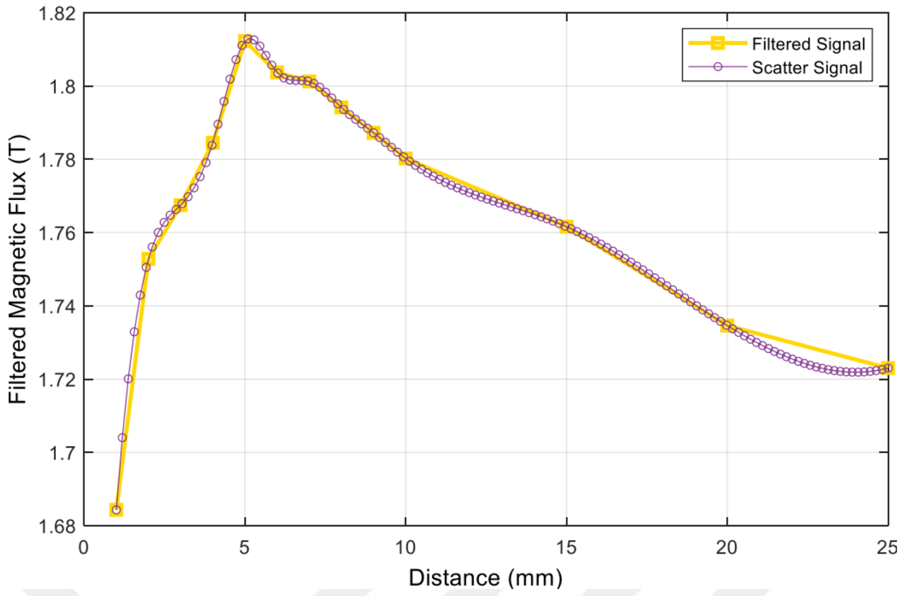

Figure 5.3. HES filtered signal using mid-pass filter

The system coefficients can be identified through an experimental approach. A series of experiments are conducted to find the currents required to levitate the object at different equilibrium positions. One such result is plotted in Figure 5.4.

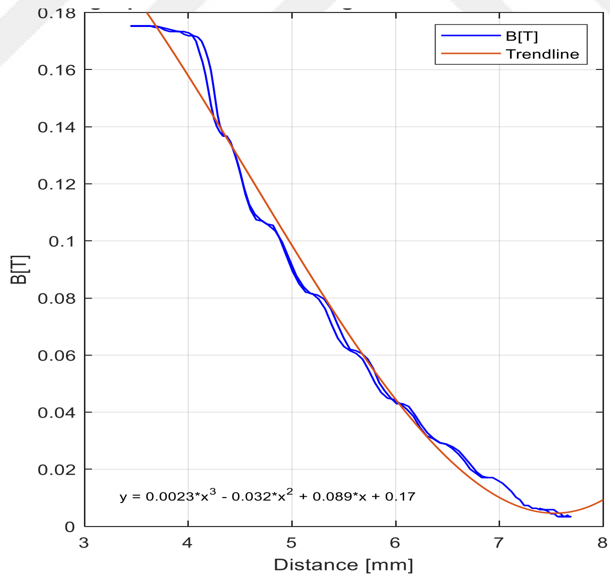

Figure 5.4. The equilibrium points and corresponding required current

The test result as shown in Figure 5.4 did not show a precise linear relationship between displacement in the vertical axis and required current for the magnetic flux expressed in Tesla on the horizontal axis to levitate the ball. However, if the ball which going to levitate only moves within a small operating range, e.g. our consideration is

0 ~ 3cm, we can get a reasonable approximation to a linear relationship from Figure 5.4.

The sampling time which show the best results were obtained at 9,37s. This value includes a delay of 1ms plus the delay associated with the computation of values in the microcontroller. Figure 5.5. shows the response of the maglev system (position in voltage form). For a levitation position of approximately 7.08 mm, the current required to maintain the sphere in the levitated position was approximately 1A, while in the model it was calculated that this would be 0.912A.

The PID controller has initial gains P = 1.4713, I = 6.0133, D = 3.2748. The regulation is carried out by real time signal filtration and results are shown in Figure 5.5.

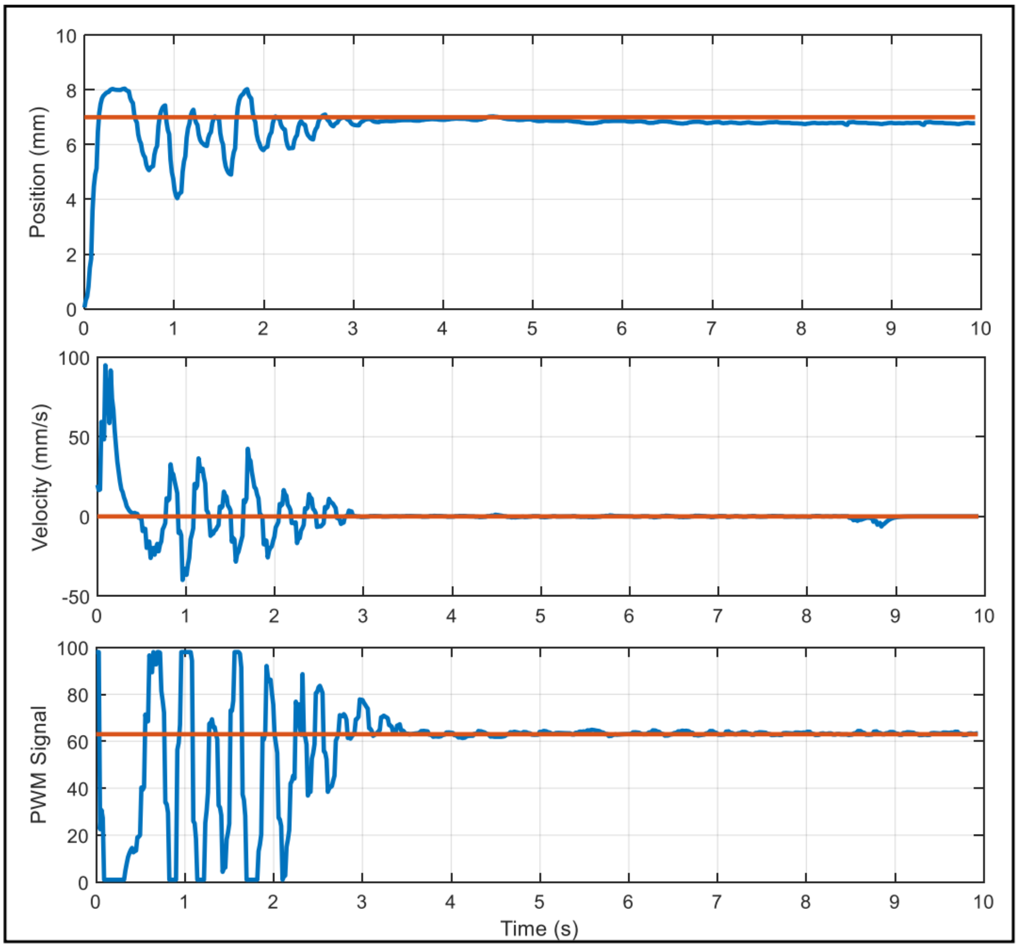

Figure 5.5. Real time response and performance of PID controller for position, Velocity and PWM signal

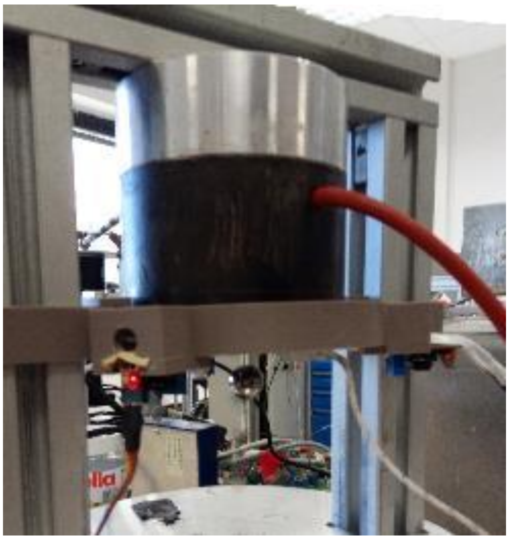

Figure 5.6. Picture of the ball controlled by PID controller

The impact of dynamic reference is investigated. To have a reasonable judgment on FLC performance, Figure 5.7 shows the performance and response of the FLC to track a reference step.

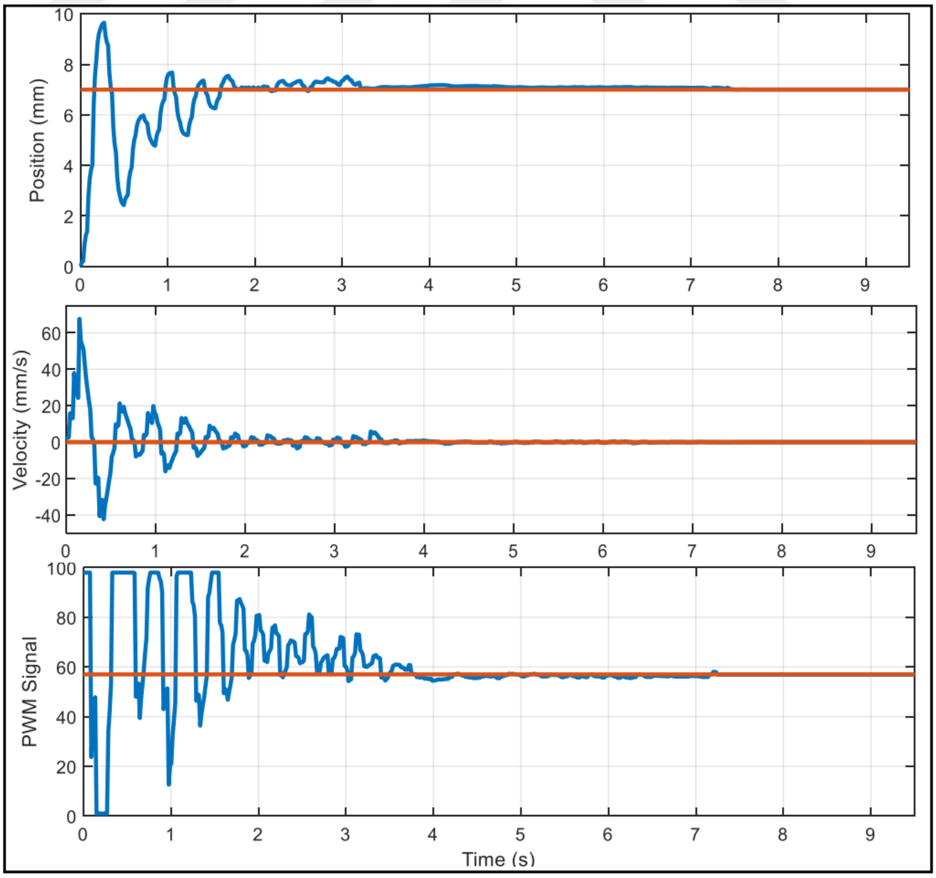

Figure 5.7. Real time response and performance of FLC for position, Velocity and PWM signal

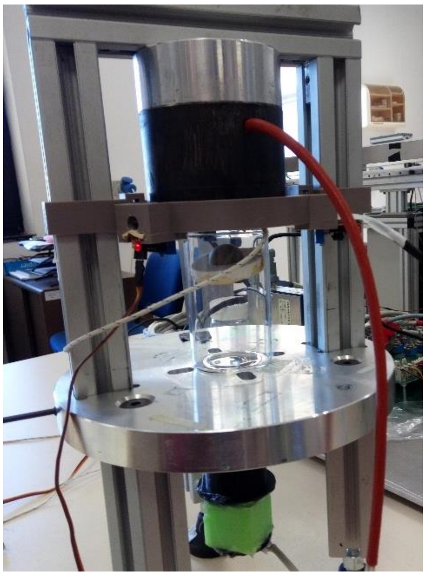

Figure 5.8. Levitation of the steel ball using a FLC

5.3. Performance Error Indices

The indices and basic performance entities considered for this project have been used extensively in the tuning of controllers to give the best performance. For this purpose, a measure known as performance index is used. The usual criterion of performance index is given using 3 expressions [41], which are the functions of an error signal.

Table 5.1. Definition of basic performance indices

Parameter	Expression	Characteristic
IAE	$IAE=\int_0^\infty \lvert e(t)\rvert\, dt$	Integral Absolute Error
ISE	$ISE=\int_0^\infty e^2(t)\, dt$	Integral Square Error
ITSE	$ITSE=\int_0^\infty te^2(t)\, dt$	Integral Time Squared Error

The error signal e(t) in a control system is given by:

$$e(t) = r(t)-c(t) \tag{5.1}$$

Where, r(t) correspond to the input or reference signal and c(t) output signal. Performance indices in the maglev system control are as follows in Table 5.2.

Table 5.2. Comparison of performance indices of the PID and FLC controllers

Controller/Criterion		Laser sensor	Distance sensor	HES
		7mm	7mm	7mm
PID Controller	IAE	9.103	9.2470	12.0941
	ISE	1.351	1.3661	1.5580
	ITSE	36.610	37.751	44.410
Fuzzy Controller	IAE	8.6431	8.7638	11.3805
	ISE	1.2510	1.2778	1.4655
	ITSE	35.342	35.985	41.397

The relative importance of the tracking performance and the amount of control effort play a central role in the selection of the controller gains. The designer can observe the changes in the expended control effort and tracking error when the controller parameters are changed. Eventually a well performing set can be fixed after a refinement process. In this study, controller performance evaluation is performed in the light of IAE, ISE and ITSE as performance criteria.

6. CONCLUSIONS AND SUGGESTIONS

Using an electromagnet with somaloy700 material in the core has proved to be an advantage offering high permeability compared to cores of steel plates, and therefore produce a greater magnetic flux, likewise, due to its ferromagnetic powder particles with coating layer composition, it allows the magnetic levitation system core to have a special cylindrical shape with a limb that starts from the center of the base of the cylinder.

The relationship between temperature and magnetic flux plays an important role in the magnetic levitation system, e.g., when the electromagnet reaches a temperature of 100 °C the coil increases its reluctance [R], consequently the magnetic flux [B] weakens at the rate of 16%, see section 3.7.

In relation to the hall effect sensor it has good advantages for the measurement of the magnetic field, e.g. The hall effect sensor has measurement capacity of up to 3T, also has a response frequency exceeding 20hz and for its physical qualities can be located in any part of the electromagnet with minimal components. A disadvantage is that the implementation of the PCB amplifier circuit for its operation requires a high level of precision in the assembly, otherwise when the measurements are carrying out the data may vary. In contrast, the laser sensor offers greater quality and reliability when it is used due to the fact that only one sensor and the amplifier circuit are presented in a single package.

To detect the position of the ball two types of sensors were used in the maglev project, one of them, the laser sensor model ZX-LD100 series which presents great sensitivity and precision in its operation, the other sensor used is a distance sensor Sharp model GP2Y0A21YK0F with standard features. The relationship in price-quality, the laser sensor turns out to be much more expensive than a sharp model distance sensor, however, the level of reliability presented by the sharp sensor is suitable to be used in the magnetic levitation system. Certainly, one of the biggest challenges in the design and control of maglev systems is the highly non-linear behavior of magnetic materials in terms of airgap, temperature, current, magnetization and hysteresis effect patterns. With help of control techniques, mathematical models and simulations, the aim was to maintain a ferromagnetic ball in a stable state of suspension under suitable parameters and conditions.

The mathematical model was able to predict the constants of the PID controller to obtain the levitation in the real prototype. The evaluation of the most optimal constants was done for the most part by simulation, and when values were found that met the design requirements the controller was implemented in the real plant. This was greatly favored due to the availability of a model and the option of observing the transitory response of the system to different constants by simulation. The obtaining of a mathematical model that largely describes the process is highlighted in the chosen linear regions.

A multidisciplinary approach was used for designing the system at all levels: physical, mathematical, electronical, mechanical, control, and software knowledge were all used. During the real implementation, it became evident the need to integrate all the concepts coming from each discipline a weight was given to the development of each component, where the need to understand all the subjects is recognized with a reasonable level of depth. For example, in reality it was found that many of the theoretical assumptions were not met 100%. Thus, in accordance with the knowledge of each discipline and the understanding of the importance of that parameter (not represented perfectly in reality) in the system, it was decided to improve it or leave it as it is, also taking into account other factors such as economic (purchase of more components) or time (increase in complexity and the need for greater purification).

Within the electronic aspect of the magnetic levitation system the development of a good sensing system and a good power system was fundamental. In both aspects, electronic problems were found, not only associated to each component, but also to the interaction between them. In particular, for good sensing it was necessary to use stable energy sources, with noises of less than 20 mV of amplitude. In the power system, a driver was used for the convention of a square signal of 5 V to 30 V (necessary to properly polarize the plant). The driver also fulfilled the function of isolating both systems.

PID and Fuzzy controllers proved to be robust and adequate controls on the actual magnetic levitation platform. Experimentally, many system parameters were varied such as mass, geometry, solenoid resistance, polarization, voltage, levitation position, as well as introducing noise into the system, such as an additional magnetic field (a using a neodymium magnet). Under moderate variations of these factors, the designed controllers responded adequately by stabilizing the object in the required levitation position.

REFERENCES

[1] Parthasaradhy P., Ranganayakulu S., Hysteresis and eddy current losses of magnetic material by Epstein frame method-novel approach, *The International Journal of Engineering and Science (IJES)*, 2014, **1**, 85-93.

[2] Jonathan S. B., Carlos V. R., Joan H. G., Comparison of a linear and nonlinear control on a magnetic levitator, *Ingenierías USBMed*, 2018, **9**(1), 112-118.

[3] Perren G., Study of the Practical Applications of the Magnetic Levitation, *Fisica III*, 2003, **2003**, 1-16.

[4] Subrata R.; Hardenberg J. L., Gozali F., The Use of PID Controller To Get The Stable Floating Condition Of The Objects In Magnetic Levitation System, *International Symposium on Electrical and Computer Engineering*, 2017, **15**, 321-324.

[5] Rairán D., Moreno J. C., Magnetic Circuit Design of a Magnetic Bearing by finite elements, *Tecnura*, 2008, **11**(22), 63-72.

[6] Delgado A., Linearization Input/Output of the Related Nonlinear using Filter, *Ing. Inv*, 2000, **0**(45), 62-66.

[7] García J. F., Control Engineering and its Actual Role in Medicine, *Ingenierías USBMed*, 2016, **7**(2), 1-3.

[8] Pradhan S. K., Singh R., Nonlinear control of a Magnetic Levitation System using feedback linearization, *International Conference on Advance Communication Control and Computing Teclmologies (ICACCCT)*, 2014, **8**(10) 152-156.

[9] Charara A., De Miras J., Caron B., Nonlinear control of a magnetic levitation system without premagnetization, *IEEE Transactions on Control Systems Technology*, 1996, **5**, 513–523.

[10] Green S. A., Craig K. C., Robust, design, nonlinear control of magnetic levitation systems, *Journal of Dynamics, Measurement, and Control*, 1998, **120**(4), 488–495.

[11] Huang C. M., Yen J. Y., Chen M. S., Adaptive nonlinear control of repulsive maglev suspension systems, *Control Engineering Practice*, 2000, **8**(5), 1357–1367.

[12] Yaghoubi H., The Most Important Maglev Applications, *Journal of Engineering*, 2013, **2013**, 19.

[13] Hrabovcova V., Jokinen T., Pyrhonen J., *Design of Rotating Electrical Machine*, 1th ed., John Wiley & Sons Ltd, United Kingdom, 2008.

[14] Thompson M. T., Eddy Current Maglev Levitation. Models and Experiments,

[15] *IEEE Potentials*, 2000, **19**, 40-44.

[16] Sangster A. J., *Electromagnetic Foundations of Solar Radiation Collection: A Technology for Sustainability*, 1th, Springer, Edinburgh, 2014.

[17] Sangster A. J., *Energy for a Warming World: A Plan to Hasten the Demise of Fossil Fuels*, 1th ed., Springer, London, 2010.

[18] Bakhsh I., *Finite Element Techniques for Three-Dimensional Skin Effect Problems*, 2012, Graz.

[19] Hui X., Evaluation of Crack Signals in Cylindrical Structures Using Eddy Current Nondestructive Evaluation Theory, Doctoral Thesis, Iowa State University, Electrical and Computer Engineering Department, Iowa, 2012, 12749.

[20] Balanis C. A., *Advanced Engineering Electromagnetics*, 1th ed., John Wiley & Sons, New York, 1989.

[21] Khali H. K., *Nonlinear Systems*, 3th ed., Prentice Hall, New Jersey, 2002.

[22] Lotha G., Hysteresis, Encyclopedia Britannica, https://www.britannica.com/-science/hysteresis (Accessed: 22 September 2018).

[23] Asari, R., A., Guo Y., Zhu J., Magnetic Properties Measurement of Soft Magnetic Composite Material (SOMALOY 700) by Using 3-D Tester, *International Conference on Applied Physics and Engineering*, 2017, **1875**(1).

[24] Slusarek B., Jankowski B., Sokalski K., Szczyglowski J., Characteristics of Power Loss in SMC a Key for Desining the Best Values of Technological Parameters, *Journal of Alloys and Compounds*, 2013, **1**, 581-699.

[25] Hoganas, A., B., Somaloy Material, http://www.hoganas.com//globalassets/-media/sharepointdocuments/BrochuresanddatasheetsAllDocuments/SomaloyMaterial-Data_November_2016_1806HOG-.pdf (Accessed: 23 mart 2017).

[26] Hurley W. G., Wolfle W. H., Electromagnetic Design of a Magnetic Suspension System, *IEEE Transactions On Education*, 1997, **40**, 2.

[27] Oguchi K., Tomigashi Y., Digital Control for a magnetic suspension system as an undergraduate project, *Int. J. Elect. Enging. Educ.*, 1990, **27**, 226-236.

[28] Boreau of Standards, *The International Annealed Copper Standard*, 1914, Government Printing Office, Washington.

[29] Sikorsky P. J., Kaufman J. G., Crosby S. R., Sizek H. W., *Electrical and Magnetic Properties of Metals*, 1th ed., ASM International, Ohio, 2000.

[30] Giancoli D. C., *Physics Principles with Applications*, 6th ed., Pearson, 590-616, 2014.

[31] Schmolz B., Magnetism and Stainless Steel, Ugitech, http://www.ugitech.com/uploads/ugitransfer/docs/GED_1591.pdf (Accessed: 03 mart 2017).

[32] Nathan I., Bastos J., P., *Electromagnetics and Calculation of Fields*, 1997,

Springer, **2**, 22-46.

[33] Wong. T. H., Design of a Magnetic Levitation Control System- An Undergraduate Project, *IEEE Transactions on Education,* 1986, **E-29**, 196- 200.

[34] Shiao Y. S., Design and implementation of a controller for a magnetic levitation system, *Proceedings of the National Science Council,* 2001, **11**(2), 88-94.

[35] Dolga V., Lia D., Modelling and Simulation of a Magnetic Levitation System, *Fascicle of Management and Technological Engineering,* 2007, **6**, 1-17.

[36] Cho D., Kato Y., Spilman D., Sliding mode and classical controllers in magnetic levitation systems, *IEEE Control Systems,* 1993, **13**(1), 42-48.

[37] Hurley W. G., Wolfle W. H., Electromagnetic Design of a Magnetic Suspension System, *IEEE Transaction on Education,* 1997, **40**, 2.

[38] Barie W., Chiasson T., Linear and nonlinear state-space controllers for magnetic levitation, *International Journal of System Science,* 1996, **27**, 11.

[39] Woodson H., Melcher J. R., *Electromechanical Dynamics*, 1th ed., John Wiley and Sons, New York, 1968.

[40] Moon F. C., *Superconducting Levitation: Applications to Bearings and Magnetic Transportation*, 1st ed., New York, Wiley, 2013.

[41] Purcell E. M., *Electricity and magnetism*, 3rd ed., Cambridge University Press, Cambridge, 2011.

[42] Valluvan M., Ranganathan S., Modeling and Control of Magnetic Levitation System, *International Conference on Emerging Trends in Science, Engineering and Technology,* 2012, **2012**, 545-548.

[43] Hajjaji A. E., Ouladsine M., Modeling and Nonlinear Control of Magnetic Levitation Systems, *IEEE Transactions on Industrial Electronics,* 2001, **48**, 831-838.

[44] Patil A., More S., Mathematical Modeling of Physics Systems, *Journal of Electrical and Electronics Engineering,* 2005, **9**, 57-64.

[45] Ogata K., Modern Control Engineering, 3rd ed., Pretince Hall, Madrid, 2010.

[46] Hurley W. G., Hynes M., Wölfle W. H., PWM Control of a Magnetic Suspension System, *IEEE Transactions on Education,* 2004, **47**(2), 165-173.

[47] Palmieri D., Pucci M., Construction and Control of a Magnetic Levitation System, *National University of Quilmes,* 2004, **1**, 1-5.

[48] Karakuzu C., An Experimental Comparison of Fuzzy, Neuro and Classical Control Techniques, *IEEE Xplore,* 2000, **21**, 160-166.

[49] Lee C. C., Fuzzy Logic in Control Systems: Fuzzy Logic Controller-Part I and Part II, *IEEE transactions on systems, man, and cybernetics,* 1990, **20**, 404-418.

[50] Middala J. R., Modeling and Analysis of Magnetic Levitation System Using Fuzzy Logic Control, *International Journal of Scientific Development and Research (IJSDR),* 2017, **2**(6), 318-323.

[51] Georgieva P. V., Fuzzy Rule-Based Systems for Decision-Making, *Engineering Science*, 2016, **3**(1), 5-16.

[52] Chonghua W., A Study of Membership Functions on Mamdani-Type Fuzzy Inference System for Industrial Decision-Making, Master Degree Thesis, Lehigh University, Mechanical Engineering Department, Pennsylvania, 2015, 1665.

[53] Rodriguez M. A., Meza R. G., Comparative Performance Analysis of Different Linear Controllers Tuned for Several Cholette's Bioreactor Steady States Using Multi-Criteria Decision Making Techniques, *Mexican Journal of Chemical Engineering*, 2015, **14**(1), 167-204.

[54] Ankit J., Losses in DC Generators, Quora, https://www.quora.com/What-are-the-losses-in-DC-generators, (Accessed: 17 July 2017).

ANNEX

ANNEX-A

```
% ============  Levitation  parameters  =====================
g=9.80665; % gravity m/s2
Nb=1090; % number of windings
Xb=0.0025; % the position of Ball in the system
Reg=6.089086;% equivalent reluctance
Rb=8; %  (coil) resistance (ohm)
Vb=30; % coil voltage
Lb = 0.15;  %  coil  inductance  (H)

lb = 0.282;    %  Length of the coil part (m)
lcb = 0.276;   %  Distance between coil and Main (m)
rbs = 0.155;   %  Radius of coil (m)
mbr = 0.110;  %  Mass of coil (kg)
%------
mT1 = 1 + mbr;      %Total mass of the  (kg)
%-------
lT1 = ((mbr)*lcb-(mbr/2+rbs)*lb)/mT1;  % Centre of gravity of the Ball (m)

av0  =  atan2((5-4),  5);  %  Initial  vertical  distance
%----------- Interface  circuit  tables

%Controller parameters
Ts = 0.2; % Sample time
Np = 20; %Prediction v
Nc = 15; % Control v
```

Figure A. 1. Parameters for maglev system using Matlab software

PUBLICATIONS AND WORKS

Zafer B., **Ayala E**., Mohammad F., Real-time PID Control for Magnetic Levitation System with special Hall Effect sensor, *International conference on theoretical and applied computer science and engineering – ICTACSE 2018*, Istanbul, Turkey, 29-30 June 2018.

BIOGRAPHY

He was born in March 1984 in Ipiales-Colombia. He completed his primary and secondary education in the same birth city. He started his university education in 2003 at the Department of Engineering in Fundación Universitaria San Martin and graduated in 2008 as an Engineer of Systems. Parallelly, He started his study in Mechatronics Technology in Servicio Nacional de Aprendizaje SENA in 2006 and graduated in 2008. He started her career as an instructor in April 2009 and worked full time in the education department of SENA between 2009-2014. Late in 2014, he earned a scholarship to study in Turkey, in 2015 he started his post-graduate education in the Department of Mechatronics Engineering at the Institute of Science, Kocaeli University in Turkey. Currently he is a candidate of the Department of Mechatronics Engineering at Kocaeli University to receive his master's degree.